

ABSTRACT

Title of Document: INVESTIGATION OF JP-8 AUTOIGNITION UNDER VITIATED COMBUSTION CONDITIONS

Casey Charles Fuller, M.S., 2011

Directed by: Professor Gregory Jackson, Chair
Department of Mechanical Engineering

Limited data on jet fuel ignition and oxidation at low-O₂, vitiated conditions has hindered the validation of kinetic models for combustion under such conditions. In this study, ignition delay time experiments of JP-8 have been performed with vitiated air at low pressures. Initially, the effects of temperature, equivalence ratio, and mole fractions of vitiated components on JP-8 ignition at 1 atm were screened to discover that temperature, O₂ and NO have the largest significance. A following detailed investigation examined the effect on JP-8 ignition of larger concentrations of NO (0 - 1000 ppm) at lower temperatures (700 - 900 K), pressure (0.5 - 1.0 atm) and O₂ mole fractions (12 - 20%). Results show that even trace amounts of NO dramatically enhance the oxidation of JP-8 with reduction in ignition delay time of up to 80%. Significant coupling exists between NO and the other design variables (temperature, oxygen level and pressure) as related to the effect of NO on ignition. An empirical model relating temperature, O₂ and NO to ignition delay time of JP-8 has also been developed.

INVESTIGATION OF JP-8 AUTOIGNITION UNDER
VITIATED COMBUSTION CONDITIONS

By

Casey Charles Fuller

Thesis submitted to the Faculty of the Graduate School of the
University of Maryland, College Park, in partial fulfillment
of the requirements for the degree of
Master of Science
2011

Advisory Committee:
Professor Gregory Jackson, Chair
Associate Professor André Marshall
Associate Professor Peter Sunderland

© Copyright by
Casey Charles Fuller
2011

Acknowledgements

This research has been supported and funded by Combustion Science and Engineering, Inc. through the following SBIR grants from the United States Air Force:

Topic # AF081-057 Contact: Barry Kiel

Phase I: FA8650-08-M-2879

Phase II: FA8650-09-C-2009

The author would like to thank P. (Gokul) Gokulakrishnan, Michael Klassen, and Richard Roby for their technical assistance and guidance. The author would also like to acknowledge Maclain Holton for his assistance in setup of the experimental apparatus and Brent Turner for his support in the design, manufacturing, assembly, and operation of the flow reactor system. Dr. Tim Edwards of the Air Force Research Laboratory at Wright-Patterson Air Force Base is acknowledged and thanked for providing the jet fuel used in this study.

Table of Contents

TABLE OF CONTENTS.....	iii
LIST OF FIGURES	v
LIST OF TABLES	vii
NOMENCLATURE	viii
CHAPTER 1: INTRODUCTION.....	1
1.1 Problem Definition.....	1
1.2 Literature Review.....	3
1.2.1 Vitiated Combustion and the Effect of NO.....	3
1.2.2 Autoignition Delay Time	8
1.3 Thesis Objectives and Chapter Summary	10
CHAPTER 2: EXPERIMENTAL SETUP AND DESIGN	13
2.1 Phase I Screening Study - Experimental Setup and Apparatus	15
2.1.1 Overview of Apparatus	15
2.1.2 Vitiated Air Supply and Heating.....	17
2.1.3 Fuel Supply and Vaporization	19
2.1.4 Steam Generation.....	21
2.1.5 Mixing Section and Diffuser.....	22
2.1.6 Flow Reactor Tube and Furnace.....	24
2.1.7 Ignition Measurement System	24
2.1.8 Temperature Profiles.....	28
2.2 Phase I Screening Study - Experiment Procedure and Design	29
2.2.1 Experimental Procedure and Methodology	29
2.2.2 Design of Experiment	30
2.2.3 Non-Vitiated Air Comparison.....	33
2.3 Phase II Detailed Investigation - Experimental Setup and Apparatus.....	34
2.3.1 Overview of Apparatus	34
2.3.2 Extension of Flow Reactor Tube	37
2.3.3 Modifications to Mixing Section and Diffuser	39
2.3.4 Improvements and Additions to Heating System	42
2.3.5 Transition Piece and Vacuum System	45
2.3.6 Fuel Vaporization and Supply	46
2.3.7 Solenoid, PMT and Data Acquisition	47
2.3.8 Temperature Profiles.....	50

2.4	Phase II Detailed Investigation - Experimental Procedure and Design.....	53
2.4.1	Experimental Procedure.....	53
2.4.2	Experimental Variables and Test Matrix.....	54
2.4.3	Baseline Comparison.....	55
CHAPTER 3:	PHASE I SCREENING STUDY - RESULTS AND DISCUSSION.....	58
3.1	Table of Results.....	58
3.2	Significance of Main and Two-Factor Interaction Effects.....	58
3.3	Examination of Main Effects.....	65
3.3.1	Effect of O ₂	66
3.3.2	Effect of Temperature.....	68
3.3.3	Effect of NO.....	70
3.4	Interaction Effect of Temperature and NO.....	72
CHAPTER 4:	DETAILED STUDY - RESULTS AND DISCUSSION.....	76
4.1	Tables of Results.....	76
4.2	Atmospheric Results.....	77
4.2.1	Direct Effects of Temperature, O ₂ and NO on Ignition Delay Time of JP-8.....	78
4.2.2	Interaction of Temperature with NO.....	81
4.2.3	Interaction of O ₂ with NO.....	84
4.2.4	Empirical Ignition Delay Time Correlation.....	87
4.3	Sub-Atmospheric Results.....	94
CHAPTER 5:	SUMMARY, CONCLUSIONS, AND FUTURE WORK.....	98
5.1	Summary of Results.....	98
5.1.1	Summary of Screening Study Results.....	98
5.1.2	Summary of Detailed Investigation Results.....	99
5.2	Conclusions.....	101
5.3	Future Work.....	102
APPENDIX	105
A.1	Measurement Variability.....	105
A.2	Test Reproducibility.....	106
A.2.1	Phase I Screening Study.....	106
A.2.1	Phase II Detailed Investigation.....	107
A.3	Phase I Screening Study Test and Effects Matrices.....	109
A.4	Phase II Detailed Investigation Test Matrices.....	114
REFERENCES	118

List of Figures

Figure 2–1:	Flow reactor apparatus used for screening study.....	16
Figure 2–2:	Flow diagram for Phase I.....	17
Figure 2–3:	Fuel and vitiated air heating system for initial screening study.....	18
Figure 2–4:	Fuel vaporizer diagram for screening study.....	20
Figure 2–5:	Vaporizer and solenoid valve schematic for screening study.....	21
Figure 2–6:	Flow reactor mixing section for screening study.....	23
Figure 2–7:	Radial species profiles of CO ₂ (a) and O ₂ (b) at 3 axial locations within the test section.....	24
Figure 2–8:	Solenoid and PMT signals CH* chemiluminescence measurements.	25
Figure 2–9:	Experimental and theoretical ignition delay time correction using prototype comparison mixtures of <i>n</i> -heptane/air	28
Figure 2–10:	Test section temperature profiles for screening study.	29
Figure 2–11:	Box-Behnken design for 7 variables.[51]	32
Figure 2–12:	Comparison of non-vitiated JP-8 IDT at atmospheric pressures to previous studies of Gokulakrishnan et al. [4][41] and Freeman & Lefebvre [39].	34
Figure 2–13:	Flow diagram for Phase II.....	35
Figure 2–14:	Flow reactor apparatus used for detailed phase experiments.....	36
Figure 2–15:	Extended flow reactor diagram and temperature capacities.	39
Figure 2–16:	Modified mixing section and diffuser.....	41
Figure 2–17:	Alignment of diffuser T/Cs.....	42
Figure 2–18:	Axial locations of T/C's in multipoint probe.....	43
Figure 2–19:	Fuel vaporizer, N ₂ bypass and solenoid valve schematic for detailed investigation.....	45
Figure 2–20:	Diagram of exhaust and vacuum transition piece.	46
Figure 2–21:	Diagram of fuel vaporizer used for detailed investigation.....	47
Figure 2–22:	Solenoid and PMT traces for OH* chemiluminescence traces.....	49
Figure 2–23:	Atmospheric test section temperature profiles for detailed study at various temperature settings.	51
Figure 2–24:	Sub-atmospheric test section temperature profiles for detailed study at various temperature settings.	52

Figure 2–25:	Comparison of atmospheric JP-8 IDT from detailed investigation to jet fuel experimental IDT data from Gokulakrishnan et. al. [4][41] and Freeman & Lefebvre [39]	55
Figure 2–26:	Comparison of atmospheric JP-8 IDT to atmospheric <i>n</i> -decane IDT data.....	56
Figure 3–1:	Main effects of experimental variables on ignition delay time of JP-8	60
Figure 3–2:	Normalized main factor and two-factor interaction effects of experimental design variables based on ignition delay time.	62
Figure 3–3:	Average IDT for each main factor of all tests for a given variable ranking.	64
Figure 3–4:	Average % change in IDT from -1 ranking of each main factor	65
Figure 3–5:	Calculated adiabatic flame temperature of Jet-A(C ₁₂ H ₂₃)/vitiated air	68
Figure 3–6:	Comparison of the averaged main, combined and two-factor interaction effect of temperature and X_{NO} . -1, 0, & +1 values for temperature and X_{NO} are	73
Figure 3–7:	Comparison of the averaged effects of temperature and X_{NO}	75
Figure 4–1:	Atmospheric ignition delay time results of JP-8 and vitiated air comprised of 20% O ₂ and 80% N ₂	77
Figure 4–2:	Atmospheric ignition delay time results of JP-8 and vitiated air comprised of 12% O ₂ and 88% N ₂	78
Figure 4–3:	Comparison of current and previous experimental IDT of JP-8 4177 to surrogate model prediction[4][41].	79
Figure 4–4:	Comparison of temperature-NO interaction on reduction of atmospheric JP-8 ignition and vitiated air comprised of 20% O ₂ and 80% N ₂	82
Figure 4–5:	Comparison of temperature-NO interaction on reduction of atmospheric JP-8 ignition and vitiated air comprised of 12% O ₂ and 88% N ₂	83
Figure 4–6:	Comparison of O ₂ -NO interaction on reduction of atmospheric JP-8 ignition and vitiated air at 850 K and 900 K.	86
Figure 4–7:	Atmospheric ignition delay time results of JP-8 and vitiated air comprised of 20% O ₂ and 80% N ₂ with emirical predictions using eq. 11.	90
Figure 4–8:	Atmospheric ignition delay time results of JP-8 and vitiated air comprised of 12% O ₂ and 88% N ₂ with emirical predictions using eq. 11.	90
Figure 4–9:	Arrhenius plot for atmospheric ignition delay time results of JP-8 and vitiated air comprised of 20% O ₂ and 80% N ₂ with emirical predictions.	92
Figure 4–10:	Sub-atmospheric ignition delay time results of JP-8 and vitiated air comprised of 20% O ₂ /80% N ₂ and 12%O ₂ /88% N ₂	95
Figure 4–11:	Comparison of the relative reduction of JP-8 ignition delay time from the 0 ppm NO condition along 900 K temperature test cases at 0.5 and 1.0 atm	96

List of Tables

Table 1-1:	Low Pressure Vitiated Combustion Envelope	2
Table 2-1:	JP-8 Fuel Properties	15
Table 2-2:	Screening Study Design Variables and Test Values.....	33
Table 3-1:	Example 8-Test Block.....	66
Table 3-2:	Phase I Tests 33-40	66
Table 3-3:	Phase I Tests 41-48	67
Table 3-4:	Phase I Tests 49-56	67
Table 3-5:	Phase I Tests 9-16	69
Table 3-6:	Phase I Tests 25-32	69
Table 3-7:	Phase I Tests 41-48	69
Table 3-8:	Phase I Tests 17-24	70
Table 3-9:	Phase I Tests 9-16	71
Table 3-10:	Phase I Tests 33-40	71
Table 4-1:	Goodness of Emperical Model Fits at 1 atm.....	89
Table A-1:	Measurement Variability - Detailed Investigation.....	108
Table A-2:	Screening Study Test Matrix and Results.....	109
Table A-3:	Matrix of Main Effects.....	111
Table A-4:	Matrix of Two-Factor Interaction Effects.....	112
Table A-5:	Detailed Investigation Atmospheric Test Matrix - Nominal Values	114
Table A-6:	Results for Atmospheric Tests of JP-8 and O ₂ /N ₂ /NO Mixtures.....	115
Table A-7:	Results for Sub-atmospheric Tests of JP-8 and O ₂ /N ₂ /NO Mixtures	116
Table A-8:	Results for all Tests of <i>n</i> -Decane (<i>n</i> -C ₁₀) and O ₂ /N ₂ /NO Mixtures	117

Nomenclature

x	Design Variable
X_i	Mole or Volume Fraction of Specie i [vol %] or [ppm]
τ_{exp}	Measured Experimental Ignition Delay Time [ms] or [s]
τ_{ig}	Ignition Delay Time (IDT) [ms] or [s]
v_{m_k}	Design Level Value (-1, 0 or +1) of Variable m for Test k
E_m	Main Effect of Design Variable m
$E_m E_n$	Interaction Effect of Design Variables m and n
R	Universal Gas Constant [cal/mol-K]
E	Activation Energy of Ignition Process [cal/mol]
T	Temperature [K]
Φ	Equivalence Ratio: $(X_{\text{fuel}}/X_{\text{oxidizer}})/(X_{\text{fuel}}/X_{\text{oxidizer}})_{\text{stoich}}$

Chapter 1: Introduction

1.1 Problem Definition

The word “vitate” finds its origin in the Latin verb *vitiare*, meaning to spoil or corrupt [1]. In scientific and medical fields, vitiated air is defined as air containing reduced amounts of oxygen. In the field of combustion, “vitiating combustion” typically refers to any combustion processes occurring in the presence vitiated air, defined as an oxidizer stream with oxygen levels less than that of normal air ($X_{O_2} < 21 \text{ vol\%}$) and/or containing other products of combustion including CO_2 , CO , H_2O , and NO_x . Vitiated conditions are often the result of flue or exhaust gas recirculation (EGR) into a fresh air stream, which can found in many practical combustion system including gas turbine combustors, automobile engines, and furnaces to reduce emissions and/or improve efficiency [2]. Vitiated combustion is also used in aircraft engines where fuel is injected into the turbine exhaust at low pressures to increase engine thrust [3].

The significance of individual vitiated air components on fuel oxidation is not fully understood. Currently, there exist several detailed kinetic models for kerosene based jet fuel and gasoline oxidation including those by Gokulakrishnan et al. [4], Curran et al. [5], Dooley et. al. [6], Dagaut et al. [7] and the CRECK modeling group [8]-[10]. However, there is considerable uncertainty in these mechanisms in terms of the kinetic effects of vitiated air on combustion as they have not been tested against experimental data sets, specifically regarding the effect of vitiated air components on the ignition of jet fuels at low pressures.

To develop an accurate chemical kinetic model for vitiated conditions, an experimental database of auto-ignition delay time under various temperatures, equivalence

ratios and vitiated air compositions is necessary to provide data for model comparison and validation. In general, kinetic models for kerosene-type fuels have thus far been validated and optimized against experimental data that were obtained using “normal” air (21% O₂) at higher pressures. The kinetic, transport and thermodynamic effects of typical vitiated species including diluent effects, third-body collision efficiencies of CO₂ and H₂O, and kinetic enhancement or inhibition of oxidation due to the presence of NO_x species in vitiated air are thought to play a role on the oxidation and ignition of jet fuels at low pressures.

Based on combustor design ranges found in the literature [3] and calculation of typical emissions for gas turbines and primary combustors the following envelope of experimental variables was determined:

Table 1-1: Low Pressure Vitiated Combustion Envelope

Variable		Min	Max
Temperature	[K]	700	1200
Pressure	[atm]	0.25	4
ϕ		lean	rich
X_{O_2}	[vol %]	12	18
X_{CO_2}	[vol %]	5	10
X_{H_2O}	[vol %]	5	10
X_{CO}	[vol %]	0.01	0.2
X_{NOX}	[ppmv]	100	1000

Therefore, the objective of this effort is to investigate the role of various vitiated combustion components and determine the significance that they have on jet fuel (JP-8) oxidation by acquiring atmospheric and sub-atmospheric pressure ignition delay time data at intermediate to high temperatures using vitiated air comprised of varying compositions of O₂, CO₂, H₂O, CO, and NO in N₂.

1.2 Literature Review

Examination of previously published works for this study consisted of two major areas: assessment of previous investigations into the effect of vitiated oxidizer components on the oxidation of hydrocarbons and an examination of methods used to measure the autoignition delay time of liquid hydrocarbons at low pressures. A review of the relevant literature for each of these areas is discussed in the following sections.

1.2.1 Vitiated Combustion and the Effect of NO

There are few reported works in the literature that investigate the effect of vitiated air compositions on jet fuel oxidation at aircraft engine relevant conditions. Some data was found in the literature examining the effects of H₂O, CO₂ and CO on fuel oxidation and ignition [11][12] however the primary vitiated species found to affect ignition and oxidation of hydrocarbons are nitrogen oxide species (NO_x). The effect of NO_x on smaller hydrocarbons, e.g. methane and butane, and hydrogen ignition [13]-[16] and oxidation [17]-[21] has been studied extensively over the years.

A study by Seiser et al. [11] investigated the influence of water vapor on the extinction and ignition of hydrogen and methane flames. The addition of up to 15 vol% H₂O to the reactant stream for both premixed and nonpremixed flames made the flames easier to extinguish due to both chemical and thermodynamic influences. In the case of ignition, nonpremixed H₂ flames were given initial reactant concentrations of H₂O up to 20 vol%. The study found that larger fractions of H₂O resulted in higher autoignition temperatures. Le Cong et al. [12] examined the effects of both CO and CO₂ from burnt gas recirculation on the oxidation of natural gas and natural gas/syngas mixtures through ignition delay, flame

structure, jet-stirred reactor (JSR), plug flow reactor (PFR) and shock tube measurements. The addition of 20% CO₂ was found to only slightly inhibit the oxidation of mixtures of CH₄/O₂/N₂ and CH₄/H₂/O₂/N₂ in JSR experiments at 1 atm and 10 atm. Experiments were also performed in the JSR at 1 atm with the addition of 0.4% CO in the reactant stream. The study found slight enhancement of the oxidation of the CH₄/H₂ fuel due to increased production of H atoms.

Significantly more data was found examining the effects of NO_x on fuel ignition and oxidation. Studies of the explosion and ignition behavior of H₂-O₂ and CH₄-O₂ mixtures in the presence of nitric oxides date back to the first half of the 20th century through the work of Thompson and Hinselwood [13] as well as Norrish and Wallace [14]. Dabora [15] investigated the effect of NO₂ on the ignition delay time of near-stoichiometric CH₄/air mixtures by varying the concentration of NO₂ in the reactant stream up to 2 vol%. It was found that addition of 0.12% NO₂ and 1% to 2% NO₂ reduced the overall activation energy for ignition by 24% and 50% respectively. Slack and Grillo [16] examined the effect of NO_x on CH₄ ignition in a shock tube study at temperatures ranging from 1310 K to 1790 K and pressures of 1.8 atm to 3.6 atm.. It was found that NO₂ has a significant effect on reducing ignition time at these temperatures and pressures. For example, at 1600 K, a mixture of 4.8% CH₄ and 19.2% O₂ balanced in Ar had an ignition delay time of approximately 300 microseconds. When a portion of the bulk Ar diluent was replaced with 0.8% NO₂ and 3.4% NO₂, the ignition delay times reduced to approximately 100 microseconds and 20 microseconds respectively.

Two studies by Bromly et al. [17][18] examined the sensitized oxidation of hydrocarbons and NO. In the first study, an isothermal, atmospheric flow reactor was used

for the experiments performed at 775 K to 975 K in which a mixture containing 440 ppm CH₄, 5% O₂ and a balance of N₂ was doped with initial concentrations of NO ranging up to 200 ppm. Increasing the initial concentration of NO was found to enhance oxidation up to 100 ppm at which point the consumption of CH₄ plateaued and then decreased slightly up to 200 ppm. The second study investigated the sensitized oxidation of NO (0.01 ppm to 200 ppm) and *n*-butane (50 ppm to 600 ppm) at atmospheric pressure and temperatures from 650 K to 720 K. Results of this study showed that low concentrations of NO promote the oxidation of *n*-butane, while low concentrations of *n*-butane mutually promote the conversion of NO to NO₂. Dagaut and Nicolle [19] performed a similar experimental and modeling study examining effect of exhaust gas on fuel combustion through the mutually sensitized oxidation of NO and methane. Results of this study show that at both 1 atm and 10 atm the presence of 200 ppm NO enhanced oxidization and reduced the temperature required for fuel oxidization for a given residence time.

Bendtsen et al. [20] investigated the oxidization of methane in the presence of NO and NO₂ in an isothermal plug flow reactor from 750 K to 1250 K in which, for the same residence time, fuel oxidation occurred at lower temperatures when NO was added to the reactants. More recently, Konnov et al.[21] performed a study in which a mixture of CH₄ (1.77%) + O₂ (0.89%) and N₂ (balance) was reacted at 832 K at 1.2 bar in a tubular flow reactor with an initial concentration of NO that was varied from 0 to 380 ppm. Results show that the addition of NO up to approximately 200 ppm promotes the oxidation of CH₄, while 200 to 380 ppm NO inhibits the oxidization of CH₄.

While the examination of the effect of NO_x on the oxidation of smaller hydrocarbons, primarily methane, is extensive, there are much fewer data sets available for larger

hydrocarbons relevant to jet fuel and even less that examine actual multi-component fuel blends relevant to kerosene, JP-8, or even gasoline oxidation. The studies in the literature primarily investigated the effect that NO_x has on oxidation of hydrocarbons through speciation and emission examinations in very diluted fuel/oxidizer mixtures [22]-[26].

Moréac et al. [22] investigated the interaction of NO and higher order hydrocarbons in a JSR at 10 atmospheres. In this work, the effect of NO on the oxidation of *n*-heptane, *iso*-octane, methanol, and toluene was examined between 600 K and 1200 K. It was observed that NO inhibited the oxidation of *n*-heptane in the low-temperature regime between 550 K and 700 K, while it enhanced the oxidation in intermediate and high temperature regions. On the other hand, NO promoted the oxidation of *iso*-octane and toluene in all temperature regions above 600 K at 10 atm. However, Moréac et al. [23] also found that NO addition had little effect on toluene oxidation in similar experiments at 1 atm. The measurements of NO and NO_2 indicate that the reaction pathways of NO-sensitized oxidation of hydrocarbons differ depending on the temperature regime [22]. These findings have implications for jet fuels and their surrogate mixtures for kinetic modeling which consist of significant proportions of *n*-alkanes, *iso*-alkanes, and aromatics [4][27]-[29].

A subsequent study in the same reactor conditions as the Moréac work was performed by Dubreuil et al. [24]. This study examined the effect of NO on the oxidation of binary mixtures of *n*-heptane/*iso*-octane and *n*-heptane/toluene, common gasoline surrogate fuels. For the fuel mixture of *n*-heptane and *iso*-octane, the addition of 50 ppm NO and 200 ppm NO enhanced the oxidation of *iso*-octane at nearly all temperatures within the NTC region (~ 625 K - 800 K) and above. For temperatures at and below the transition point from the NTC to low temperature regime, the addition of NO was found to inhibit *iso*-octane oxidation.

Both the enhancement and inhibition of *iso*-octane oxidation was stronger when the higher concentration of NO was added to the reactant stream. In the case of the *n*-heptane/toluene mixture, the addition of 50 ppm NO enhanced oxidation of both fuels at temperatures above the NTC regime and inhibited oxidation for all temperatures below. A similar study examining the effect of NO on a highly diluted gasoline surrogate (*n*-heptane/toluene) was performed by Anderlohr et al. [25]. This study also found that the presence of NO inhibits oxidation in the low temperature oxidation regime (600 to 800 K), while enhancing the oxidation in the high temperature oxidation regime (800 to 1000 K).

A study by Kowalski [26] examined the effect of NO on diluted mixtures of actual gasoline blends as well as an *iso*-octane/*n*-heptane blend with an 87 octane rating in a variable pressure plug flow reactor at 6 atm. Based on the product mole fractions of O₂, the addition of 50 ppm to the reactant stream had the same effect on a real gasoline blend as it did on the surrogate blend. At lower temperatures in the NTC regime, the presence of NO inhibits oxidation however at higher temperatures it enhances it based on smaller product fractions of O₂.

Each of these experiments examining the effect of NO on gasoline and jet-fuel relevant hydrocarbons utilized heavily diluted mixtures (0.1 mol% to 0.9 mole% of fuel in the reactant stream) to limit the effect of heat release on speciation measurements. They were also performed at high pressures more relevant to internal combustion engines and HCCI systems rather than low pressure combustion devices that are of interest in the current study. This data provides insight into the oxidation effects of NO on hydrocarbons relevant to jet fuels but it does not examine the effects on fuel mixture concentrations relevant to low pressure vitiated combustion and ignition.

Overall, the literature describes the effect of NO_x on the oxidation of hydrocarbon relevant to jet fuel as one that enhances in the intermediate to high temperature regime and inhibits oxidation through the NTC region and the low temperature regime. This is true not only for primary surrogate fuel components but for surrogate mixtures and actual fuel (gasoline) blends as well. Studies that examined the effect of NO_x and other vitiated or EGR components play on the actual ignition of jet fuels were not found by the author.

While the current published literature does provide valuable data and insight into the effect that vitiated air species have on fuel oxidation and in some cases ignition, there are gaps in the available data that need to be filled to better understand the effects of vitiation on the ignition of jet fuels. Two major pieces of data are missing. The first is ignition data under the conditions provided in **Table 1-1** that is critical to develop a well validated kinetic model. The second is an analysis of the significance of the major vitiated components (temperature, Φ , and composition) when compared to one another. By only looking at single or perhaps two components at a time, the overall scope of the driving factors of vitiated combustion are not fully understood. In order to find this information and conduct autoignition experimentation, methods to acquire the necessary ignition data were investigated as well.

1.2.2 Autoignition Delay Time

For understanding the autoignition delay time and oxidation characteristics of liquid fuels, ignition delay measurements have been made using varying apparatuses including: constant volume bombs [30][31], rapid compression machines (RCMs) [32][33], shock tubes [34]-[38], and flow reactors [4][39]-[41]. The references listed here are just a representative view on the vast quantity of literature on this topic.

Ignition measurements using the constant volume bomb approach date back to the first half of the last century through the work of Starkman [30] who investigated the ignition delay time of diesel fuels in lower temperature regions for engine data comparisons. The work of Geir [31] used a constant volume bomb to investigate the ignition and combustion processes of liquid fuels to develop correlations between fuel composition and ignition properties. Rapid compression machines have also been used to investigate ignition and knocking properties of liquid fuels. Granata et al. [32] used ignition delay time data from RCMs for the validation of cyclohexane models at low temperatures. Würmel et al. [33] examined the effect that various diluents (He, Ar, Xe, and N₂) have on the ignition delay time of 2,3-dimethylpentane, a *n*-heptane isomer, due to thermodynamic effects.

Shock tubes have been used extensively to measure the ignition delay time of liquid fuels, especially at elevated pressures. Mullaney [34] began using shock tubes to look at the autoignition of liquid fuel sprays in 1958. In 1975, Myasaka and Mizutani [35] attempted to obtain pure ignition delay time data of cetane (hexadecane) and tetralin free from the atomization and mixing processes. Ciezki and Adomeit [36] investigated the autoignition of *n*-heptane/air mixtures at elevated pressures relevant to engine conditions. Using high pressure shock tube facilities, Dean et al. [37] and Vasu et al. [38] measured the ignition delay time of Jet-A and JP-8 respectively in both the high and low temperature regions.

The use of flow reactors to measure ignition delay time at both low and high pressures can also be found in the literature. Freeman and Lefebvre [39] as well as Spadaccini and TeVelde [40] measured ignition delay time of Jet-A using their respective flow reactor apparatuses at atmospheric and high-pressure (10-30 atm) conditions. The ignition delay time measurements of JP-7, JP-8, and S-8 made by Gokulakrishnan et al.

[4][41] were performed using an atmospheric flow reactor to measure ignition delay time in the intermediate and high temperature region (800 K - 900 K) to aid in the development of surrogate models for kerosene based fuels.

While these ignition measurement techniques all provide valid data regarding the autoignition of liquid fuels, the use of the flow reactor method was found to be most appropriate for the scope of this study based on its ability to measure ignition at conditions relevant to low-pressure vitiated combustion processes. Therefore, the apparatus used by Gokulakrishnan et al. [4][41] serves as the base apparatus used for ignition delay measurements made in this study.

Two major conclusions can be drawn from a review of current published literature:

1. Given the lack of data currently available for ignition of undiluted jet fuel mixtures and the effect that vitiated products, especially NO, play on oxidation, ignition delay time measurements of jet fuel ignition, with vitiated oxidizers, and at low pressures are required.
2. The best method to make the necessary ignition delay time measurements is through the use of a flow reactor due to the ability to measure ignition at low pressures and across the range of desired temperatures and oxidizer compositions.

Parts of the work presented in this thesis have been previously published in two papers by Fuller et al. [42][43].

1.3 Thesis Objectives and Chapter Summary

This goal of this study is to correlate ignition delay time of jet fuel on several of the

vitiated combustion variables relevant to low pressure applications, e.g. atmospheric and sub-atmospheric EGR combustion devices, namely temperature, pressure, equivalence ratio (Φ) and oxidizer composition. To accomplish this task, the study has been broken down into two phases with the following objectives.

- **Phase I - Screening Study**

- Using an existing experimental flow reactor apparatus [4][41], measure the ignition delay time of JP-8 at atmospheric pressure with varying equivalence ratios and oxidizer compositions relevant to vitiated combustion due to exhaust gas recirculation.
- Determine the significance of seven (7) design variables (temperature, Φ , X_{O_2} , X_{CO_2} , X_{CO} , X_{H_2O} , and X_{NO}) at constant pressure through the use of design of experiment (DOE) and response surface methodology techniques.

- **Phase II - Detailed Investigation**

- Apply findings of Phase I to determine which variables should be studied in greater detail.
- Modify the flow reactor apparatus to measure a greater range of experimental conditions and improve upon methods used in Phase I.
- Investigate the main and interaction effects of significant experimental design variables across expanded ranges compared to those in Phase I as well as pressure variation.
- Develop an empirical model that predicts ignition delay time within the experimental envelope that provides insight into the physical and chemical processes effecting ignition delay.

This thesis has been divided into several chapters that provide detailed explanation, analysis, and results. Chapter 2 is divided into several sections that describe the experimental setup and design for both phases of this study. The sections on experimental set up describe the flow reactor apparatus for each experimental phase in detail, including the reasons for the multiple modifications that were made to transition from Phase I to the Phase II. The experimental design sections describe the procedures used to acquire ignition delay time data as well as the experimental design technique used to develop efficient test matrices for the screening study.

Chapter 3 discusses the results of the Phase I screening portion of this study, including the experimental findings as well as the analysis of the main and two-factor interaction effects of the 7 design variables: temperature, Φ , O_2 , CO_2 , CO , H_2O , and NO . The effects are analyzed using a cumulative probability method to determine their relative significance to one another within the test envelope.

Chapter 4 discusses the results of the Phase II detailed investigation of the variables found significant in Phase I: temperature, O_2 , and NO . The results are also broken down into atmospheric and sub-atmospheric cases. The direct effect of each design variable, as well as the interaction of temperature and NO and O_2 and NO are also examined. This chapter details the development of an empirical correlation to predict the ignition delay time of JP-8 within the atmospheric experimental envelope of this study. The recorded ignition delay time data for all test conditions in this study can be found in the Appendix.

Chapter 5 summarizes the results of both Phase I and Phase II of this study and also provides conclusions based on the overall findings and scope of this effort. Avenues for future investigation are also examined in this section.

Chapter 2: Experimental Setup and Design

This study aims to determine the level of significance that major components of vitiated combustion have on autoignition of jet fuel and more specifically the effect of the significant variables. In practical combustors, vitiated combustion is typically due to the mixing of fresh air with the exhaust gas from another combustor. This can also result in fuel-oxidizer mixtures that fall in the intermediate to high temperature regime for ignition. The vitiated air species of interest in this study are: O₂, CO₂, CO, H₂O, and NO_x in a bulk diluent of N₂. The concentration of O₂ in the oxidizer was varied from 12 vol% to 21 vol %. The oxidizer concentrations of CO₂ and H₂O were varied up to 6 vol% and up to 0.2 vol% for CO. The oxidizer concentration of NO_x, supplied as NO in this study, was varied from 0 to 1000 ppm. A multi-component jet fuel, JP-8, was used at the primary test fuel with equivalence ratios, Φ , ranging from 0.5 to 1.5. Based on the combustor operating envelope shown in **Table 1-1**, the pressure and temperature ranges examined were 0.5 atm to 1.0 atm and 700 K to 1125 K respectively.

The ignition delay time of JP-8 was measured through the use of two separate but related flow reactors in this ignition study. The apparatus used in Phase I, the screening study, was nearly identical to the reactor used by both Gokulakrishnan et al. [4][41] and Holton et al. [44]. It was comprised of an atmospheric tubular reaction zone made out of alumina (aluminum oxide – Al₂O₃) that was heated to a steady temperature ranging from 950 K to 1125 K. The head end mixing zone consisted of a radial pre-mixer and a stainless steel expanding duct designed to supply a homogenous, laminar flow to the entrance of the test section. Ignition events were measured using a photomultiplier tube (PMT) equipped with a narrow band pass filter to identify CH* emissions.

In Phase II, the detailed investigation, modifications were made to the initial flow reactor apparatus to reduce reactor temperature, improve heating uniformity, improve mixing, and allow for sub-atmospheric conditions. In order to accommodate these expanded conditions, the modifications included: extension of the overall length of the reactor to provide a longer residence time for lower temperature and sub-atmospheric tests; modification of the injection section to improve mixing of the fuel and oxidizer; and replacement of the narrow band pass filter to identify OH* rather than CH* emissions during ignition events in order to reduce signal noise. Both setups will be discussed below.

The fuel and oxidizer components were the same for both phases of testing. Flow reactor ignition measurements were made for three fuels: *n*-heptane, *n*-decane, and JP-8. The *n*-alkanes were used for mixing and transport time correlations as well as comparison data due to their similarity to typical surrogate components of typical kerosene type fuels. The jet fuel used in these experiments was a JP-8 blend obtained from the Air Force Research Laboratory (AFRL) in Dayton, OH, AFRL ID# 02-POSF-4177. Throughout the remainder of this report, this fuel is referenced as JP-8 or JP-8 4177. **Table 2-1** lists the chemical properties of JP-8 02-POSF-4177 acquired through standardized ASTM testing for aviation fuels [45][46]. The vitiated air oxidizer was supplied to the flow reactor by blending individual gaseous components to match the prescribed test conditions. Air was supplied to the system via an industrial compressor. Oxidizer species N₂, O₂, and CO₂, were supplied as pure gases from high pressure cylinders. For test cases including CO and/or NO, these components were supplied via high pressure cylinders from CO/N₂ and NO/N₂ mixtures respectively. For test cases including H₂O in the oxidizer, tap water was filtered for chlorine and particulate removal then vaporized and supplied as steam to the system.

Table 2-1: JP-8 Fuel Properties

Fuel Type WPAFB ID		JP-8 02-POSF-4177	
ASTM D2425 [45]	vol %	ASTM D6379 [46]	vol %
(n + iso) Alkanes	51.3	Monoaromatics	16.1
Cycloalkanes	18	Diaromatics	1.2
Dicycloalkanes	11.8	Total Aromatics	17.3
Tricycloalkanes	1.6	Total Saturates	82.7
Alkylbenzenes	9.3		
Indan and Tetralins	6.7	API gravity	42.4
Indenes C _n H _{2n-10}	<0.2	Specific gravity	0.814
Naphthalene	<0.2	Avg. Boiling Pt. [C]	218
Naphthalenes	1	H mass %	13.7
Acenaphthenes	<0.2	H/C atomic ratio	1.9
Acenaphthylenes	<0.2	Molecular Weight	162
Tricyclic Aromatics	<0.2		
Total	100		

2.1 Phase I Screening Study - Experimental Setup and Apparatus

2.1.1 Overview of Apparatus

The first phase of experimentation used a slightly modified version of the flow reactor apparatus used by Gokulakrishnan et al.[4][41] and Holton et al. [44]. **Figure 2–1** displays the apparatus as used in the initial screening portion of this study. A basic flow and equipment diagram of the apparatus is shown in **Figure 2–2**. The system was designed to be a flow reactor heated in ramped and steady temperature sections in order to test ignition delay from 925 K to 1125 K. Liquid fuel was vaporized and radially injected into a vitiated air stream prior to entering an alumina flow reactor tube as a homogenous plug. Ignition delay time was measured using a photomultiplier tube and corresponding narrow band filter to detect the presence of CH* visible during an ignition event.

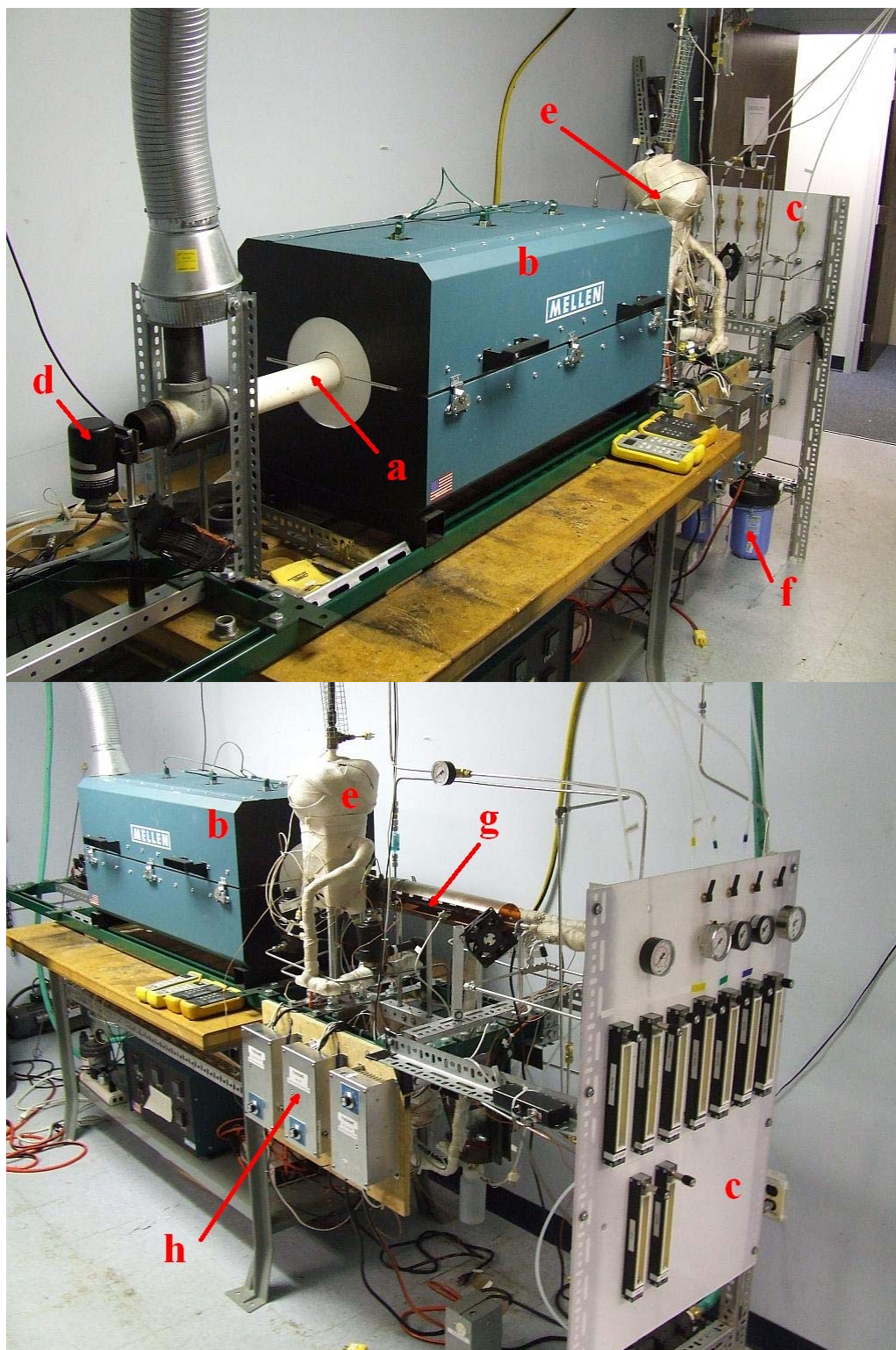


Figure 2-1: Flow reactor apparatus used for screening study.
Key: **a**) - flow reactor tube, **b**) tube furnace, **c**) flow control panel,
d) photomultiplier tube, **e**) fuel vaporizer, **f**) water filtration,
g) main vitiated air heater, and **h**) heater controllers

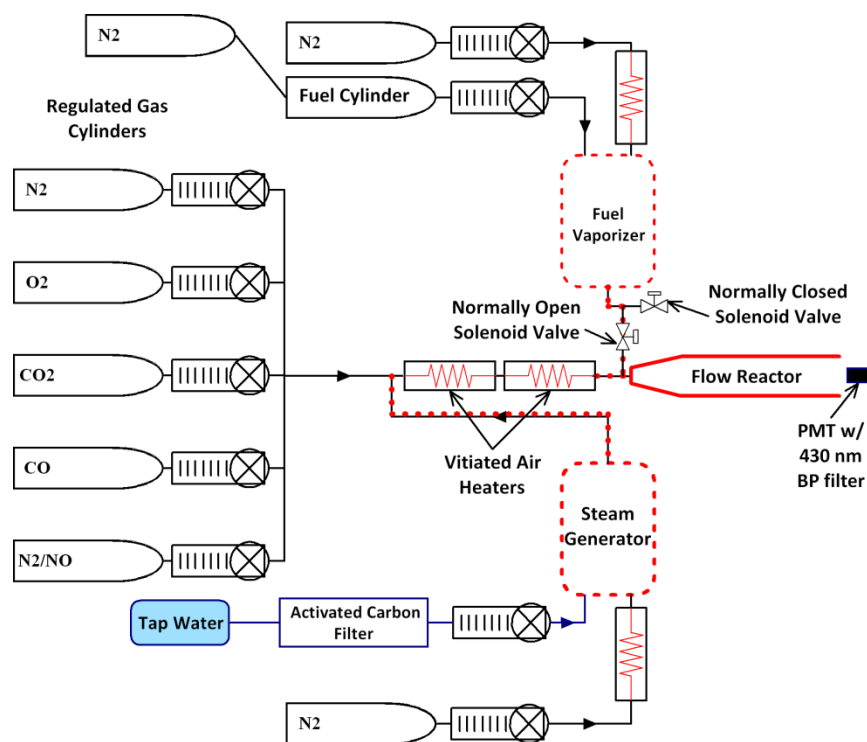


Figure 2–2: Flow diagram for Phase I. Red lines represent heated sections.

2.1.2 Vitiated Air Supply and Heating

The screening study consisted of 48 different vitiated air mixtures comprised of O₂, CO₂, CO, NO and H₂O in a bulk diluent of N₂. The number of mixture combinations as well as the inclusion of steam necessitated a gaseous control and manifold system that allowed for each component to be individually supplied to the vitiated air heater. **Figure 2–2** shows the flow paths of the vitiated air components and vaporized fuel/diluent stream. Each vitiated air component was metered using a Matheson 600 series rotameter. The dry components (N₂, O₂, CO₂, CO and NO) were mixed downstream of their rotameters and sent to the vitiated air manifold. Explanation of the rotameter calibration and variability is provided in the Appendix. The steam was metered as liquid water then vaporized with an N₂ dilution flow and superheated to 725 K. The superheated N₂-H₂O stream was mixed with the other gaseous components and sent through inline air heaters to be heated to 1000 K prior to

mixing with the fuel.

The bulk diluent, N_2 , was the largest component of each of the vitiated air mixtures and was used as a carrier gas for both the steam and fuel vaporizers. Three separate N_2 streams were metered and sent to the fuel vaporizer, steam generator, and dry gas manifold respectively as needed for a given test. For each test, the overall vitiated air flowrate of the system was 100 slpm. Included in the total vitiated air flow was 20 slpm of N_2 that was diverted through the fuel vaporization circuit to aid in fuel injection. This flow was heated separately from the remaining vitiated air prior to entrance to the fuel vaporizer.

Each gaseous component was mixed in a tubing manifold prior to entering a customized inline gas heater assembly. The vitiated air heater consisted of two separate 3/8" 1.6 kW Osram-Sylvania inline pipe heaters (P/N 038821) aligned in series. Two heaters were used to boost gas temperatures to a maximum of 1000 K and reduce the temperature gradient between the mixing section and steady temperature test section of the flow reactor. The heaters assembled as part of the flow reactor apparatus are shown in **Figure 2–3**.

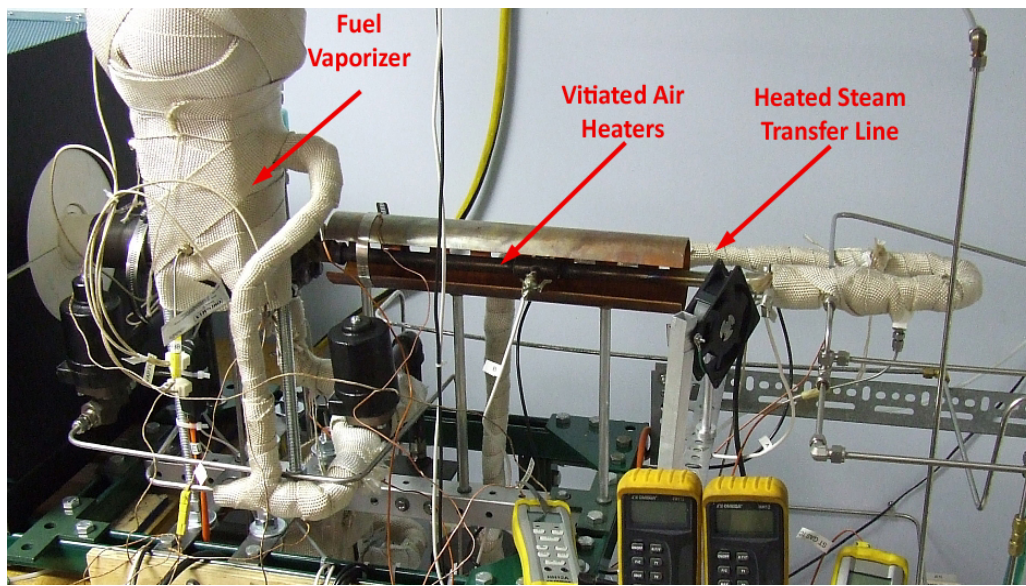


Figure 2–3: Fuel and vitiated air heating system for initial screening study.

2.1.3 Fuel Supply and Vaporization

Two fuels were used in this study: JP-8 as the main test fuel and *n*-heptane for calibration. Identical methods were used to control, vaporize and inject each fuel into the flow reactor system. To examine the autoignition of liquid fuel from a vapor state, fuel was vaporized, in a manner similar to Gokulakrishnan's work [4], prior to injection into the flow reactor mixing section. Liquid fuel was supplied via pressurized cylinders and controlled using rotameters individually calibrated for JP-8 and *n*-heptane. The liquid flowrate of JP-8 varied from 3.7 sccm to 15.5 sccm ($5.0\text{E-}05$ kg/s to $2.1\text{E-}04$ kg/s). The liquid fuel was injected into a heated vaporizer and mixed with a heated N₂ stream that served as a carrier gas. For all tests, the flowrate of the N₂ carrier gas was set to 20 slpm. Rather than maintaining a constant N₂/fuel ratio, the N₂ flowrate was kept constant to normalize the flowrate through the fuel injectors as well as the vitiated air heater. By doing this, fuel injection dynamics were relatively constant between tests. Also, the constant flowrate of 80 slpm through the flow reactor between tests maintained temperature uniformity in the test section.

A diagram of the fuel vaporizer is shown in **Figure 2–4**. The unheated liquid fuel was injected from the bottom of the heated vaporizer through a bed of heated stainless steel balls, each one 6.4 mm in diameter. The N₂ was injected directly from an inline pipe heater at the top of the vaporizer. N₂ was injected at 750 K and the vaporizer walls were heated to 675 K. The transfer line from the vaporizer to the mixing section was heated to 650 K. Fuel and N₂ passed through the vaporizer for several minutes prior to injection into the mixing section to ensure steady output concentrations for each test. Ignition measurements were made to determine the minimum flow time of fuel through the vaporizer required to fall

within the overall repeatability error of the flow reactor system. Throughout the screening study, no fuel coking was observed in the vaporizer or lines.

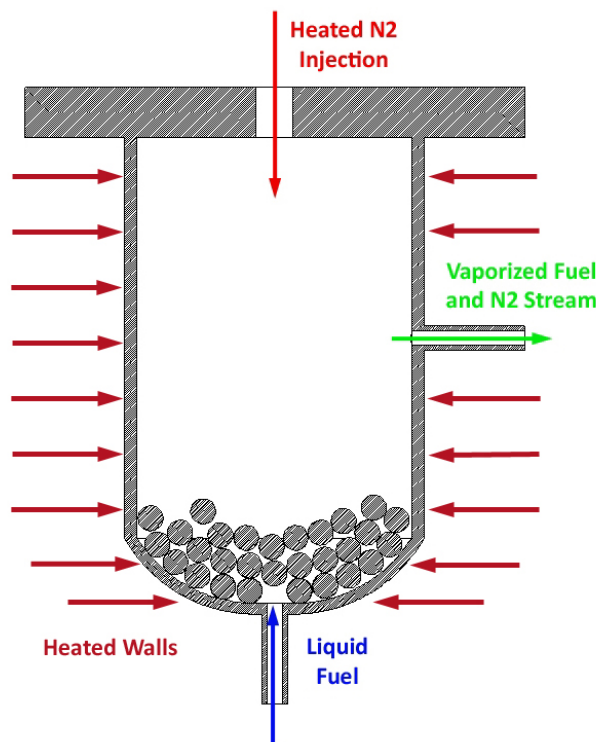


Figure 2–4: Fuel vaporizer diagram for screening study.

Unlike other flow reactors that are used to measure steady state flows, ignition measurements made in a flow reactor require an intermittent injection of fuel. To quickly inject and then stop the flow of fuel into the flow reactor, the automated solenoid valve system shown in **Figure 2–5** was used. The fuel injection system was comprised of two solenoid valves: a normally closed valve on the transfer line going to the mixing section of the flow reactor and a normally open valve located on the transfer line to the exhaust hood and condenser. Between ignition tests, the vaporized fuel flowed through the normally open valve to a condenser where the N_2 vented to an exhaust hood while the fuel was recondensed and collected for disposal. At the time of an ignition test, both valves were energized thereby

closing the line to the condenser and opening the line to the mixing section. When an ignition test was completed, the valves were de-energized, reverting fuel flow back to the exhaust path. The time at which the valves were initially energized was logged in a data acquisition system and tagged as the initial time for an individual ignition test.

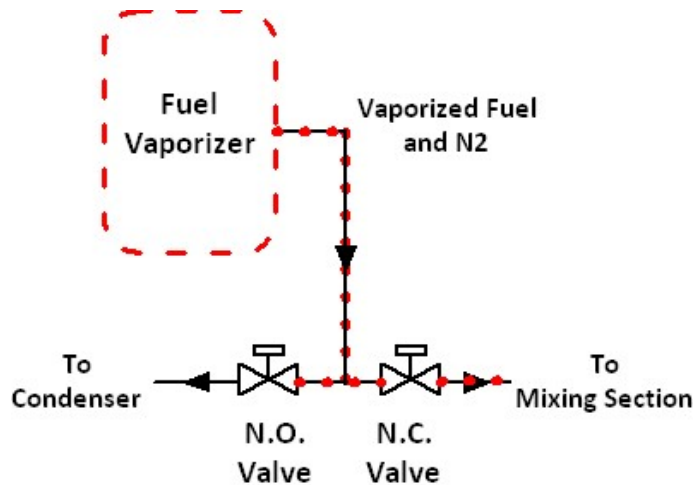


Figure 2–5: Vaporizer and solenoid valve schematic for screening study. A combination of normally open (N.O.) and normally closed (N.C.) valves was used to direct the flow.

2.1.4 Steam Generation

The inclusion of H₂O as a component of vitiated combustion and an experimental variable required steam to be supplied to the vitiated oxidizer stream. Steam was generated by vaporizing tap water that had undergone activated carbon filtration to reduce chlorine levels by at least 90% followed by particulate filtration. The water flowrate (2.2 to 4.4 liquid sccm) was controlled using a Matheson 600 series rotameter.

Liquid water was injected into a vaporizer with wall temperatures of 725 K along with a pre-heated N₂ stream heated to 700 K that served as a carrier gas. The molar dilution ratio of N₂ to H₂O varied between 4.0 and 5.0 depending on the specific test case. The superheated steam/N₂ mixture was carried through a heated transfer line and injected into the

vitiated air manifold at 725 K. The H₂O/N₂ stream mixed with the dry gas components prior to entering the primary inline gas heaters. The temperature of the vitiated stream once the H₂O had been added was no less than 1.5 times the dew point temperature of the mixture for all test cases that involved H₂O. The flow path and apparatus for the steam line are shown in **Figure 2–2** and **Figure 2–3** respectively. The N₂ stream was preheated using an inline pipe heater while the vaporizer and transfer lines were heat traced with Samox heating tapes.

2.1.5 Mixing Section and Diffuser

The fuel and vitiated air were mixed in a stainless steel mixing section, shown in **Figure 2–6**, and then flowed through a custom expanding duct (diffuser) prior to entering the flow reactor test section. The inline pipe heater consisted of a spiraled heating element that acted to mix the vitiated air components prior to the mixing section. Upon entrance to the mixing section, the vitiated air was swirled inside an annular duct. Immediately downstream of the swirler, the fuel/N₂ mixture was injected radially from six injection orifices located on the outer wall of the duct. Prior to injection, the fuel/N₂ mixture was passed from the heated transfer line into an annular plenum to improve injection uniformity.

The fuel/N₂ stream was injected through six equally distributed injectors that were 1.5 mm in diameter. The outer diameter of the mixing annulus was 13 mm with an inner diameter of 9 mm. The jet penetration of the fuel/N₂ mixture into the swirled axial flow was approximately 45% of the annular gap height. Using the hydraulic diameter of the annulus (outer diameter minus the inner diameter) as the characteristic length, the Reynolds number of the fuel/air mixture in the annulus after injection was approximately 3000. Upon leaving the mixing section, the fuel/air flow entered the diffuser to provide a homogenous, laminar

plug to the entrance of the flow reactor. The diffuser duct expanded in diameter from 13 mm to 51 mm over a distance of 178 mm. In Phase I, the Reynolds number of the flow exiting the diffuser and entering the test section ranged from 1100 to 1200.

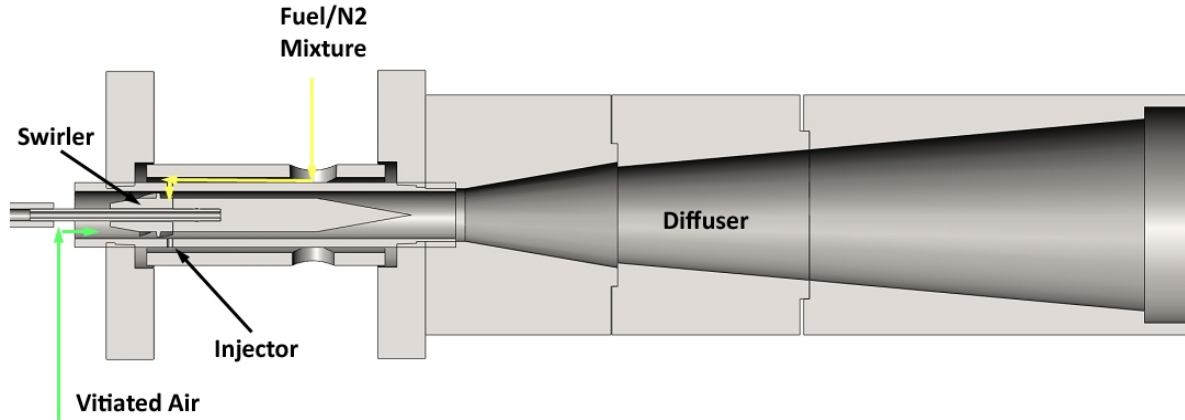


Figure 2–6: Flow reactor mixing section for screening study.

The effectiveness of the mixing section and diffuser was characterized in a previous study using this flow reactor apparatus by Gokulakrishnan et al.[41] as shown in **Figure 2–7**. The fuel stream was substituted with CO₂ and injected into the flow reactor. The momentum ratio of CO₂ and air was selected to match that of the fuel/air mixture to ensure similar mixing conditions. A gas analysis probe was inserted from the tail end of the flow reactor tube measure CO₂ and O₂ concentrations at the transition of the diffuser to the flow reactor tube test section.

Measurements were made in increments of 1 mm along the radial direction of the test section and at axial distances of 25, 50, and 75 mm from the transition of the expanding duct to the test section.. The flow has negligible radial variation along the radius along both the radial and axial directions denoting a well-mixed plug.

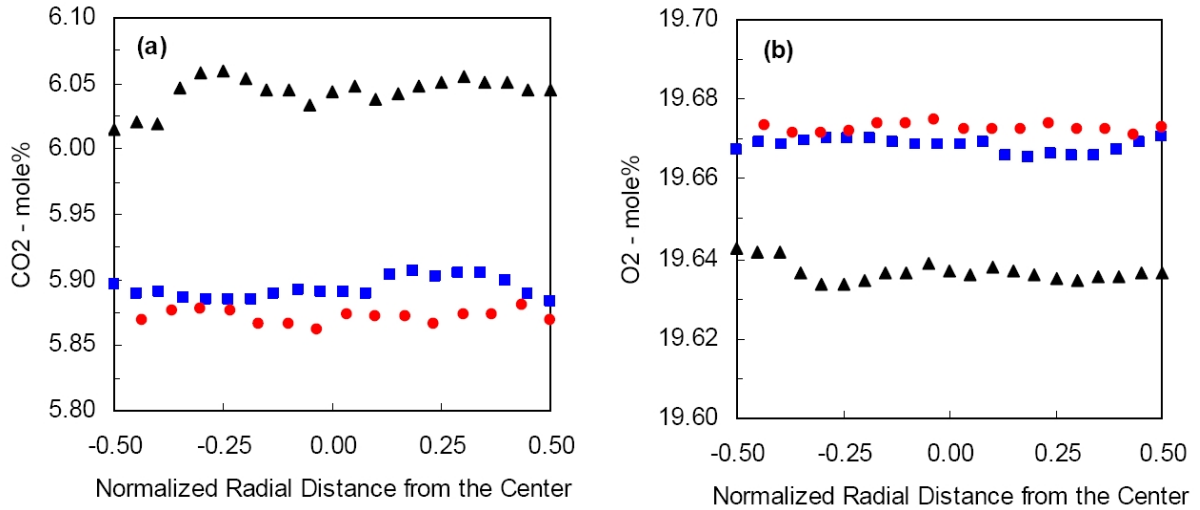


Figure 2-7: Radial species profiles of CO₂ (a) and O₂ (b) at 3 axial locations within the test section. Axial distance from the exit of the diffuser in meters: ▲ - 25 mm; ● - 50 mm; ■ - 75 mm. Figure taken directly from Gokulakrishnan et. al[41]

2.1.6 Flow Reactor Tube and Furnace

The primary test section of the flow reactor, where autoignition occurred, was an alumina (Al₂O₃) tube that measured 1.32 meters in length with an internal diameter of 0.051 meters. The test section was enclosed in a well-insulated ceramic furnace with three independently controlled heating zones. The tube furnace and test section are shown in **Figure 2-1**. The furnace (P/N SV13) and control system (P/N PS205-230) were manufactured by Mellon.

The furnace heated the test section to a steady temperature and provided what can be assumed to be adiabatic conditions inside the flow reactor. The tube functioned as a plug flow reactor. The fuel and air mixture travelled down the tube as a well-mixed plug until the mixture ignited at some distance along the reactor.

2.1.7 Ignition Measurement System

Ignition was measured inside the flow reactor by detecting the chemiluminescence of

CH* radical excitation. The emission of CH* was observed using a Hamamatsu R298 photomultiplier tube (PMT) equipped with a 430 nm narrow band pass filter. The PMT was located at the exhaust end of the flow reactor with direct line of sight down the axis of the test section through a quartz window. During an ignition event, CH* radicals emitted light at 430 nm that was registered by the PMT. The time of light emission (ignition) was recorded in into a data acquisition system on the same temporal axis as the activation of the fuel supply solenoid (injection). The signals were logged at a rate of 10 kHz giving the ignition delay time measurements a resolution of 0.1 ms. An example of the solenoid and PMT signal traces is shown in **Figure 2–8a**.

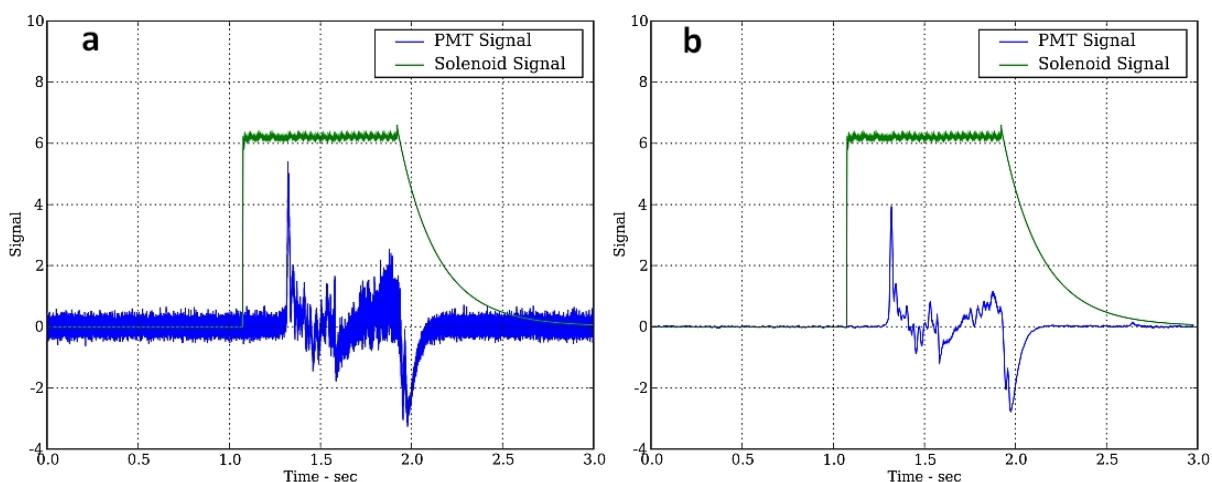


Figure 2–8: Solenoid and PMT signals CH* chemiluminescence measurements. Raw (a) and smoothed (b) PMT signal data are shown as blue traces.

To calculate the time of ignition, a Python script was used to determine the time corresponding to the initial peak of the PMT signal (approximately 1.32 s in **Figure 2–8**). Due to significant signal noise in the raw signal (**Figure 2–8a**) data averaging was applied. The data averaging smoothed out the noise from the signal, as shown in (**Figure 2–8b**), to provide a clean curve for determining the point of ignition. The time of the solenoid signal,

representing the time of fuel injection into the system, was also determined using the Python script. The time of injection was measured as the time in which the solenoid signal had the largest gradient, signified by a nearly vertical signal spike (approximately 1.07 s in **Figure 2–8**) and denoting the activation point of the valve. The time difference between fuel injection (activation of the solenoid) and an ignition event (excitation of the PMT) was recorded as the measured experimental ignition delay time for a given fuel/oxidizer mixture, τ_{exp} .

Due to transit and mixing time of the fuel and oxidizer, the measured ignition delay time, τ_{exp} , accounts for more than just the desired autoignition delay time, τ_{ig} , of the fuel/oxidizer for the given furnace temperature. This not only leads into added delay prior to ignition but also induction chemistry effects such as possible fuel decomposition prior to the fuel/oxidizer mixture entering the test section. The temperature gradient at the entrance to the test section of the flow reactor introduces additional uncertainty in the ignition delay time as well. The issue of accounting for the mixing of the fuel and oxidizer components in a flow reactor has been approached through various methods. These include: the time shifting method [47], the quasi-steady-state approach [48], and the entrainment model approach [49]. The time-shifting approach has been used extensively in the Princeton Variable Pressure Flow Reactor whose mixing and expanding duct sections served as the basis for the flow reactors used in this current study. Gokulakrishnan et al. [50] compared the time shifting method to numerical PSR-PFR modeling for *n*-heptane oxidation experiments and determined that the impact of induction chemistry is sufficiently accounted for through the use of time shifting.

To account for the induction time delay, the time-shifting method has been applied to the flow reactor data acquired from the apparatus used in the Phase I screening portion of this

study. The ignition delay time for the given furnace temperature of the mixture, τ_{ig} , was calculated through the use of a well-characterized comparison fuel for which theoretical ignition delay time could be calculated through validated kinetic models. In the screening study, this comparison fuel was HPLC grade *n*-heptane. The use of *n*-heptane to determine the time shift in the ignition delay time of kerosene based jet fuels due to fuel injection, transit, and mixing was previously performed in the study by Gokulakrishnan et al. [4] to determine the ignition delay time of JP-8, JP-7 and S-8 in the same flow reactor apparatus used in this screening study.

Mixtures of *n*-heptane and air (21 vol% O₂/79 vol% N₂) were ignited in the flow reactor at test temperatures of 950 K, 1038 K and 1125 K as well as test equivalence ratios of 0.5, 1.0 and 1.5. The experimental τ_{exp} from these tests was compared to the theoretical ignition delay time values using the kinetic mechanism experimentally validated for *n*-heptane and developed by Curran et al. [5]. For a given Φ , the experimental τ_{exp} for all three test temperatures was plotted against the corresponding theoretical ignition delay times to determine the linear correction functions shown in **Figure 2–9**. These correction functions were applied to each JP-8 test in the screening study based on the equivalence ratio for a specific test and used to determine the value for each experimental condition. In the following sections that discuss the results of the screening study, the ignition delay times given will be the corrected values of τ_{ig} .

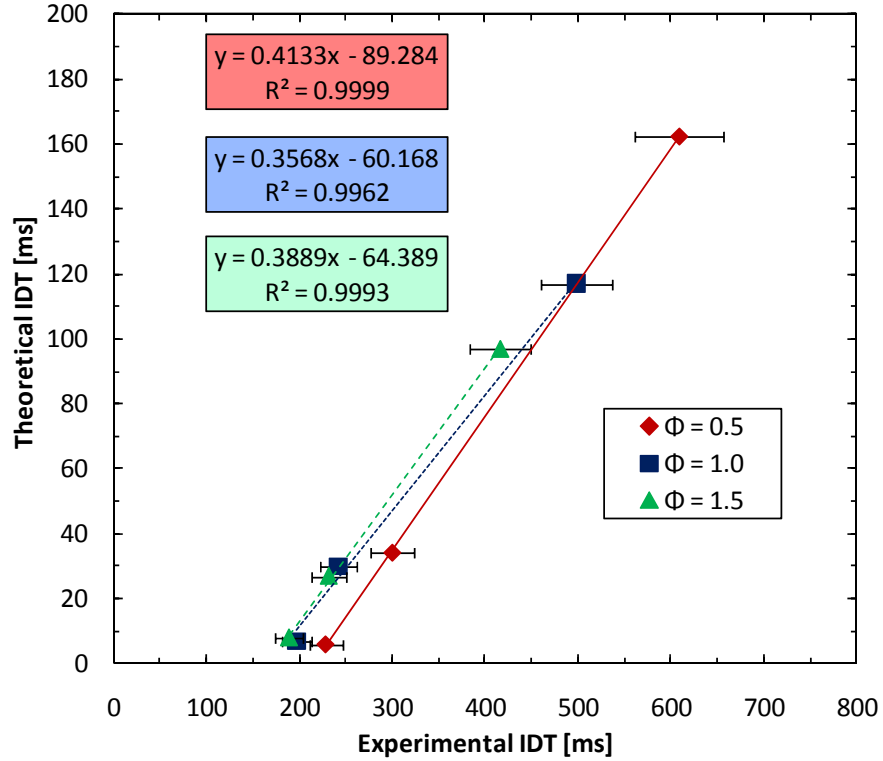


Figure 2-9: Experimental and theoretical ignition delay time correction using prototype comparison mixtures of *n*-heptane/air. Error bars represent 95% confidence based on overall test measurement error.

2.1.8 Temperature Profiles

The screening study examined ignition at three separate steady temperature levels: 950 K, 1037 K, and 1125 K. The temperature profiles, shown in **Figure 2-10**, were determined by taking temperature measurements in 6 inch (15.2 cm) increments starting at the transition from the diffuser to the alumina test section. The temperatures denoting each of the profile curves represent the steady, flat temperature portion of the test section, which are the same temperatures used as design variables in the screening study test matrix.

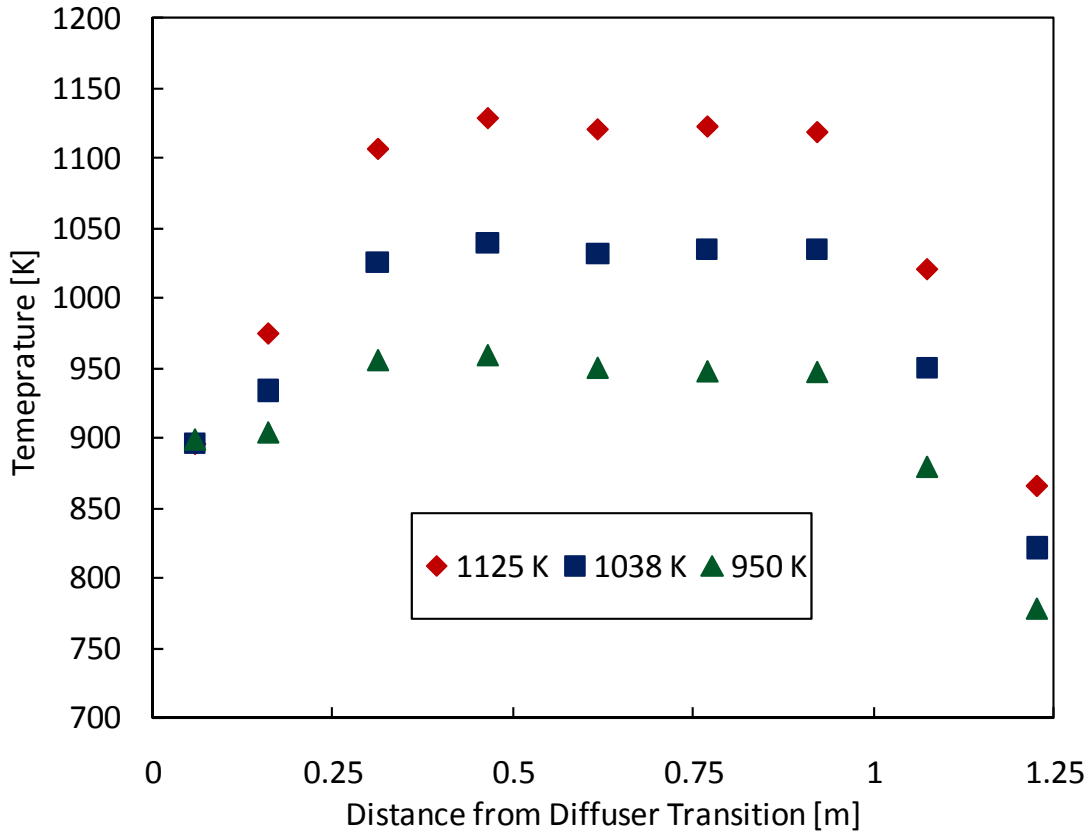


Figure 2-10: Test section temperature profiles for screening study.

2.2 Phase I Screening Study - Experiment Procedure and Design

2.2.1 Experimental Procedure and Methodology

The experimental procedure involved three stages: setting the flow reactor conditions, injecting the fuel and oxidizer, and determining the ignition delay time. This procedure was used for each of the tests covered by the test matrix as well as tests made in non-vitiated conditions and with *n*-heptane for flow reactor characterization purposes. A given test began by setting the flowrates for the main oxidizer stream, fuel vaporizer and steam generator to their corresponding test values and by setting the tube furnace, heat tracing and gas heaters to their test temperatures. Execution of a test began with the injection of the fuel/N₂ mixture into the oxidizer stream through activation of the solenoid fuel control valves and was

completed when the solenoid valves were deactivated. Ignition time of the fuel/oxidizer mixture was determined by measuring the difference between the time in which the PMT registered and ignition event and the time of fuel injection denoted by the activation of the control valves.

Setup of the system for injection measurements began with heating the flow reactor apparatus and setting the flow rates through the different flow reactor components. For all tests, the flow of the oxidizer stream was 80 slpm, made up of the necessary flow rates of N₂, O₂, CO, CO₂, H₂O and NO to meet the test condition requirements. The flow rate through the fuel vaporizer was made up of a constant 20 slpm flow of N₂ and a variable flowrate of fuel based on test requirements. Prior to injection of the fuel, these flows were set and the heating elements (tube furnace, heat tracing and inline gas heaters) on the flow reactor apparatus were allowed to reach steady temperatures corresponding to the test being performed. Upon completion of a measurement, the system was allowed to return to steady temperature levels.

2.2.2 Design of Experiment

The goal of the screening study was to determine the significance of the effects on ignition delay time of the major variables of low pressure (1 atm) vitiated combustion of jet fuel. For this study, seven (7) independent design variables were chosen to represent the various components of vitiated combustion: temperature, equivalence ratio, and the concentration of five (5) vitiated air species: O₂, CO₂, CO, H₂O, and NO (all balanced in a bulk diluent of N₂). Because the study aimed to investigate a large number of variables, a design of experiment (DOE) technique was used to systematically examine the role that each

has on JP-8 ignition under vitiated combustion conditions.

Due to the high non-linearity of combustion processes, the experiments were performed so that each design variable was examined at a minimum of 3 levels. Examination of every combination of these variables at 3 levels would have required 3^7 (2187) tests, which were far too many experiments to perform in a timely and efficient manner. Thus, a DOE technique was applied to reduce the number of tests while providing enough information from the gathered data regarding the effect of each independent variable (known as the *main effect*) and the synergy of two variables (known as the *two-factor interaction effect*) on ignition delay time. To acquire this information and optimize test efficiency, the Box-Behnken Design (BBD) [51], a second-order response surface methodology, was chosen. The BBD design matrix for seven variables is shown in **Figure 2–11**. For a seven variable case, the BBD method reduces the number of tests from 2187 to 56 (7 blocks of 8) while the design still accounts for the non-linear response of the variables. In the case of this study, 60 tests were run: 7 blocks of 8 + 4 independently examined center points. In the design matrix, the three levels for each variable are -1, 0 and +1, representing the low, middle and high values respectively.

The BBD chosen for this study is a *resolution V* design [52], which entails that the main effects are not *confounded* (confused) with the two-factor interaction effects, rather the main effects are confounded with the four-factor interaction effects, while the two-factor interaction effects are confounded with three-factor interaction effects. Generally, the interaction effects higher than two-factors are considered insignificant [52]. Therefore, the main effects and the two-factor interaction effects can be obtained with reasonable accuracy in the current BBD. In addition, the use of the BBD is beneficial due to its rotatability and

spherical shape in a seven variable design. A design is rotatable if the variance of the predicted response at any point \mathbf{x} depends only on the distance of \mathbf{x} from the design center point. A design with this property can be rotated around its center point without changing the prediction variance at \mathbf{x} [53].

$$\mathbf{D} = \begin{bmatrix} x_1 & x_2 & x_3 & x_4 & x_5 & x_6 & x_7 \\ \mathbf{0} & \mathbf{0} & \mathbf{0} & \pm\mathbf{1} & \pm\mathbf{1} & \pm\mathbf{1} & \mathbf{0} \\ \pm\mathbf{1} & \mathbf{0} & \mathbf{0} & \mathbf{0} & \mathbf{0} & \pm\mathbf{1} & \pm\mathbf{1} \\ \mathbf{0} & \pm\mathbf{1} & \mathbf{0} & \mathbf{0} & \pm\mathbf{1} & \mathbf{0} & \pm\mathbf{1} \\ \pm\mathbf{1} & \pm\mathbf{1} & \mathbf{0} & \pm\mathbf{1} & \mathbf{0} & \mathbf{0} & \mathbf{0} \\ \mathbf{0} & \mathbf{0} & \pm\mathbf{1} & \pm\mathbf{1} & \mathbf{0} & \mathbf{0} & \pm\mathbf{1} \\ \pm\mathbf{1} & \mathbf{0} & \pm\mathbf{1} & \mathbf{0} & \pm\mathbf{1} & \mathbf{0} & \mathbf{0} \\ \mathbf{0} & \pm\mathbf{1} & \pm\mathbf{1} & \mathbf{0} & \mathbf{0} & \pm\mathbf{1} & \mathbf{0} \\ \mathbf{0} & \mathbf{0} & \mathbf{0} & \mathbf{0} & \mathbf{0} & \mathbf{0} & \mathbf{0} \end{bmatrix}$$

Figure 2–11: Box-Behnken design for 7 variables.[51]

By using the BBD in this experimental study, the results obtained provide a broad look at each of these variables individually and their interactions with one another to determine their overall significance on auto-ignition delay time as well as to determine the validation of kinetic models. **Table 2-2** lists the variables and their values at each of the three levels that were investigated in the screening study.

The low-level (-1) values of each vitiated air component derived from main combustor exhaust, H₂O, CO₂, CO, and NO, were considered zero, while the high-level values (+1) were assumed to be upper limit of typical vitiated conditions of air combined with turbine exhaust as listed in **Table 2-2**. In the case of O₂, however, 21 vol% is defined as the minimum (-1) value and 15 vol% is defined as the maximum (+1) value. This was done

to examine the effect of O₂ reduction as it applies to increasing air vitiation. The low level (-1) values: 950 K and 0.5 and high level (+1) values: 1125 K and 1.5 were used for temperature and equivalence ratio respectively. The values of these variables were chosen to bracket the range of conditions of non-vitiated air and the mixture of fresh air with typical exhaust gases from common jet fuel combustors.

Table 2-2: Screening Study Design Variables and Test Values

Variable:	x_1	x_2	x_3	x_4	x_5	x_6	x_7
Level (v)	Temp. [K]	Φ	X_{O_2} [vol %]	X_{CO_2} [vol %]	X_{CO} [vol %]	X_{H_2O} [vol %]	X_{NO} [ppm]
-1	950	0.5	21	0	0	0	0
0	1038	1	18	3	0.1	3	50
1	1125	1.5	15	6	0.2	6	100

2.2.3 Non-Vitiated Air Comparison

In addition to the use of *n*-heptane for calibration of the flow reactor, several JP-8 ignition delay time experiments were performed at $\Phi = 1.0$ and in normal air (21 vol% O₂/79 vol% N₂) compare the results of this study with previous work. Tests were performed at the three test temperatures listed as variables in the DOE matrix: 950 K, 1038 K and 1125 K. Non-vitiated testing followed the same procedure as all other tests performed in the screening study. The results of the non-vitiated cases are given at the bottom of **Table 0-2** and plotted against experimental data and validated detailed model predictions in **Figure 2-12**.

In **Figure 2-12**, all sets of comparison data were acquired from atmospheric flow reactors, the results plotted from Gokulakrishnan et al.[41] coming from the base apparatus of the flow reactor used in this screening study. The non-vitiated ignition delay time data acquired in this screening study match reasonably well with similar experimental data and kinetic model predictions for JP-8.

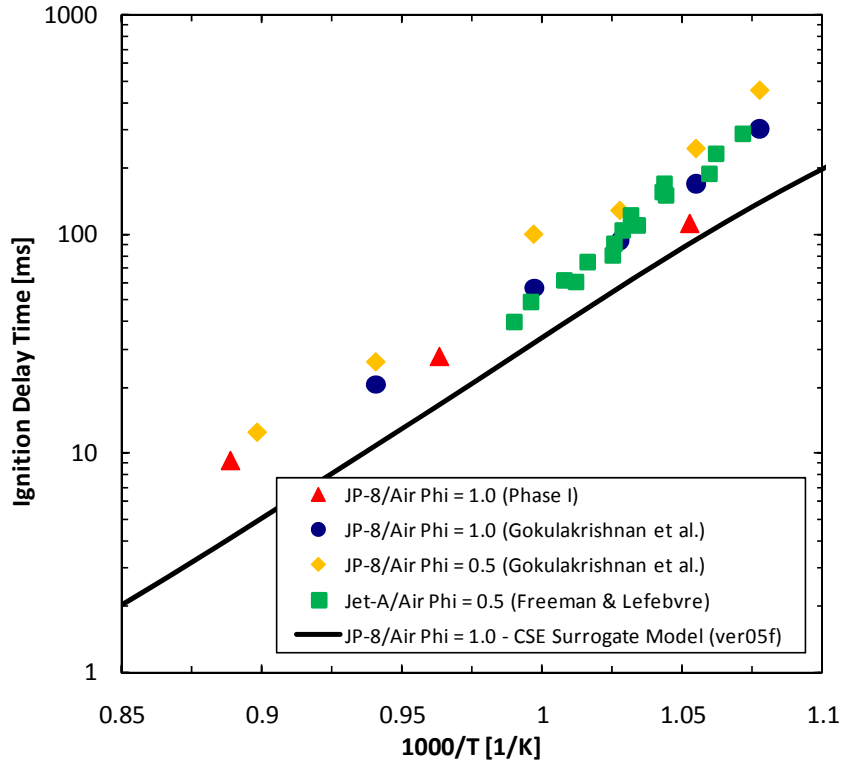


Figure 2–12: Comparison of non-vitiated JP-8 IDT at atmospheric pressures to previous studies of Gokulakrishnan et al. [4][41] and Freeman & Lefebvre [39].

2.3 Phase II Detailed Investigation - Experimental Setup and Apparatus

2.3.1 Overview of Apparatus

Upon completion of the Phase I screening study and the determination of the desired experimental envelope for the Phase II detailed investigation, several limitations with the initial experimental apparatus were addressed to properly modify the flow reactor: insufficient residence time, changes in flowrates and mixing, reactor temperature uniformity, sealing for sub-atmospheric operation, and solenoid and PMT signal issues.

Expansion of capabilities and improvements to the test methods of the screening portion of this study resulted in numerous changes made to the flow reactor apparatus to improve capabilities as well as the accuracy and efficiency of the system. The modified

apparatus is shown in **Figure 2–14**. The modified system was designed to measure the autoignition of liquid fuels at temperatures from 700 K to 900 K and at pressures down to 0.5 atm. The major changes to the system included extension of the length of the flow reactor, redesign of the front end mixing section, improved temperature control, and the addition of a vacuum system. A basic flow and equipment diagram of the modified system is shown in **Figure 2–13**.

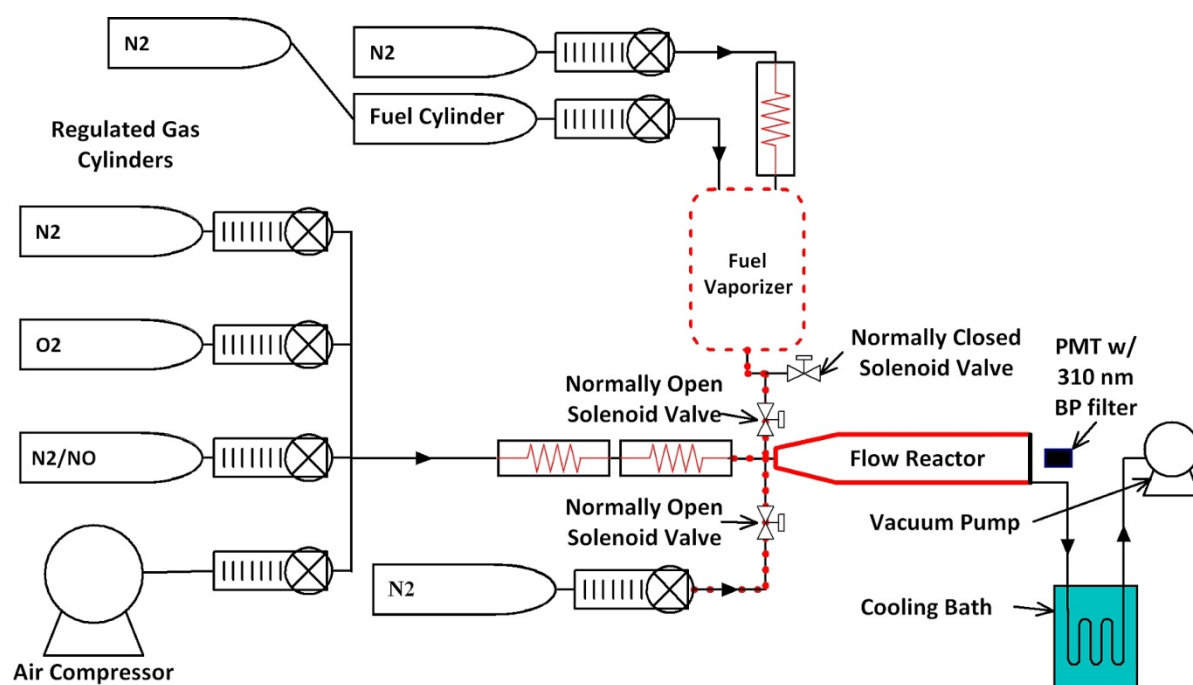


Figure 2–13: Flow diagram for Phase II. Red lines represent heated sections.



Figure 2–14: Flow reactor apparatus used for detailed phase experiments.
 Key: a) flow reactor tube, b) tube furnace, c) flow control panel,
 d) solenoid manifold, e) fuel vaporizer, f) heater controls,
 g) photomultiplier tube, and h) transition piece.

2.3.2 Extension of Flow Reactor Tube

The most significant issue in transitioning from the screening to detailed study was the limitation that the residence time of the original system placed on the experiments. In the detailed study it was desirable to examine lower temperatures (700 K – 900 K) and pressures (0.5 – 1.0 atm) than those used in the screening study. These conditions result in longer ignition times and therefore require that the fuel/air mixtures have longer residence times inside the test section. Two options existed to increase residence time: extending the flow reactor test section and/or reducing the axial velocity of the fuel/air plug. Advantages and disadvantages existed for either option.

There were two main advantages to extending the test section. First, it allowed for continued use of the original test apparatus with minor modifications rather than increasing the tube diameter tube and purchasing a furnace. Second, by maintaining the diameter of the test section, the design of the diffuser, which had been previously characterized, did not need modifications that significantly altered the fluid dynamics of the fuel/air plug. The disadvantages of extending the test section were the need for more lab space due to the increased overall length and having to overcome length limitations of alumina tubing that required multiple sections with connector joints between each tube.

The alternative solution to increasing residence time by lengthening the test section was lowering the flow velocity. The primary advantage of this solution was the ability to limit the overall length of the flow reactor, requiring less lab space. However, the possible methods of lowering the velocity have their own disadvantages. One option was to reduce the flowrates of fuel and air flowing through the reactor. While this would lower the velocity, it also would have required new gas heating equipment due to heating element

limitations of the original equipment. Re-characterization of the diffuser and mixing section would also have been required based on changes in the fluid dynamics of the system. Alternatively, increasing the diameter of the test section to lower the axial velocity would mitigate some of the issues regarding reduced flow rates. This method, however, would have meant that the diffuser and mixing section would have been totally redesigned and the furnace used in the screening study would likely have needed to be replaced.

It was determined that the flow reactor to be used in the detailed investigation would be extended in length by adding alumina tubes of the same dimension as the original test section. This required that the flow reactor be moved to a new lab, but limited the necessary modifications to the front end of the system and allowed for the use of the pre-existing heating equipment.

In the screening study, approximately 0.9 m of the alumina test section was heated, the initial portion undergoing a steep temperature gradient shown in **Figure 2–10**. In the detailed investigation, the flow reactor tube was extended by three additional tubes and the heated section was increased to 5.3 meters. Not only was the length of the test section increased, but the front end temperature gradient seen in the screening study was removed due to an improved heating scheme and lower overall test temperatures. The flow reactor extension allowed for the residence time within the test section to exceed three seconds. A schematic of the lengthened flow reactor is shown in **Figure 2–15**.

The reactor was lengthened by using four separate alumina tubes joined by stainless steel connectors and graphite ring gaskets. The option of using a single long tube was not possible due to individual tube length limitations set by the manufacturing process. Connector pieces, placed between the alumina sections, were machined from stainless steel

pipe to slip over the alumina tube ends. Each connector rested on a stand that allowed it to slide axially as the graphite gaskets were compressed to form a seal between the tubes and connectors. Graphite ring gaskets were also used to seal the connections between alumina tubes and the diffuser and exhaust transition piece. A combination of 3.2 mm and 1.6 mm thick graphite gaskets were used in the detailed study while only 1.6mm gaskets were used in the Phase I apparatus.

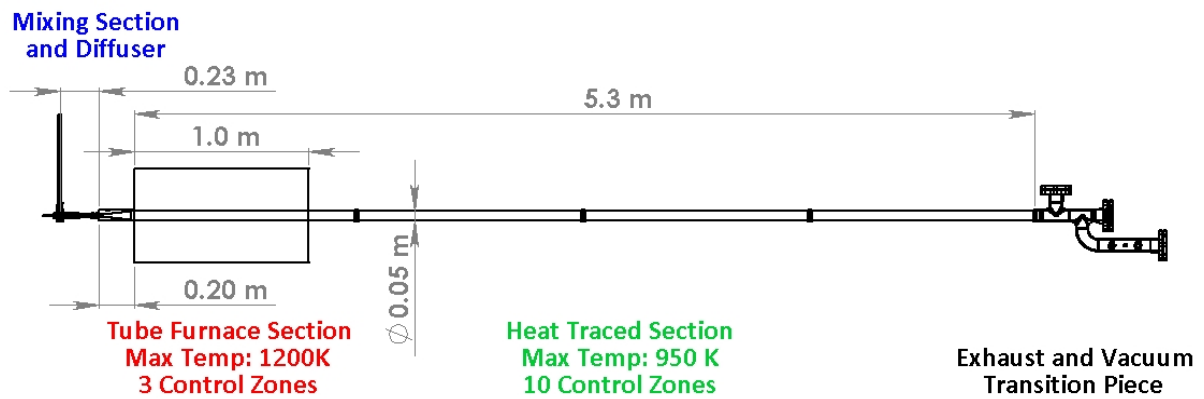


Figure 2–15: Extended flow reactor diagram and temperature capacities.

2.3.3 Modifications to Mixing Section and Diffuser

Characterization of the flow reactor mixing and diffuser section performed in the study by Gokulakrishnan et al. [41] supported that the original apparatus used in the screening study provided a well-mixed plug flow to the steady temperature test section. However, future testing with the flow reactor apparatus, for the detailed investigation and other studies, required the ability to run tests at lower overall flow rates and sub-atmospheric conditions. These flows resulted in reduced Reynolds numbers and less turbulence in the mixing section in this test series. To improve mixing, the radial injectors and the length of the mixing section were both modified. Fuel injector changes increased the penetration of

fuel into the vitiated air stream and extension of the mixing section increased the mixing length for the fuel/air stream prior to entering the diffuser.

The original diffuser was comprised of three separately welded parts and lacked ports for instrumentation. During early shakedown tests for the screening study, fuel and air were found to leak from the fittings connecting the diffuser to the mixing section due to breakdown of the graphite gaskets at test temperatures. The diffuser and mixing section were welded together for to prevent leaking, but this also removed the ability to modify the injectors or mixing section. To improve sealing and allow for interchangeability of mixing sections in the detailed investigation and future studies, the parts were connected with compression fittings in the redesigned apparatus.

The modified mixing and diffuser components are shown in **Figure 2–16**. Two major modifications were made to the mixing section and diffuser to improve mixing as well as measurement capabilities in the head end of the flow reactor. The first modification was to the radial fuel injectors. In the screening study, the fuel and N₂ were injected through 6 injectors (1.5 mm in diameter) with a calculated jet penetration of approximately 45% of the distance between the outer annular wall and the center body. To improve mixing, the number of injectors was increased to 8 and the diameter was reduced to 0.8 mm. This modification increased the calculated jet penetration to 67% as well as added additional streams to penetrate and mix into the swirling, vitiated air flow.

The second modification was the lengthening of the center body and mixing annulus. This modification was made to extend the mixing time of the fuel and air prior to their entrance to the diffuser. The cylindrical portion of the solid body was lengthened from 3.8 cm to 15.2 cm, increasing the length-to-hydraulic diameter ratio of the mixing annulus from

10 to 40. The diameter of the solid body remained 9 mm and the length of the tapered end length remained 25 mm. The primary reason for these modifications was to overcome the reduction in Reynolds number for sub-atmospheric tests and future tests with lower overall flow rates. The dimensions of the diffuser were the same as those of the screening study apparatus; however, the diffuser was machined from a single piece of metal rather than 3 separate sections, thereby smoothing the wetted surface.

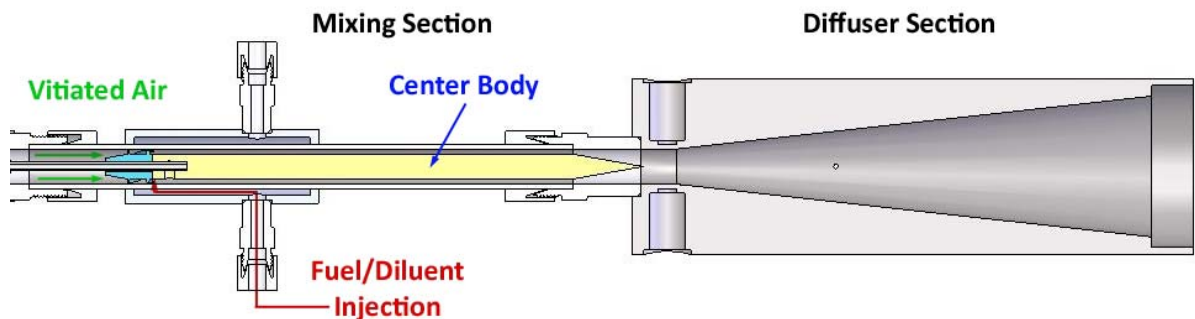


Figure 2–16: Modified mixing section and diffuser.

To provide long enough residence times, all flowrates in sub-atmospheric tests were reduced to maintain velocity (i.e. fuel/air flowrates at 1 atm were nominally 100 slpm while tests at 0.5 atm were nominally 50 slpm). Although velocity was maintained, the Reynolds numbers in the annulus were reduced from 3000 to 1500 due to changes in mixture density. The additional mixing length provided more mixing time for less turbulent flows prior to their entrance to the diffuser, both for sub-atmospheric tests in this study and future tests with this apparatus. In Phase II, the Reynolds number of the flow exiting the diffuser and entering the test section ranged from 1250 to 1450.

Thermocouple (T/C) ports were also added to the modified diffuser to improve temperature profiles and monitor diffuser temperatures during tests. When temperature

profiles were taken (**Figure 2–17a**), a thermocouple, located 5.8 cm from the transition of the mixing section to the diffuser, was placed at a depth that intersected the flow reactor axis. During test conditions, the thermocouple was moved to the wall of the diffuser to avoid flow disruptions (**Figure 2–17b**). For temperature monitoring purposes, a second thermocouple was located inside the diffuser body close to the wall of the expanding duct, 0.12 m from the transition of the mixing section to the diffuser. These thermocouples were used to improve the overall resolution and flatness of the temperature profile throughout the reactor. The fittings on the mixing section were changed to compression fittings rather than the threaded pipe and graphite gaskets used in the apparatus from the screening study. This modification limited leakage in the head end of the system during the sub-atmospheric testing portion of the study. It also provided the ability to switch out mixing sections for future testing.

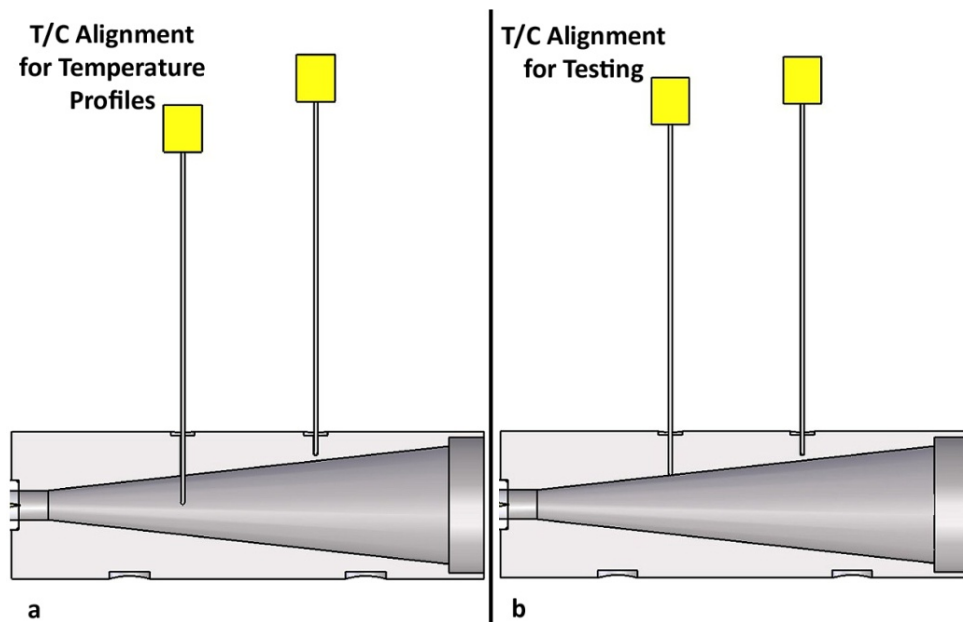


Figure 2–17: Alignment of diffuser T/Cs. Full apparatus not shown.

2.3.4 Improvements and Additions to Heating System

Extension of the flow reactor required additional heating and control in order to

maintain a constant temperature test section for longer ignition tests. The initial temperature ramp seen in the screening study temperature profiles, **Figure 2–10**, was eliminated in the detailed investigation apparatus. This was possible through the combination of lower test temperatures and several modifications made to the heating and temperature control of the apparatus. For the detailed investigation, temperature profiles taken within the test section were made using a custom multipoint T/C probe. The probe was 6 m long with a diameter of 6.4 mm and consisted of fifteen type K thermocouples spanning from the tip to 5.18 m down the length of the probe. Temperature measurements were taken within the flow reactor at two offset probe depths 15.25 cm (6 in) apart. The axial locations along the flow reactor that were measured by the probe are shown in **Figure 2–18**.

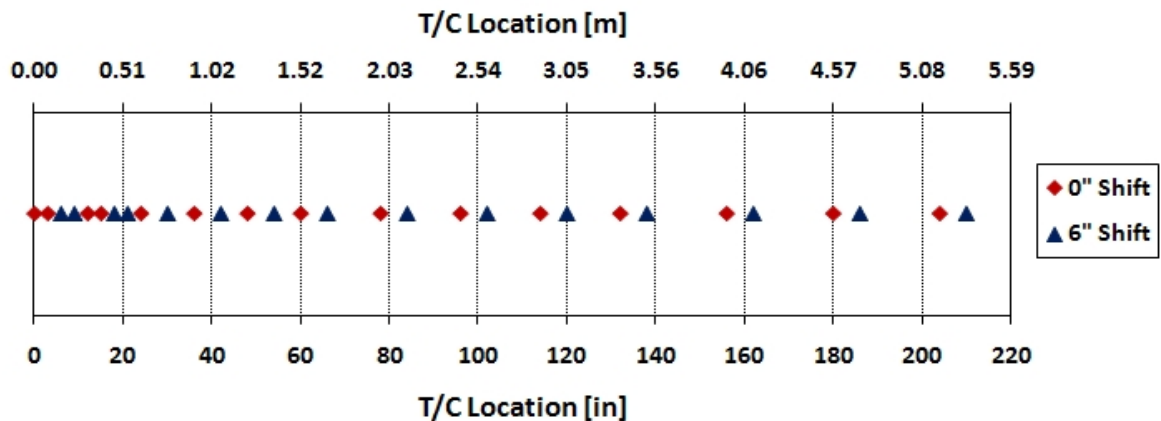


Figure 2–18: Axial locations of T/C’s in multipoint probe. To increase the resolution of temperature profile through measurements, the T/C probe was shifted 6 inches.

The front end of the flow reactor tube was heated and controlled by the Mellon tube furnace system used in the screening and previous studies of Gokulakrishnan et al. [4][41] and Holton et al. [44]. The additional alumina tubing was traced with Samox heating tapes that could raise the gas temperature of the extended flow reactor section to 950 K. The heat tracing was controlled in ten separate zones along the length of flow reactor downstream of

the tube furnace. The entire mixing section and diffuser were also heat traced and controlled to match the temperature of the fuel/air mixture entering the diffuser to the steady temperature along the test section.

The flowrate used to measure the profile differed from the flowrate of the fuel/air mixture during an actual ignition test. In the screening study, 80 slpm of air was used to set the heater controllers and determine the temperature profile of the flow reactor. This was done to match the settings of the flow reactor immediately prior to an ignition test, at which point the additional flowrate of fuel and N₂ is added to the system for a few seconds. This method reduced the accuracy of the temperature profile for the duration of an ignition test. The use of *n*-heptane to calibrate the flow reactor mixing and temperature ramping helped to account for this method in the screening study, however for the detailed investigation the system was adjusted with additional N₂ to account for the fuel injection flowrate that occurs with ignition tests. This provided for more accurate conditions during the temperature profile measurements.

A fuel injection bypass system, shown in **Figure 2–19**, that replaced the fuel/diluent stream with heated N₂ (20 slpm at atmospheric conditions, 10 slpm at 0.5 atm) was added to the system for the detailed investigation. During temperature profile measurements and between ignition tests, all three solenoid valves were de-energized, sending the fuel/N₂ stream to the condenser and the heated N₂ stream through the injectors in the mixing section. To begin an ignition test, the solenoids were activated by the data acquisition and control system, shutting off N₂ flow to the injectors and re-directing the fuel/N₂ stream to the mixing section. By replacing the fuel/N₂ flow with heated N₂ between tests, the temperature profiles measured in the flow reactor were more accurate representations of the conditions

experienced by a fuel/air plug during an ignition test.

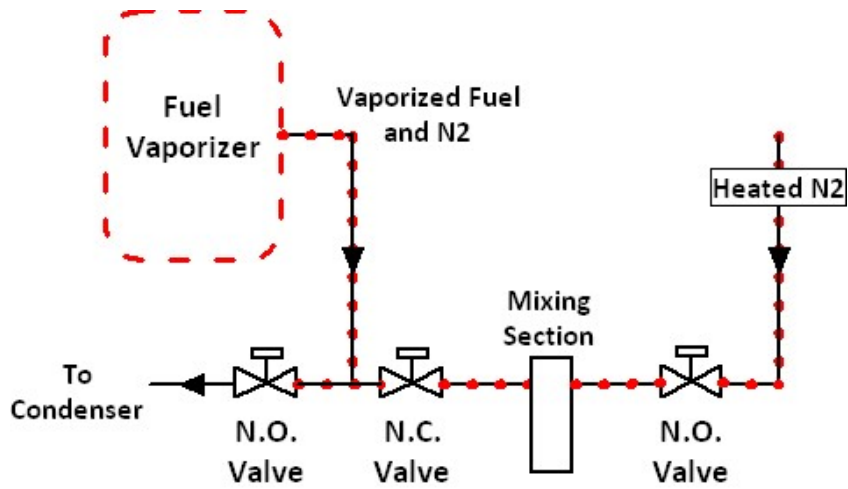


Figure 2–19: Fuel vaporizer, N₂ bypass and solenoid valve schematic for detailed investigation. A combination of normally open (N.O.) and normally closed (N.C.) valves was used to direct the flow.

2.3.5 Transition Piece and Vacuum System

The transition piece, **Figure 2–20**, was manufactured from stainless steel to connect the alumina tube test section to the exhaust and vacuum systems. For atmospheric tests, exhaust from the flow reactor vented directly to a fume hood. For sub-atmospheric tests, the exhaust was transferred to a rotary vane vacuum pump after passage through 2.54 cm diameter copper tubing submerged in a cooling bath. Inlet temperature limitations of the rotary vane vacuum pump made this cooling system necessary. The transition piece was placed on rollers with the ability to move along the axis of the flow reactor. Movement was controlled by manually adjusting four lead screws that connected the transition piece to the Unistrut frame supporting the flow reactor. The flow reactor tubes were sealed by adjusting the position of the transition piece to compress the graphite gaskets located between the diffuser, flow reactor tubes, tube connectors and the transition piece itself. The transition

piece also served as part of the instrumentation apparatus. A flanged port with a quartz window was placed perpendicular to the axis of the test section to allow for the PMT to register ignition events. There were also several Swagelok compression fittings, used as bosses for thermocouples and ports for gas analyzers, welded onto the transition piece.

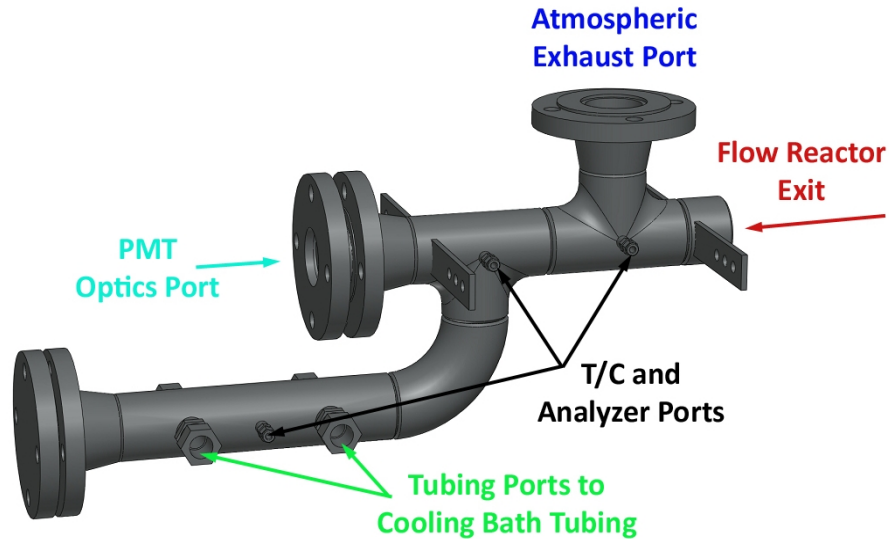


Figure 2–20: Diagram of exhaust and vacuum transition piece.
Flow moves from right to left.

2.3.6 Fuel Vaporization and Supply

Modifications were made to the fuel supply system and vaporizer in the detailed investigation to improve the vaporization and safety of the system. The screening apparatus made use of a previously installed vaporizer (**Figure 2–4**) that injected fuel from the bottom while exhausting through the side. While rebuilding the flow reactor apparatus and moving to a larger space for the detailed investigation, the vaporizer was modified to inject fuel from the top. The heated N_2 was injected from two ports on opposite sides of the vaporizer wall. The fuel/ N_2 mixture exited from the bottom of the vaporizer and flowed to the injection manifold and solenoid valve system. The vaporizer used in the detailed investigation, shown

in **Figure 2–21**, reached steady temperatures faster than the apparatus used in the screening study. Fuel coking was not found in the vaporizer, injector or plumbing throughout Phase II.

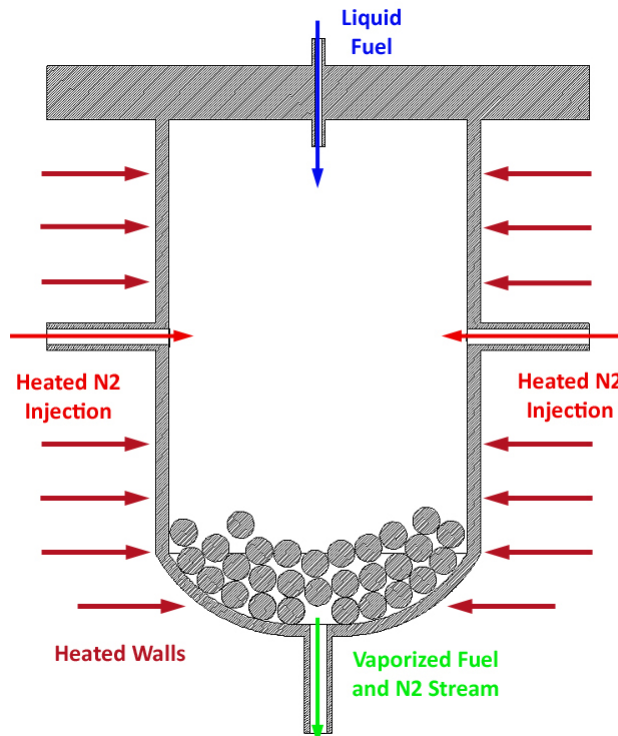


Figure 2–21: Diagram of fuel vaporizer used for detailed investigation.

The fuel supply system was also modified to improve efficiency and safety. The transfer line from the fuel control rotameter was reduced in diameter and length to reduce transfer time to the vaporizer. Toggle valves were put in place to facilitate fast shut down of the liquid fuel flow to the vaporizer and to provide N₂ purge of the system. The purge system allowed for the transition of fuels, i.e. JP-8 to *n*-decane, to occur with more efficiency than in the screening study.

2.3.7 Solenoid, PMT and Data Acquisition

Minor issues were found with the solenoid valve, PMT and data acquisition setups

used for the screening study. The mechanical switch to activate the valves for fuel injection and shutdown led to some injection times not registering in the data acquisition system. On the other hand, the PMT signal noise made it difficult in some tests to define the ignition time. Ambient lighting in the room caused cyclic noise in the PMT signal that made ignition events with CH* emissions of small magnitude difficult to identify.

The modifications made to the solenoid, PMT, and data acquisition systems of the flow reactor were done primary to improve test efficiency and accuracy. The solenoid injection system was further automated and coupled with the data acquisition system through the use of a solid state relay that responded to an output voltage sent by Labview to activate the solenoid valves. Rather than recording the signal sent during manual activation of the solenoid valves, the modified system sent the signal for a specific amount of time and automatically closed the valves to end a test. The use of a manual control switch for the solenoid valves was maintained for emergency shutdown purposes.

The optic filter on the PMT was changed from a 430 nm narrow band filter used to measure the emission of CH* to a 310 nm narrow band filter to measure OH* emission. This change was made to eliminate much of the cyclic noise from the recorded PMT signal filtered for CH* seen in **Figure 2–8a** compared to the signal recorded when the PMT filtered to measure OH* shown in **Figure 2–22**. This modification improved accuracy when determining the time of an ignition event as well as efficiency by reducing the need for post processing and data averaging. This was especially useful for fast ignitions that physically occurred close to the head end of the flow reactor and registered low amplitude signals on the PMT.

For the detailed investigation, the experimental ignition delay time, τ_{exp} , for a given

test run was determined in the same manner as the screening study. A Python script was used to determine the time corresponding to the initial peak of the PMT signal (approximately 2.286 s in **Figure 2–22**). The script was also used to determine the time of fuel injection into the system represented as the solenoid activation time. As in the screening study, the solenoid activation time is the time in which the signal gradient is at a maximum, signified by a nearly vertical spike (approximately 1.06 s in **Figure 2–22**).

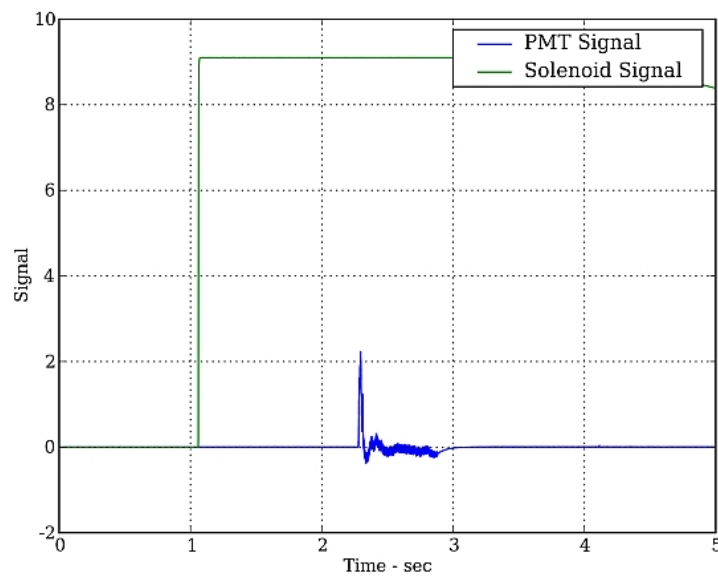


Figure 2–22: Solenoid and PMT traces for OH* chemiluminescence traces. PMT signal is shown as a blue trace.

The time difference between fuel injection (activation of the solenoid) and an ignition event (excitation of the PMT) was recorded as the measured experimental ignition delay time, τ_{exp} , for a given fuel/oxidizer mixture. This recorded value is different from the autoignition delay time, τ_{ig} , of the fuel/oxidizer due to its inclusion of transit, mixing and heat-up time of the mixture. Unlike the screening study, the heat-up time of the mixture was greatly reduced due to the flattening of the temperature profiles, shown in **Figure 2–23** and **Figure 2–24**, for the observed test conditions. Rather than using a comparison fuel, the

nominal transit time from the normally closed solenoid fuel injection valve to the transition from the mixing section to the diffuser was calculated to be 25 ms. This transit time was used as a step-function the correction factor for all tests performed in the detailed investigation to convert τ_{exp} to τ_{ig} . Therefore, in the case shown in **Figure 2–22**, the τ_{exp} value of 1.226 s results in a τ_{ig} of 1.201 s. In the detailed study, measured ignition times, τ_{exp} , approximately range from 0.12 s to 3.2 s, resulting in mixing time effects of 20% down to 0.8% of the total ignition time. This is a vast improvement from the screening study which saw measured ignition delay times, τ_{exp} , ranging from 2.5 to 20 times larger than the corrected autoignition delay time, τ_{ig} due to larger temperature ramps between the mixing and test sections.

2.3.8 Temperature Profiles

As shown in **Figure 2–10** and other studies using the initial version of the flow reactor [54], the temperature profiles of the test section have a significant initial temperature ramp. This ramp was due to the inability to heat the mixing section and diffuser to the temperature level of the tube furnace. In the screening study, this temperature ramp and corresponding induction time delay required adjustment to the measured ignition delay time based on *n*-heptane calibrations. In the detailed investigation, the temperatures examined were lower than those of the screening study, which allowed for the diffuser and mixing section to be heated to the same level, flattening the profiles as shown in **Figure 2–23** and **Figure 2–24**.

The atmospheric portion of the detailed investigation examined ignition at the following temperatures: 700 to 900 K. The sub-atmospheric portion only recorded ignition

events at 800 K, 850 K and 900 K. The use of the 15 point thermocouple probe and the thermocouple located in the diffuser provided temperature measurements far into the diffuser. In the temperature profiles shown in **Figure 2–23** and **Figure 2–24**, the temperature at the 0.0 meters location corresponds to the temperature measured by the thermocouple probe located in the flow stream in **Figure 2–18a**. The effect of the lower overall temperatures and improved heating system provided temperature profiles that were much flatter than those obtained in the screening study, nearly eliminating the temperature ramp seen in **Figure 2–10**. By doing so, the uncertainty that exists in the use of the time shift method to account for induction chemistry of the fuel/oxidizer prior to entering the test section is reduced.

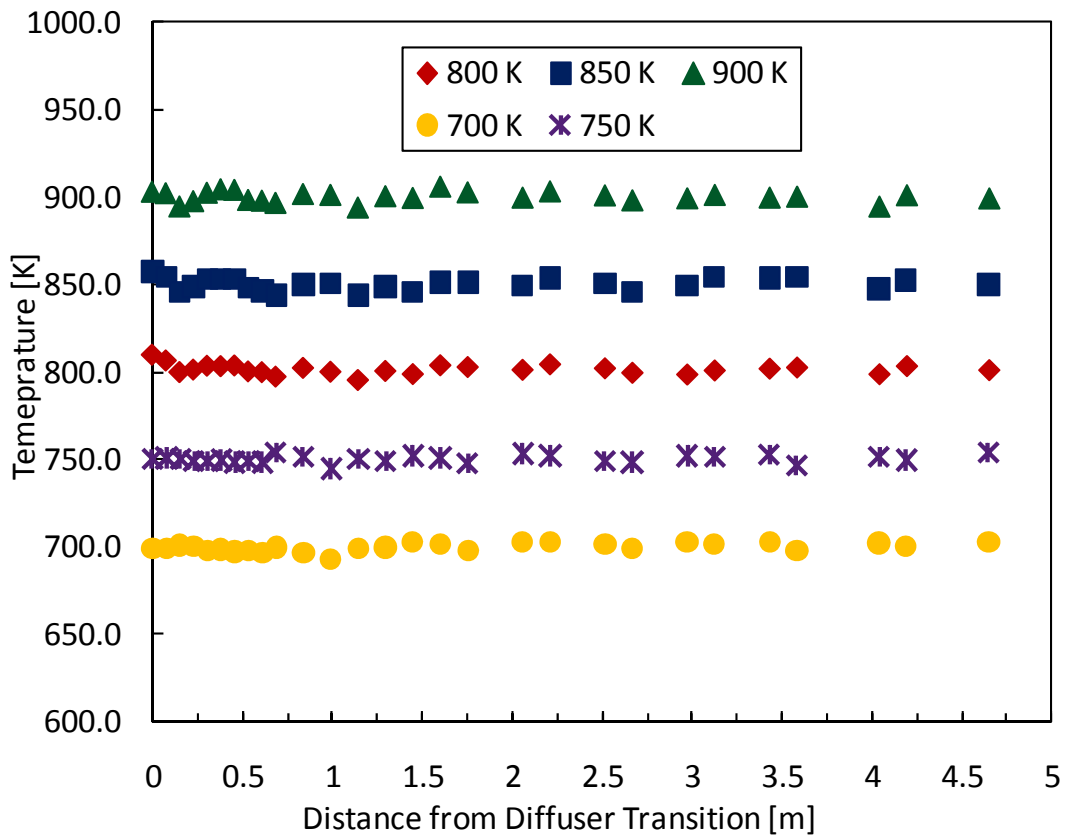


Figure 2–23: Atmospheric test section temperature profiles for detailed study at various temperature settings.

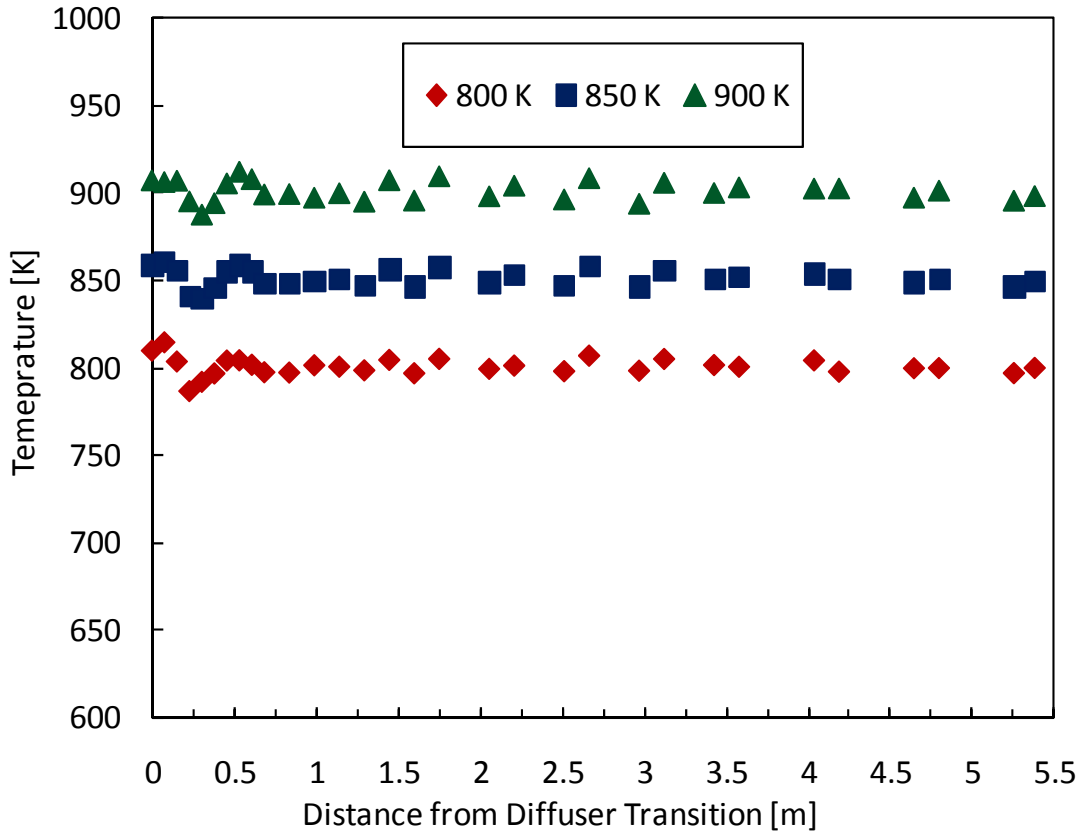


Figure 2–24: Sub-atmospheric test section temperature profiles for detailed study at various temperature settings.

2.4 Phase II Detailed Investigation - Experimental Procedure and Design

2.4.1 Experimental Procedure

The experimental procedure of the detailed investigation involved the same three stages as the screening study: setting the flow reactor conditions, injecting the fuel and oxidizer, and determining the ignition delay time. This overall procedure was used for all JP-8 and *n*-alkane tests, both atmospheric and sub-atmospheric.

Setup of the system for injection measurements began with heating the flow reactor apparatus and setting the flow rates through the different flow reactor components. For all tests, the flow of the oxidizer stream (80 slpm for atmospheric tests, 40 slpm for 0.5 atm tests) was made up of the necessary flow rates of air, N₂, O₂, and NO to meet the test condition requirements. The flow rate through the fuel vaporizer was made up of a constant flow of N₂ (20 slpm for atmospheric tests, 10 slpm for 0.5 atm tests) and a variable flowrate of fuel based on test requirements. An additional heated N₂ stream was added to the system that was injected through the fuel system between tests that had a flowrate equal to the flow rate of N₂ through the fuel vaporizer for a corresponding test condition.

Prior to a test, these flows were set and the heating elements (tube furnace, heat tracing and inline gas heaters) on the flow reactor apparatus were allowed to reach steady temperatures corresponding to the test being performed. Upon completion of a test, the system was allowed to return to steady temperature levels. To refer back to the flow and heating diagram of the modified apparatus for the detailed investigation, see **Figure 2–13**.

An ignition test was initiated by the activation of the fuel control valves, a combination of three solenoid valves that directed the fuel/N₂ flow to either the mixing section of the flow reactor or a condenser and exhaust hood. Ignition events during the

detailed investigation were measured by a PMT equipped with a 310 nm narrow band pass filter to record ignition events by observing the chemiluminescent of OH* radical which is present at the time of ignition, as discussed in Section 2.3.7.

2.4.2 Experimental Variables and Test Matrix

The screening study determined that temperature, NO concentration and O₂ concentration were of the largest significance to the ignition delay time of JP-8 in vitiated environments high temperatures (See Chapter 3). Correspondingly, the purpose of the detailed investigation was to examine these variables in further depth and at values extending beyond the scope of the screening study. For the atmospheric tests, temperature was varied from 700 K to 900 K in 50 K increments. The NO concentration of the oxidizer was nominally varied at the following levels: 0, 50, 100, 250, 500 and 1000 ppm. The concentration of O₂ was examined at 20 vol% and 12 vol% balanced with N₂ as the bulk diluent. These ranges bracketed the values seen in vitiated combustors used in many aircraft operations. All tests were performed at $\Phi = 1.0$. The other components of vitiated air examined in the screening study (CO₂, CO, and H₂O) were not included in the vitiated stream for the detailed examination. The reduction in design variables simplified the test matrix and experimental design for this portion of the study. If ignition occurred for all combinations of each test temperature, NO and O₂ concentration at atmospheric pressure, it would have resulted in the 60 test cases that are shown in **Table 0-5**.

This phase of the study investigated the effect of these design variables at sub-atmospheric conditions. These tests were performed at 0.5 atm and mirrored the atmospheric test matrix down to the point where ignition would not occur due to insufficient residence

time inside the flow reactor, even with the extended length of the flow reactor test section.

2.4.3 Baseline Comparison

As was done in the screening study, the non-vitiated ignition delay time of JP-8 was measured and compared to other non-vitiated experimental data. The ignition delay time results for the atmospheric JP-8 tests in 20% O₂/80% N₂ mixtures without NO addition are compared to other atmospheric jet fuel/air data in **Figure 2–25**. When compared to the ignition delay time data of JP-8/air mixtures from the screening and previous studies[4][39][41], the data obtained from the detailed investigation appears to follow the same trend.

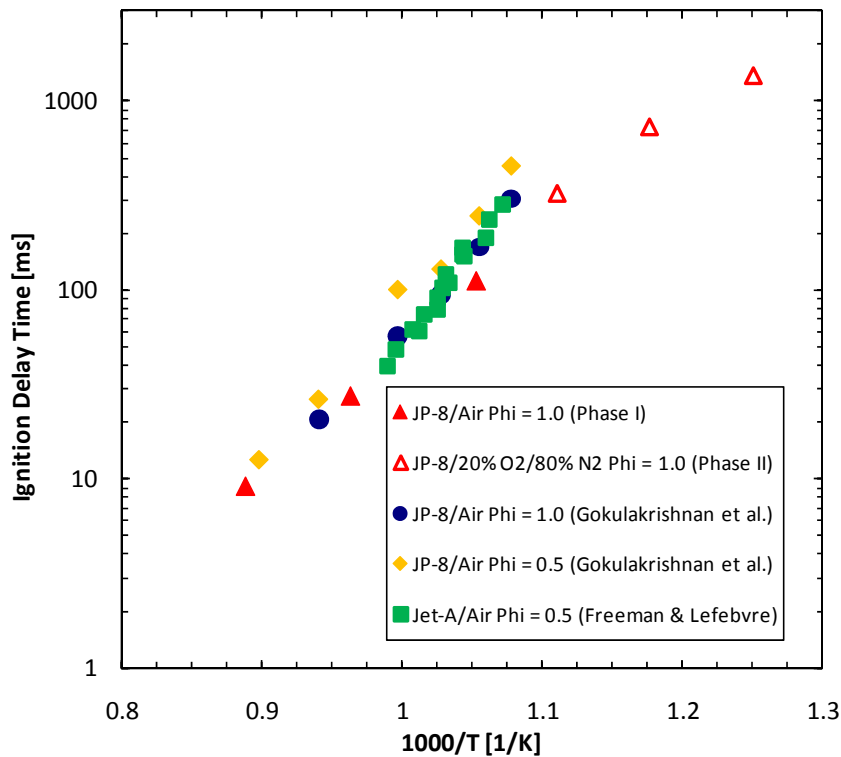


Figure 2–25: Comparison of atmospheric JP-8 IDT from detailed investigation to jet fuel experimental IDT data from Gokulakrishnan et. al. [4][41] and Freeman & Lefebvre [39]

In **Figure 2–26**, the atmospheric ignition delay time data for both JP-8 and *n*-decane

in the 20% O₂/80% N₂ mixture without NO addition are compared to the JP-8/Air ignition delay time results from the screening study. Of note in this plot is the effect of temperature on the ignition delay time of JP-8 compared to *n*-decane. In the temperature range of 800 K to 900 K, JP-8 has a lower ignition delay time than *n*-decane at atmospheric pressures. Below 800 K, however, this relationship reverses. In the temperature regime of 700 K to 800 K, the ignition delay time of *n*-decane is much lower than that of JP-8, so much so that the residence time of the modified flow reactor was insufficient to measure the ignition delay time of JP-8 without NO addition.

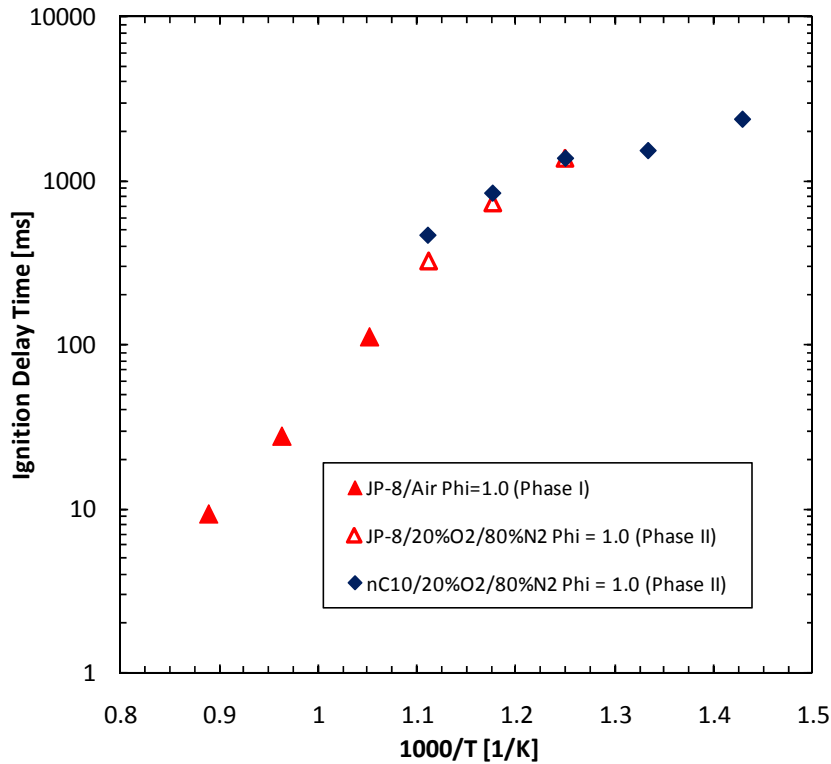


Figure 2–26: Comparison of atmospheric JP-8 IDT to atmospheric *n*-decane IDT data.

While decane and other *n*-alkanes are significant components of jet fuels, the remaining major components, typically aromatics, *iso*-alkanes and cyclo-alkanes, are kinetically different in the temperature ranges examined in the detailed investigation.

Specifically, cyclo-alkanes have been found, in both experimental and theoretical analysis, to have ignition delay times on the order of those of *n*-alkanes at the upper end of the temperature range examined in the detailed investigation [55]. As temperatures are reduced, however, their ignition delay times increase dramatically, similar to the effect that low temperatures have on JP-8 in this study.

Chapter 3: Phase I Screening Study - Results and Discussion

3.1 Table of Results

Experimental results from the screening study are shown in **Table 0-2** in the **Appendix**. Listed at the top of **Table 0-2** is the center point test (Test 0) which represents the combined overall average and standard deviation of all runs for the four separately run 0 point test cases. Listed at the bottom of the matrix are three cases using non-vitiated air. For each 56 tests as well as the Test 0 and the non-vitiated cases, the experimental ignition delay time, τ_{exp} , its corresponding standard deviation of measured values, and the corrected ignition delay time, τ_{ig} , are given.

3.2 Significance of Main and Two-Factor Interaction Effects

The experimental data obtained from the 56 test cases determined in the BBD test matrix was used to examine the significance of the 7 main effect and the 21 two-factor interaction effects that the design variables of temperature, Φ , O_2 , CO_2 , CO , H_2O , and NO have on the autoignition time of JP-8. As discussed in section 2.2, the resolution V design of this experiment avoids confounding of the main and two-factor interaction effects of the variables and allows the examination of all 7 main effects and 21 interaction effects independently.

As defined by Box et al. [52], the *effect* of a factor is the change in response to a variable due to the move from the -1 value to the +1 value, e.g. from 950 K to 1125 K for the temperature variable. For this study, the main effect of the 7 design variables is determined first by taking the level of the design variable for a specific test (-1, 0 or +1) and multiplying

it with the ignition delay time for that test. The sum of this value across all 56 tests is the main effect for that design variable:

$$E_m = \sum_k v_{mk} \tau_{igk} \quad \text{eq. 1}$$

where E_m is the main effect for a given variable m while v_{mk} and τ_{igk} are the design level for variable m and the ignition delay time respectively for a given test k . For example, the main effect of temperature is calculated as follows. The value of τ_{ig} for each test case, k , is multiplied by the corresponding variable level, v_m , for the temperature variable of that test: -1 for 950 K, 0 for 1038 K, or +1 for 1125 K. Ignition delay time values therefore have a negative value for low level for temperature cases and a positive value for high level for temperature cases. The value of tests performed at the midpoint temperature becomes zero. The summation of these values is then taken to calculate the overall effect of the given variable. In the case of temperature, the values sum to -780.6, denoting a negative effect i.e. as temperature increases ignition delay time decreases and vice versa. The effect of temperature was found to be the largest in magnitude of all main and two-factor interaction effects.

The full main effect matrix is shown in **Table 0-3**. The main effects of the 7 design variables are normalized to the largest effect, temperature whose magnitude is set equal to 1 and shown in **Figure 3-1**. A negative effect denotes that increasing the BBD design level of a given design variable (from -1 to +1) results in a reduction of ignition delay time whereas a positive value denotes an increase in ignition delay time as the design level increases. It should be noted that in the case of O_2 , an increase in the design level from -1 to +1 denotes a decrease of the O_2 concentration in the oxidizer stream which is due to the presence of more

vitation products in the oxidizer stream. The value of the variable itself, e.g. [K] for temperature, [ppm] for X_{NO} , [vol %] for X_{O_2} , etc. does not matter in this calculation. This is due to the fact that the effects are being calculated in relationship to each other within the bounds of the experimental envelope. The effect of temperature in the range of 950 K to 1125 K is of interest in comparison to the effect of X_{NO} in the range of 0 ppm to 100 ppm, X_{O_2} in the range of 21 vol% to 15 vol %, etc. Normalization to the largest effect, temperature, is done to simplify comparisons made between each effect.

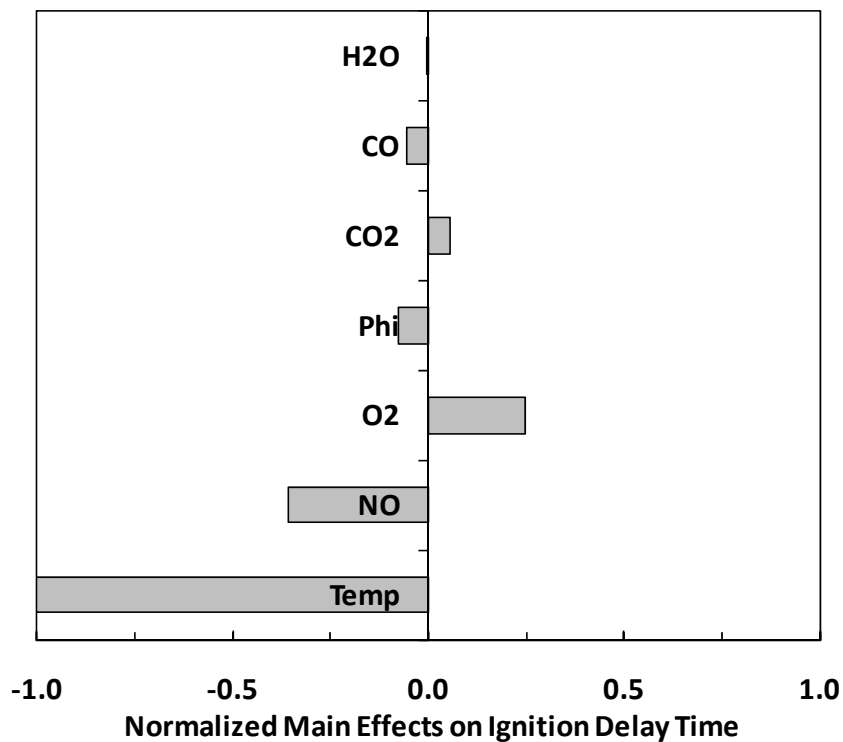


Figure 3–1: Main effects of experimental variables on ignition delay time of JP-8. Effects are normalized based on temperature having the largest effect. Positive results indicate an increase in ignition delay time as the BBD design level for a given design variable is increased from -1 to +1.

Not surprisingly, temperature has the largest effect on ignition delay time due to its non-linear relationship with oxidation kinetics. The addition of NO in the vitiated oxidizer

stream has the second largest effect of the design variables on ignition delay time. Nitric oxide, which is known for its catalytic effect on promoting the oxidation of fuel-lean hydrocarbon mixtures at low temperatures [17], not only has the largest significance of the oxidizer composition variables, but also occurs with trace quantities in the vitiated air stream. Oxygen concentration is the third design variable that has a significant effect, resulting in longer ignition delay times at lower O₂ concentrations. Equivalence ratio, CO₂, and CO concentrations have less significant effects on ignition delay time, with Φ and CO reducing ignition delay time while CO₂ increases ignition delay time. For the conditions studied, H₂O is found to have a negligible effect on ignition delay time compared to the other design variables.

Along with main effects, two-factor interaction effects of design variables can have a substantial influence on the response variable of a given system, in the case of this study, ignition delay time. Box et al. [52] determines the value of the *interaction effect* by taking the difference between the average of effect m with the high and low value averages of effect n ; where m and n represent the two unlike design variables for whose interaction effect is being determined. Similar to the calculation of the main effects, the 21 two-factor interaction effects are calculated by taking the level of two design variables for a specific test and multiplying their product with the ignition delay time for that given test. The sum of these values across all tests is the two-factor interaction effect $E_m E_n$ for those design variables m and n .

$$E_m E_n = \sum_k v_{mk} v_{nk} \tau_{igk}$$

eq. 2

where v_{mk} and v_{nk} are the design levels (i.e. -1, 0, or +1) for variables m and n . τ_{igk} is the

ignition delay time for a given test k . The 7 main effects and 21 two-factor interaction effects are normalized based on the largest effect and listed in **Table 0-3** and **Table 0-4** respectively.

In **Figure 3-2**, the cumulative probability of the 28 main and two-factor interaction effects are plotted with 24 of the 28 effects fall within the following range:

$$R = m \pm \frac{s}{2} \tag{eq. 3}$$

where R is the range of effects that fall between one half of a standard deviation, s , above and below the median, m , of the 28 effects.

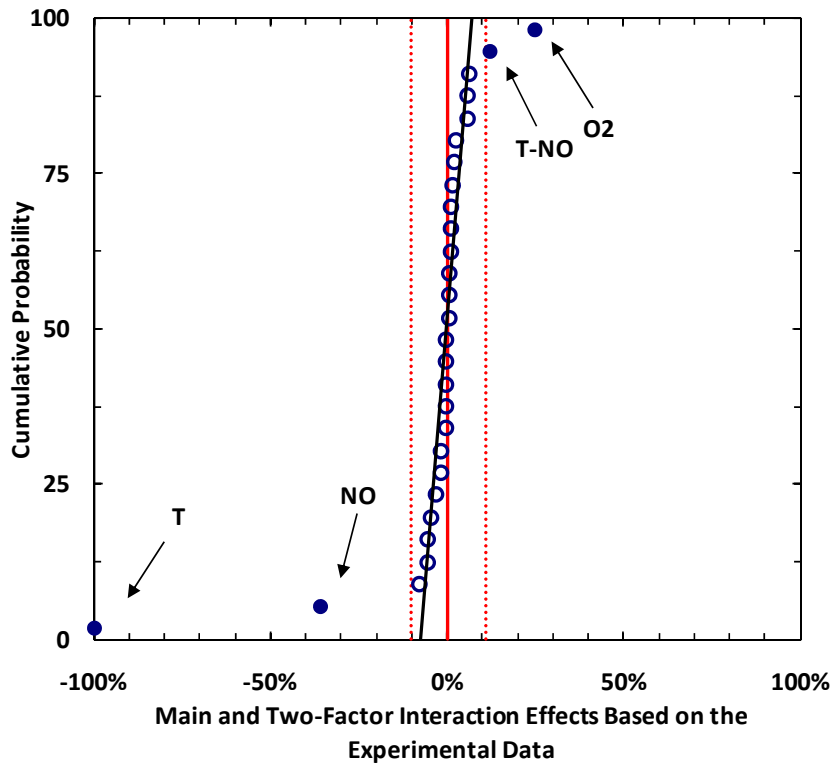


Figure 3-2: Normalized main factor and two-factor interaction effects of experimental design variables based on ignition delay time.

In **Figure 3-2**, the solid red line, —, represents the normalized median of the interaction effects. The dotted red lines, ····, represent \pm one half of the standard deviation of

the normalized main and two-factor effect data. The cumulative probabilities of the 24 main and two-factor effects that fall within R, between the dotted lines, are plotted with open circles, \circ . A linear regression fit through these variables has an R^2 value of 0.9, denoting a relatively straight line and consequently follows a normal distribution. The remaining four effects that are plotted with closed circles, \bullet , fall outside of the normal distribution and represent main and two-factor interactions effects that have a statistically significant effect on the ignition delay time of JP-8. The four outlying effects are: temperature, NO concentration, O₂ concentration as well as the two-factor interaction of temperature and NO concentration.

Figure 3–3 looks at the average ignition delay time for each design variable at each variable level defined by:

$$\tau_{ig_{m,v}} = \frac{\sum \tau_{ig_{m,v}}}{N_{m,v}} \quad \text{eq. 4}$$

where $\tau_{ig_{m,v}}$ is the average ignition delay time for all tests in which one of the 7 design variables, m , is at a specific design level, v . $N_{m,v}$ is the number of tests for which the design variable, m , is at the specified design level, v . **Figure 3–3a** shows the average ignition delay time across design levels for the significant main effects noted above: temperature, NO concentration and O₂ reduction while **Figure 3–3b** shows the average ignition delay time across design levels for the less significant effects of Φ , CO₂, CO and H₂O concentration. For all design variables it can be seen that the ignition delay time of the zero value for each is very close to the overall ignition delay time average of all tests: 41 milliseconds. The agreement between the midpoint of each main effect and the overall ignition delay time average supports the rotatability of the experiment and the effectiveness of the BDD.

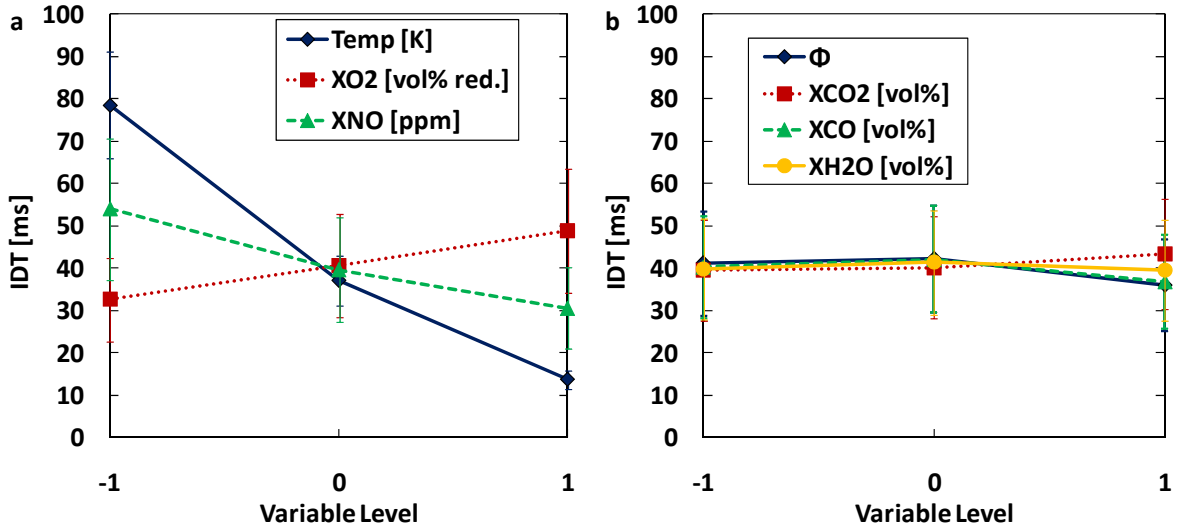


Figure 3-3: Average IDT for each main factor of all tests for a given variable ranking. Error bars represent standard deviation for averaged set of tests for a given design variable across all three levels. **Note:** X_{O_2} is represented as the reduction in O_2 from 21% at -1 to 15% at +1.

To further highlight the significance of temperature, NO concentration and O_2 reduction, **Figure 3-4** plots the average change in ignition delay time from the -1 to +1 value for each main affect as a percent change from the value for $\tau_{ig_{m,-1}}$ for all 7 main effects. In **Figure 3-4a**, the changes in ignition delay time from the -1 to +1 level for temperature, O_2 and NO are -82%, -43% and +49% respectively. The changes in ignition delay time for these three variables can be compared to a maximum change of $\pm 13\%$ for the remaining main factors shown in **Figure 3-4b**. Based on the significance of temperature, NO concentration and O_2 reduction, these main effects as well as the two-factor interaction effect of temperature and NO will be discussed in more detail in the following sections.

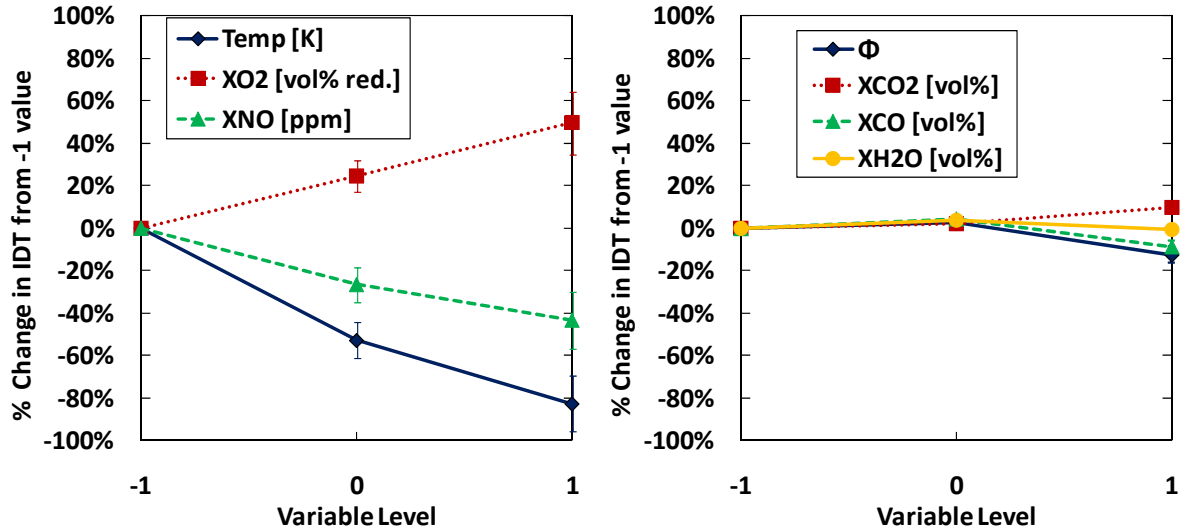


Figure 3-4: Average % change in IDT from -1 ranking of each main factor. Error bars represent standard deviation for averaged set of tests for a given design variable across all three levels. **Note:** X_{O_2} is represented as decrease in O_2 from 21% at -1 to 15% at +1.

3.3 Examination of Main Effects

Given the BBD of the test matrix, **Table 0-2**, for a given design variable there are 6 cases in which the chosen design variable is tested at its -1 and +1 levels while all other variables remain constant. The matrix is also made up blocks of 8-tests in which 4 design variables remain constant at their 0 level values while the other 3 are varied between their -1 and +1 values. For reference, these -1, 0 and +1 values are noted in **Table 2-2**. An example of one of these 8-test blocks can be seen in **Table 3-1**. In this block, temperature, Φ , X_{O_2} , and X_{NO} remain constant at their values for 1038 K, 1.0, 18 vol%, and 50 ppm respectively for all tests while X_{CO_2} , X_{CO} , and X_{H_2O} are varied between their high and low values of 0% - 6%, 0.0% - 0.2%, and 0% - 6% respectively. This blocking allows for the examination of 2 design variables at their high and low values, while 5 variables remain constant as shown in Tests 1-4 and 5-8 where X_{CO_2} is constant across for each 4-test block. These test blocks will be used to look more specifically into the effect of the significant design variables.

Table 3-1: Example 8-Test Block. Dynamic design variables are shaded.

	x_1	x_2	x_3	x_4	x_5	x_6	x_7	Experimental	Corrected	
Test #	Temp. [K]	Φ	X_{O_2}	X_{CO_2}	X_{CO}	X_{H_2O}	X_{NO}	τ_{exp} [ms]	Std. Error %	τ_{ig} [ms]
1	1038	1.0	18%	6%	0.20%	6%	50	285	0.7%	41.4
2	1038	1.0	18%	6%	0.20%	0%	50	277	1.3%	38.7
3	1038	1.0	18%	6%	0.00%	6%	50	285	1.0%	41.4
4	1038	1.0	18%	6%	0.00%	0%	50	268	2.4%	35.5
5	1038	1.0	18%	0%	0.20%	6%	50	256	2.6%	31.2
6	1038	1.0	18%	0%	0.20%	0%	50	254	1.8%	30.5
7	1038	1.0	18%	0%	0.00%	6%	50	268	1.4%	35.4
8	1038	1.0	18%	0%	0.00%	0%	50	261	2.2%	33.0

3.3.1 Effect of O₂

The effect of O₂ reduction from 21 vol% to 15 vol% can be directly examined in the experimental results through the following test blocks:

Tests 33-40: Temp., Φ , X_{CO} , X_{H_2O} constant; X_{O_2} , X_{CO_2} , X_{NO} varied (Table 3-2)

Tests 41-48: Φ , X_{CO_2} , X_{H_2O} , X_{NO} constant; X_{O_2} , Temp, X_{CO} varied (Table 3-3)

Tests 49-56: Temp., X_{CO_2} , X_{CO} , X_{NO} constant; X_{O_2} , Φ , X_{H_2O} varied (Table 3-4)

Table 3-2: Phase I Tests 33-40

Test	Temperature [K]	Φ	X_{O_2} [vol%]	X_{CO_2} [vol%]	X_{CO} [vol%]	X_{H_2O} [vol%]	X_{NO} [ppm]	τ_{ig} [ms]	% Change in τ_{ig}
40	1038	1.0	21%	0%	0.10%	3%	0	34	0%
36	1038	1.0	15%	0%	0.10%	3%	0	69	101%
39	1038	1.0	21%	0%	0.10%	3%	100	21	0%
35	1038	1.0	15%	0%	0.10%	3%	100	42	102%
38	1038	1.0	21%	6%	0.10%	3%	0	45	0%
34	1038	1.0	15%	6%	0.10%	3%	0	66	47%
37	1038	1.0	21%	6%	0.10%	3%	100	26	0%
33	1038	1.0	15%	6%	0.10%	3%	100	41	54%

Table 3-3: Phase I Tests 41-48

Test	Temperature [K]	ϕ	X_{O_2} [vol%]	X_{CO_2} [vol%]	X_{CO} [vol%]	X_{H_2O} [vol%]	X_{NO} [ppm]	τ_{ig} [ms]	% Change in τ_{ig}
48	950	1.0	21%	3%	0.0%	3%	50	62	0%
46	950	1.0	15%	3%	0.0%	3%	50	86	38%
47	950	1.0	21%	3%	0.2%	3%	50	60	0%
45	950	1.0	15%	3%	0.2%	3%	50	85	41%
44	1125	1.0	21%	3%	0.0%	3%	50	15	0%
42	1125	1.0	15%	3%	0.0%	3%	50	21	37%
43	1125	1.0	21%	3%	0.2%	3%	50	12	0%
41	1125	1.0	15%	3%	0.2%	3%	50	13	12%

Table 3-4: Phase I Tests 49-56

Test	Temperature [K]	ϕ	X_{O_2} [vol%]	X_{CO_2} [vol%]	X_{CO} [vol%]	X_{H_2O} [vol%]	X_{NO} [ppm]	τ_{ig} [ms]	% Change in τ_{ig}
56	1038	0.5	21%	3%	0.1%	0%	50	27	0%
54	1038	0.5	15%	3%	0.1%	0%	50	42	55%
55	1038	0.5	21%	3%	0.1%	6%	50	31	0%
53	1038	0.5	15%	3%	0.1%	6%	50	42	36%
52	1038	1.5	21%	3%	0.1%	0%	50	26	0%
50	1038	1.5	15%	3%	0.1%	0%	50	39	48%
51	1038	1.5	21%	3%	0.1%	6%	50	31	0%
49	1038	1.5	15%	3%	0.1%	6%	50	39	29%

In each test block given in **Table 3-2**, **Table 3-3**, and **Table 3-4**, the three variables that are examined at their -1 and +1 levels are shaded along with the change in ignition delay time from the cases at the -1 O_2 level (21 vol%) to the +1 O_2 level (15 vol%). In all cases, the reduction of O_2 from 21 vol% to 15 vol%, while all other design variables remain constant, results in an increase of the ignition delay time of JP-8 ranging from 12% to 102%, with an average increase of 50%. This effect is not surprising given that the reduction of O_2 in the oxidizer stream results in an increase in the fraction of third body species, primarily N_2 in this study. The increased fraction of N_2 also works as a diluent that absorbs a portion of

the exothermic energy of the combustion process. This effect can also be seen in **Figure 3–5** through the reduction in the adiabatic flame temperature of jet fuel as O_2 in a system is replaced by N_2 while the remaining vitiated species concentrations, Φ , and temperature remain the same.

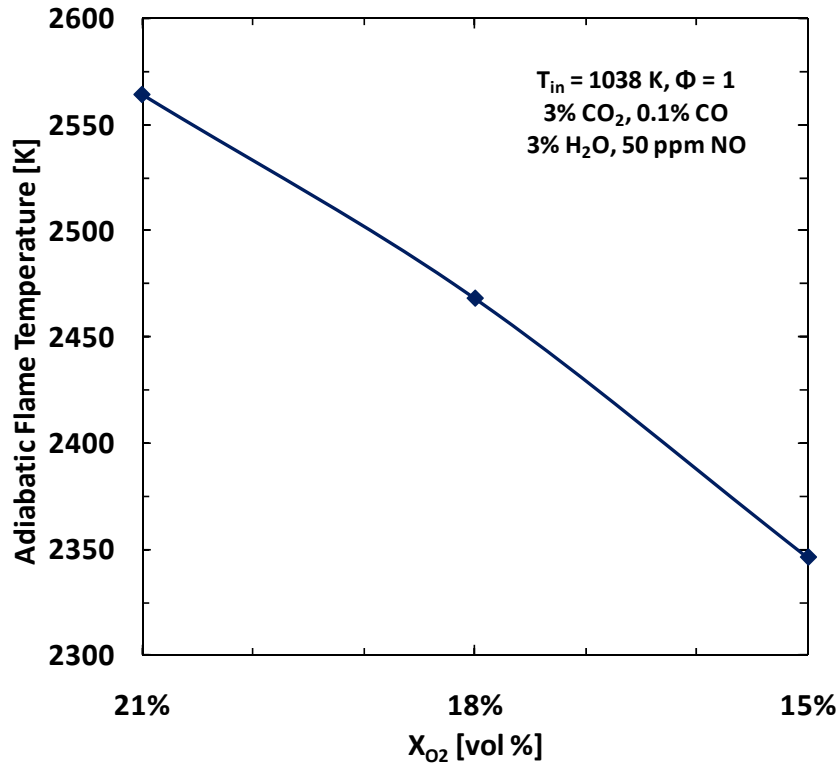


Figure 3–5: Calculated adiabatic flame temperature of Jet-A($C_{12}H_{23}$)/vitiated air mixtures. Jet-A acquired from Burcat [56] and Gracia-Salcedo et al. [57]. O_2 concentration varied from 21 vol% to 15 vol%. Remaining design variables are constant at their corresponding 0 level values.

3.3.2 Effect of Temperature

The effect of temperature from 950 K to 1125 K can be directly examined in the experimental results through the following test blocks:

Tests 9-16: Φ , X_{O_2} , X_{CO_2} , X_{CO} , constant; Temp., X_{H_2O} , X_{NO} varied (**Table 3-5**)

Tests 25-32: X_{O_2} , X_{CO} , X_{H_2O} , X_{NO} constant; Temp, Φ , X_{CO_2} varied (**Table 3-6**)

Tests 41-48: Φ , X_{CO_2} , X_{CO} , X_{NO} constant; Temp, X_{O_2} , X_{CO} varied (**Table 3-7**)

Table 3-5: Phase I Tests 9-16

Test	Temperature [K]	ϕ	X_{O_2} [vol%]	X_{CO_2} [vol%]	X_{CO} [vol%]	X_{H_2O} [vol%]	X_{NO} [ppm]	τ_{ig} [ms]	% Change in τ_{ig}
16	950	1.0	18%	3%	0.1%	0%	0	118	0%
12	1125	1.0	18%	3%	0.1%	0%	0	18	-85%
15	950	1.0	18%	3%	0.1%	0%	100	61	0%
11	1125	1.0	18%	3%	0.1%	0%	100	9	-85%
14	950	1.0	18%	3%	0.1%	6%	0	97	0%
10	1125	1.0	18%	3%	0.1%	6%	0	21	-79%
13	950	1.0	18%	3%	0.1%	6%	100	49	0%
9	1125	1.0	18%	3%	0.1%	6%	100	16	-67%

Table 3-6: Phase I Tests 25-32

Test	Temperature [K]	ϕ	X_{O_2} [vol%]	X_{CO_2} [vol%]	X_{CO} [vol%]	X_{H_2O} [vol%]	X_{NO} [ppm]	τ_{ig} [ms]	% Change in τ_{ig}
32	950	0.5	18%	0%	0.1%	3%	50	86	0%
28	1125	0.5	18%	0%	0.1%	3%	50	11	-87%
31	950	0.5	18%	6%	0.1%	3%	50	94	0%
27	1125	0.5	18%	6%	0.1%	3%	50	6	-94%
30	950	1.5	18%	0%	0.1%	3%	50	73	0%
26	1125	1.5	18%	0%	0.1%	3%	50	9	-87%
29	950	1.5	18%	6%	0.1%	3%	50	71	0%
25	1125	1.5	18%	6%	0.1%	3%	50	14	-80%

Table 3-7: Phase I Tests 41-48

Test	Temperature [K]	ϕ	X_{O_2} [vol%]	X_{CO_2} [vol%]	X_{CO} [vol%]	X_{H_2O} [vol%]	X_{NO} [ppm]	τ_{ig} [ms]	% Change in τ_{ig}
48	950	1.0	21%	3%	0.0%	3%	50	62	0%
44	1125	1.0	21%	3%	0.0%	3%	50	15	-75%
47	950	1.0	21%	3%	0.2%	3%	50	60	0%
43	1125	1.0	21%	3%	0.2%	3%	50	12	-80%
46	950	1.0	15%	3%	0.0%	3%	50	86	0%
42	1125	1.0	15%	3%	0.0%	3%	50	21	-76%
45	950	1.0	15%	3%	0.2%	3%	50	85	0%
41	1125	1.0	15%	3%	0.2%	3%	50	13	-85%

For each test block given in **Table 3-5**, **Table 3-6**, and **Table 3-7** the three variables that are examined at their -1 and +1 levels are shaded along with the change in ignition delay time from the cases at the -1 temperature level (950 K) to the +1 temperature level (1125 K). The increase of temperature from 950 K to 1125 K, while all other design variables remain constant, results in a decrease of the ignition delay time of JP-8 for all cases ranging from 67% to 94% with an average decrease of 82%. Given the temperature dependence of the ignition delay time of jet fuel found in previous studies at non-vitiated conditions and this temperature range [4][39][41], as shown in **Figure 2–12**, the large effect that temperature has on the ignition delay time of JP-8 in vitiated air is generally expected.

3.3.3 Effect of NO

The effect of NO concentration on the ignition delay time of JP-8 can be directly examined in the experimental results of the following test blocks:

Tests 9-16: Φ , X_{O_2} , X_{CO_2} , X_{CO} , constant; X_{NO} , Temp., X_{H_2O} varied (**Table 3-8**)

Tests 17-24: Φ , X_{O_2} , X_{CO_2} , X_{CO} constant; X_{NO} , Temp, X_{H_2O} varied (**Table 3-9**)

Tests 33-40: Temp., Φ , X_{CO} , X_{H_2O} constant; X_{NO} , X_{O_2} , X_{CO_2} varied (**Table 3-10**)

Table 3-8: Phase I Tests 17-24

Test	Temperature [K]	Φ	X_{O_2} [vol%]	X_{CO_2} [vol%]	X_{CO} [vol%]	X_{H_2O} [vol%]	X_{NO} [ppm]	τ_{ig} [ms]	% Change in τ_{ig}
24	1038	0.5	18%	3%	0.0%	3%	0	58	0%
23	1038	0.5	18%	3%	0.0%	3%	100	30	-48%
22	1038	0.5	18%	3%	0.2%	3%	0	42	0%
21	1038	0.5	18%	3%	0.2%	3%	100	24	-42%
20	1038	1.5	18%	3%	0.0%	3%	0	39	0%
19	1038	1.5	18%	3%	0.0%	3%	100	26	-33%
18	1038	1.5	18%	3%	0.2%	3%	0	40	0%
17	1038	1.5	18%	3%	0.2%	3%	100	23	-41%

Table 3-9: Phase I Tests 9-16

Test	Temperature [K]	Φ	X_{O_2} [vol%]	X_{CO_2} [vol%]	X_{CO} [vol%]	X_{H_2O} [vol%]	X_{NO} [ppm]	τ_{ig} [ms]	% Change in τ_{ig}
16	950	1.0	18%	3%	0.1%	0%	0	118	0%
15	950	1.0	18%	3%	0.1%	0%	100	61	-49%
14	950	1.0	18%	3%	0.1%	6%	0	97	0%
13	950	1.0	18%	3%	0.1%	6%	100	49	-50%
12	1125	1.0	18%	3%	0.1%	0%	0	18	0%
11	1125	1.0	18%	3%	0.1%	0%	100	9	-50%
10	1125	1.0	18%	3%	0.1%	6%	0	21	0%
9	1125	1.0	18%	3%	0.1%	6%	100	16	-22%

Table 3-10: Phase I Tests 33-40

Test	Temperature [K]	Φ	X_{O_2} [vol%]	X_{CO_2} [vol%]	X_{CO} [vol%]	X_{H_2O} [vol%]	X_{NO} [ppm]	τ_{ig} [ms]	% Change in τ_{ig}
36	1038	1.0	15%	0%	0.1%	3%	0	69	0%
35	1038	1.0	15%	0%	0.1%	3%	100	42	-39%
34	1038	1.0	15%	6%	0.1%	3%	0	66	0%
33	1038	1.0	15%	6%	0.1%	3%	100	41	-39%
40	1038	1.0	21%	0%	0.1%	3%	0	34	0%
39	1038	1.0	21%	0%	0.1%	3%	100	21	-40%
38	1038	1.0	21%	6%	0.1%	3%	0	45	0%
37	1038	1.0	21%	6%	0.1%	3%	100	26	-42%

In each test block given in **Table 3-8**, **Table 3-9**, and **Table 3-10**, the three variables that are examined at their -1 and +1 levels are shaded along with the change in ignition delay time from the cases at the -1 NO level (0 ppm) to the +1 NO level (100 ppm). The addition of NO to the vitiated stream from 0 ppm to 100 ppm, while all other design variables remain constant, results in a decrease of the ignition delay time of JP-8 for all applicable test cases. The percentage of ignition delay time reduction ranges from 22% to 50% with an average decrease of 41%. This reductive effect occurs regardless of the temperature, Φ , or balance concentration of the vitiated air.

This measurable effect of NO on the ignition and oxidation of JP-8 is supported by numerous previous studies examining the effect of nitric oxides on the ignition and oxidation of H₂ and hydrocarbon fuels, including kerosene and gasoline surrogates [13]-[26][58]. Although the presence of 100 ppm of NO decreased ignition delay time for all tests in this study, the relative effect of NO on ignition diminishes as the concentration increases. This can be seen by looking at the averaged ignition delay time curve based on NO in **Figure 3–4**. By noting that the percent change in ignition delay time from the 0 to +1 variable rank (50 to 100 ppm NO) is less than the percent change in ignition delay time from the -1 to 0 variable rank (0 to 50 ppm NO), the decrease of effectiveness at higher concentrations is shown. A similar trend noting the decreased effect of NO at higher concentrations was observed by Bromly et al.[17]. In that study, increasing the initial concentration of NO enhanced oxidation up to 100 ppm at which point the consumption of CH₄ plateaued and then decreased slightly up to 200 ppm. Norrish et al.[14] also noted an inhibiting effect of NO at higher concentrations. While the results of the screening study show an apparent reduction in the effectiveness of NO, further examination across a larger range of concentrations is required to better determine the asymptotic behavior and possible inhibition effects that NO has on jet fuel ignition.

3.4 Interaction Effect of Temperature and NO

Statistically, the majority of the 21 two-factor effects of the 7 design variables on ignition delay are not significant within the ranges inspected by the DOE of the screening study. The exception to this finding is the two-factor interaction effect of temperature and NO. As shown in **Figure 3–2**, the two-factor effect of temperature and NO is positive, rather

than negative, as is the case for the effect of both temperature and NO as main factors. The positive value for the temperature-NO effect implies that the role of NO promoting the oxidation of JP-8 would decrease as the temperature is increased. This point is further illustrated in **Figure 3–6** and **Figure 3–7**.

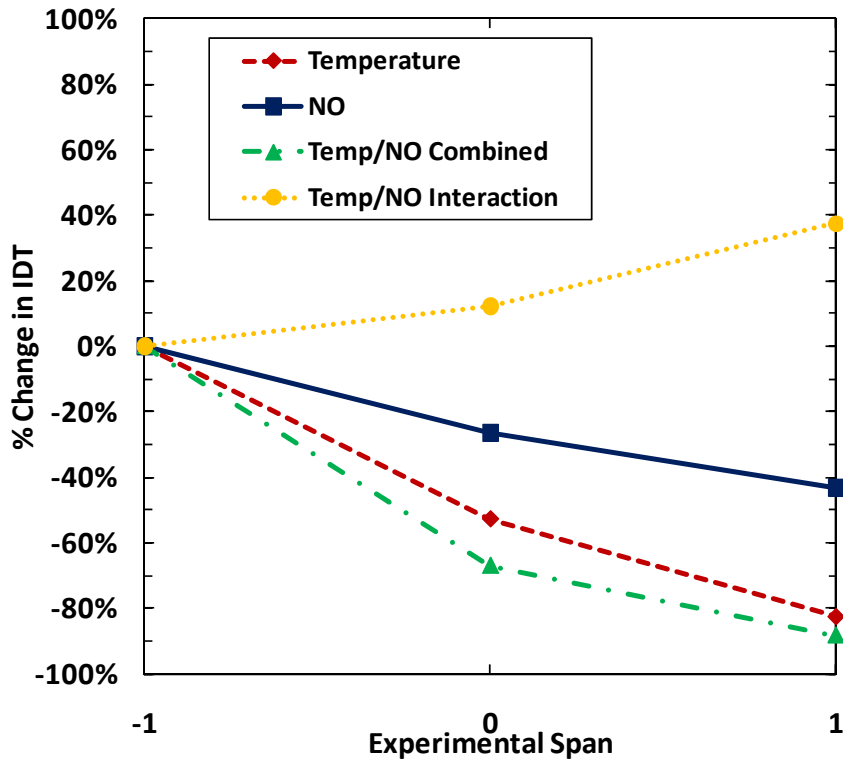


Figure 3–6: Comparison of the averaged main, combined and two-factor interaction effect of temperature and X_{NO} . -1, 0, & +1 values for temperature and X_{NO} are 950, 1038, and 1125 K and 0, 50, and 100 ppm respectively.

Figure 3–6 compares the effect of temperature, NO, and temperature-NO on the ignition delay time of JP-8 over the rank of the design variables. The three points in each curve represent average ignition delay time data for the specific main or combined effect at each of the three variable rankings, -1, 0 and +1. In the case of NO they represent the average of all the tests that contain 0 ppm (12 tests), 50 ppm (32 tests) and 100 ppm NO (12 tests). For the temperature curve they represent the average of tests that were run at 950K

(12 tests), 1038 K (32 tests) and 1125 K (12 tests). In the combined temperature-NO curve, the points represent the average of tests that were run at each of the -1, 0 and +1 levels for both variables i.e. 0 ppm NO and 950 K (2 tests), 50 ppm NO and 1138 K (20 tests), and 100 ppm NO and 1125 K (2 tests). The two-factor interaction effect of temperature and NO is obtained by taking the difference between the combined effect and the sum of both main factor effects. As seen in both **Figure 3–2** and **Figure 3–6**, the interaction effect is positive since the combined effect of temperature and NO does not result in the expected reduction of ignition delay time based on combining the effect of each individual variable.

This significance is further shown through the comparison of the averaged effects of temperature and NO in **Figure 3–7** where the data from **Figure 3–6** is broken down to examine the change in average ignition delay time from the low to high rankings versus both temperature and NO. A reduction, while slightly diminishing, of ignition delay time as temperature increases is shown in **Figure 3–7a**, regardless of the level of NO in the vitiated air. In **Figure 3–7b**, however, it is found that at higher temperatures the relative effect of NO reduces from 50 ppm NO to 100 ppm NO, to the point where the additional 50 ppm has virtually no effect in the highest temperature case.

The reduced effect of nitric oxides on hydrocarbon oxidation as temperature increases has been seen in previous work. Looking again at the study by Bromly et al.[17], experiments were performed using an isothermal flow reactor study examining the oxidation of 200 ppm CH₄ in 5% O₂ and 112 ppm NO (balanced by N₂). Species measurements were made at temperatures ranging from approximately 830 K to 975 K over a residence time of 2.8s. Measurements found that the mole fraction of CH₄ decreases with the rise in temperature, becoming nearly fully oxidized at 930K. The mole fraction of NO was

increasingly consumed in flows with temperatures up to 875 K. However, at higher temperatures, the NO concentration began to rise back up towards initial levels. This finding signifies the reduced ability of the NO to enhance reaction rates at higher temperatures.

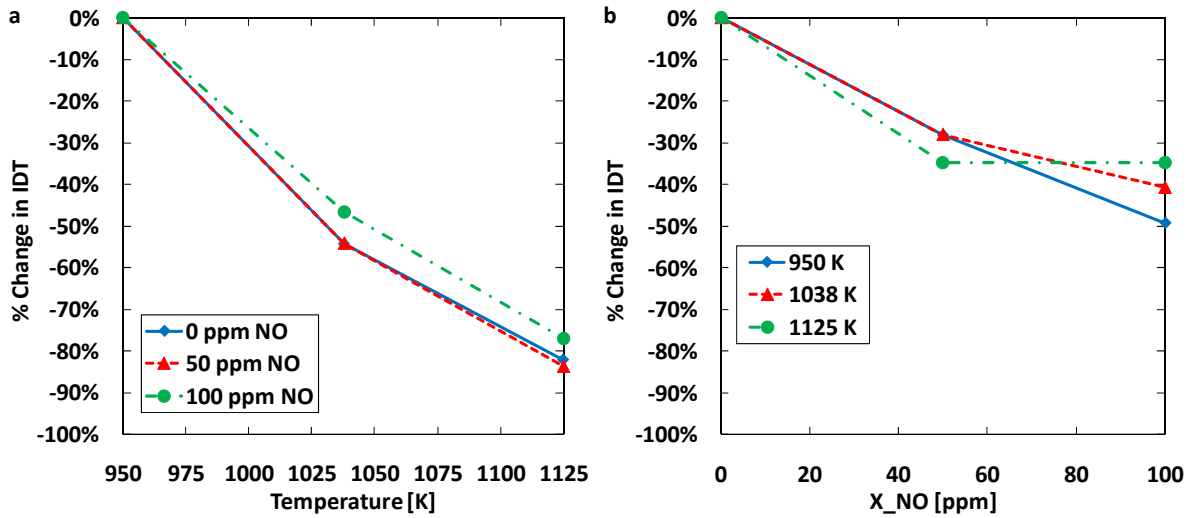


Figure 3-7: Comparison of the averaged effects of temperature and X_{NO} .

Chapter 4: Detailed Study - Results and Discussion

4.1 Tables of Results

A tabular version of the results of the detailed investigation are located in the **Appendix** in **Table 0-6**, **Table 0-7**, and **Table 0-8** and are broken up into three categories: atmospheric results of JP-8 and O₂/N₂/NO mixtures, sub-atmospheric results of JP-8 and O₂/N₂/NO mixtures, and all results of *n*-decane and O₂/N₂/NO mixtures respectively. Test conditions are represented along with τ_{ig} and the standard error for each test.

Experimental results for the atmospheric JP-8 tests are given in **Table 0-6**. For atmospheric tests conducted with 20% O₂ in the oxidizer, experiments were performed from 700 K to 900 K. Atmospheric tests with 12% O₂ in the oxidizer were conducted from 800 K to 900 K. The temperature range was reduced for 12% O₂ tests due to residence time limitations of the flow reactor apparatus. For both O₂ levels, several tests points did not register ignition or were not performed. These points are shaded out in **Table 0-6**. Experimental results for the sub-atmospheric (0.5 atm) JP-8 tests are given in **Table 0-7**. The sub-atmospheric testing was based off the atmospheric test matrix, **Table 0-5**. Tests were only performed from 800 K to 900 K due to residence time limitations of the flow reactor. Tests for which an ignition event did not occur are shaded out in the table.

In addition to JP-8 ignition testing, the ignition delay time of *n*-decane was examined in this study at certain test conditions in order to compare JP-8 results to a component typically found in surrogate mixtures for chemical kinetic modeling. Baseline tests (free of NO in the oxidizer) were conducted at atmospheric pressure from 900 K to 700 K with 20 vol% O₂ and at 900 K and 850 K with 12 vol% O₂ in the oxidizer. Several tests looking at

the effect of NO across the experimental test spectrum at both of the experimental O₂ concentrations were also conducted with *n*-decane. The results for *n*-decane testing are provided in **Table 0-8**.

4.2 Atmospheric Results

The atmospheric pressure experimental results for JP-8 ignition delay time listed in **Table 0-5** are plotted in **Figure 4-1** and **Figure 4-2** as a functions of initial NO concentration at varying reactor temperatures with 20% O₂ and 12% O₂ in the oxidizer stream, respectively.

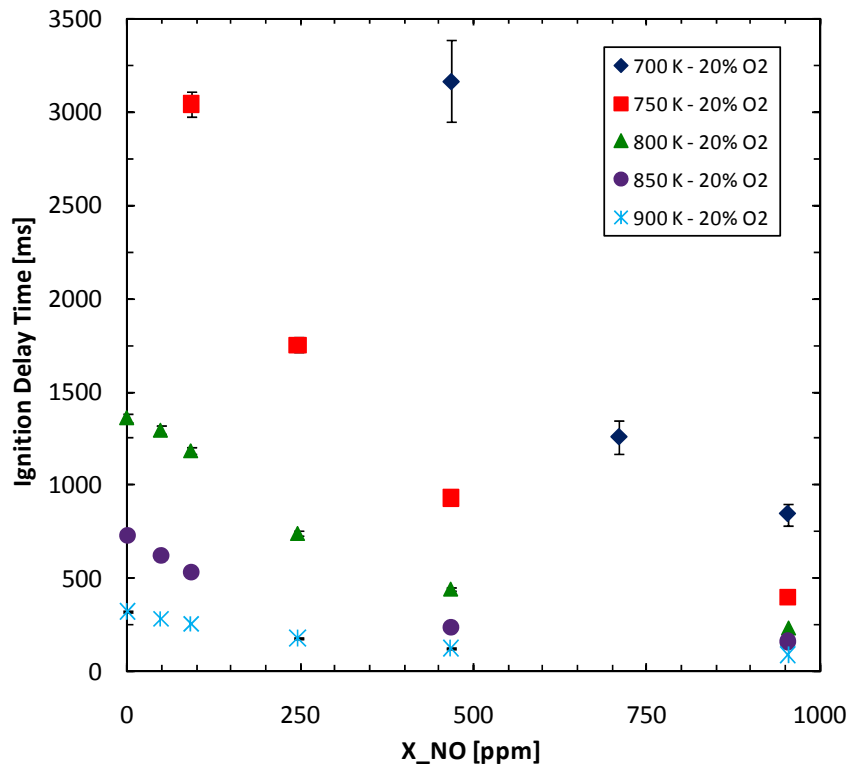


Figure 4-1: Atmospheric ignition delay time results of JP-8 and vitiated air comprised of 20% O₂ and 80% N₂. The average 95% confidence interval for these tests is $\tau_{ig} \pm 2.4\%$.

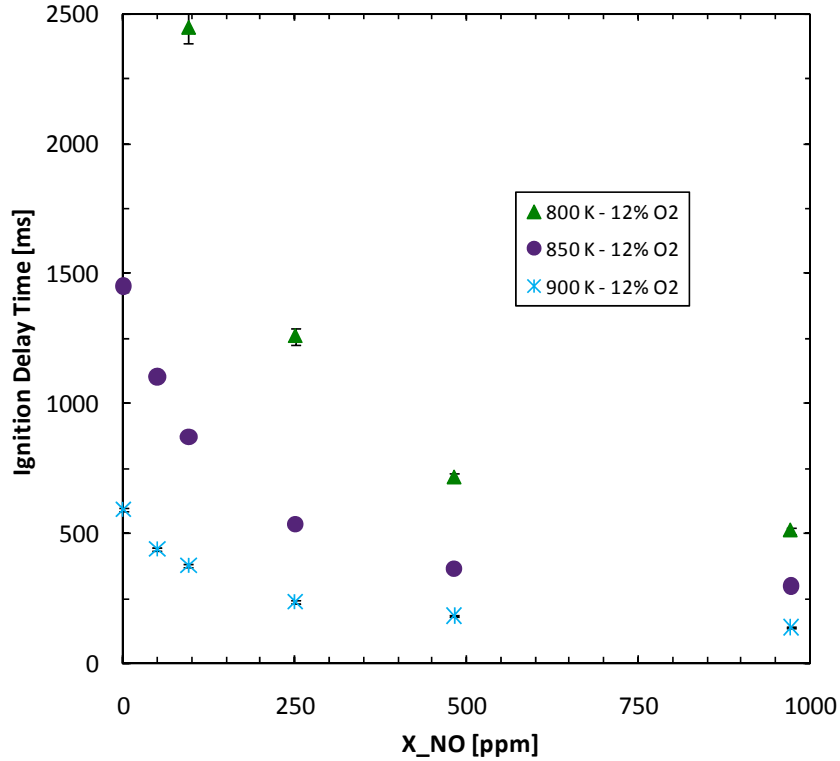


Figure 4–2: Atmospheric ignition delay time results of JP-8 and vitiated air comprised of 12% O₂ and 88% N₂. The average 95% confidence interval for these tests is $\tau_{ig} \pm 1.7\%$.

4.2.1 Direct Effects of Temperature, O₂ and NO on Ignition Delay Time of JP-8

In the screening portion of this study, test temperature as well as the concentrations of O₂ and NO in the oxidizer stream of the reactor were all found to significantly affect ignition of JP-8 at atmospheric conditions, as shown in **Figure 3–1**. Through expanded investigation, the direct effect of each of these design variables are found to be akin to the screening results in the intermediate to high temperature range.

For JP-8/oxidizer mixtures consisting of the same levels of O₂ and NO, increasing temperature by any increment from 700 K to 900 K results in a reduction in ignition delay time. Experimental ignition delay time results of stoichiometric mixtures of JP-8 and air (free of NO in the oxidizer) for both phases of testing in this study are plotted along with previous experimental findings and a surrogate model prediction [4][41] in **Figure 4–3**.

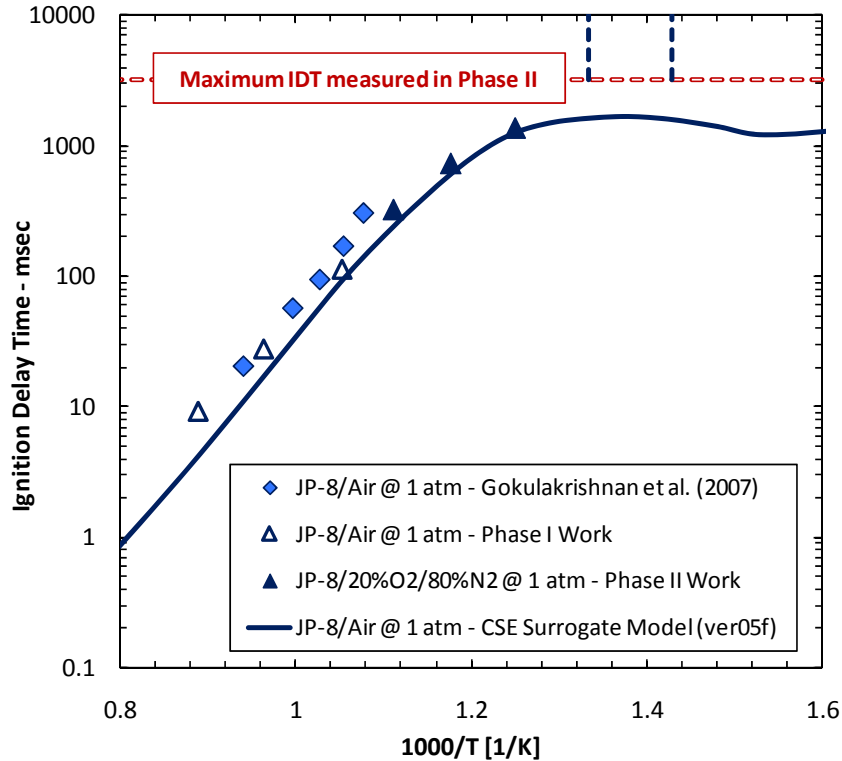


Figure 4-3: Comparison of current and previous experimental IDT of JP-8 4177 to surrogate model prediction[4][41].

For the temperature range in which ignition of atmospheric mixtures of JP-8 and air were measured in study, 800 K to 1125 K, experimental results follow the expected ignition delay time trend based on model predictions within the intermediate to high temperature regime. However, JP-8 ignition was not witnessed at temperatures below 800 K for 20% O₂ cases that did not have NO in the oxidizer stream. Based on calculations of the system residence time and the longest measured ignition delay time in this study, NO-free ignition of JP-8 with 20% O₂ in the oxidizer is at least 3200 milliseconds for the 700 K and 750 K temperature in the current flow reactor rig. As shown in **Figure 4-3**, ignition delay time at these temperatures deviates from the detailed model prediction. Possible reasons for this disparity include the following:

1. The chemical kinetic model used to predict ignition in the transition range from

intermediate to low temperatures over-predicts the NTC effect, resulting in lower ignition times or;

2. The reactor model does not account for aspects of the experimental setup, including the test apparatus and long residence times, that may affect ignition in the NTC region. These include surface effects and diffusion of radicals to the reactor wall that are relevant to NTC kinetics.

Future analysis will examine the role of the apparatus on ignition delay time at low temperatures and apply these experimental findings to modeling techniques.

The results show the effect that varying the O₂ concentration in the oxidizer has on ignition delay time is consistent with the results from the screening study. Reducing the O₂ concentration results in a significant increase in ignition delay time. Results from the screening study show that the average increase in ignition delay time is 50% as O₂ mole fraction is reduced from 21% to 15%. In the detailed investigation, O₂ mole fraction is reduced from 20% to 12% at atmospheric pressure which results in an average increase in ignition delay time of approximately 70%. The maximum and minimum increases are found to be 115% and 32% respectively. This indicates that the two apparatuses are giving consistent results.

As mentioned previously, the effect of even trace concentrations of NO (50 ppm) in the oxidizer significantly affects the ignition time of JP-8. Increasing the oxidizer concentration of NO from 50 ppm to approximately 1000 ppm consistently leads to shorter ignition delay times. This follows suit with the findings of previous studies [22][24], in which the presence of NO in the intermediate to high temperature range enhances the oxidation of highly diluted mixtures of jet fuel surrogates and air. Although the effect that

NO has on JP-8 ignition increased with concentration, it was found to be exponential as shown in **Figure 4-1** and **Figure 4-2**, with ignition reduction reaching a maximum of approximately 80% for the highest concentrations of NO examined. For example, in **Figure 4-1**, at 850 K, approximately 500 ppm NO reduces the ignition delay time from 730 milliseconds to 240 milliseconds, approximately a 67% reduction. However, further addition of up to a total of approximately 1000 ppm NO has a marginal reduction of less than 100 ms in ignition delay time and a total reduction of only 78% from the 0 ppm case as the effect of NO levels off.

4.2.2 Interaction of Temperature with NO

In the screening study, the 21 two-factor interaction effects of all 7 design variables were examined and plotted on a cumulative probability plot, **Figure 3-2**. Results show that a significant interaction between temperature and NO exists in regard to JP-8 ignition at atmospheric pressure and temperatures of 950 K - 1125 K. Continued significance of this interaction is found in the intermediate to high temperature regime of 700 K to 900 K. Evidence of this interaction is seen through the temperature-NO dependence discovered in development of an empirical ignition model, as shown later in **eq. 9** and discussed in section **4.2.4**, as well as through the examination of the level of ignition delay time reduction due to NO as varying test temperatures.

Figure 4-4 and **Figure 4-5** show comparisons of the reduction of the ignition delay time of JP-8 due to NO at atmospheric pressure and with 20% O₂ and 12% O₂ in the oxidizer respectively. **Figure 4-4** shows the ignition delay time results for cases where ignition could occur at 20 % O₂ without any added NO at 800 K, 850 K and 900 K. Similarly at 12 % O₂,

only the 850 K and 900 K cases are shown **Figure 4–5** given for the same reason. For the 20% O₂ cases, the percent reduction in ignition delay time at 850 K is consistently higher than that of 900 K for all cases with an initial concentration of NO in the oxidizer. A similar trend is found for the 12% O₂ cases, in which reduction is higher at 850K compared to 900 K for all initial NO concentration of 100 ppm and higher. For the 20% O₂ case, the average difference in reduction between these two temperatures is ~6% while the average difference is only ~4% for the 12% O₂ case.

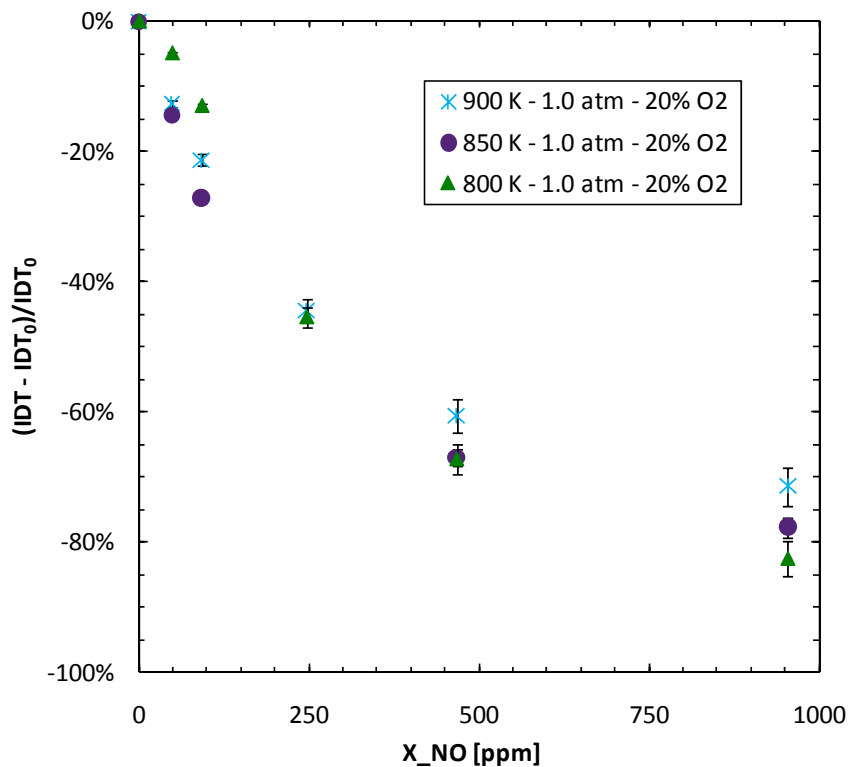


Figure 4–4: Comparison of temperature-NO interaction on reduction of atmospheric JP-8 ignition and vitiated air comprised of 20% O₂ and 80% N₂.

The reduction in ignition delay time at 800 K trends differently than at 850 K and 900 K cases at 20% O₂ level as shown in **Figure 4–1** and **Figure 4–4**. While the overall shape of the ignition delay time and reduction curves at 850 K and 900 K are exponentially convex,

for initial NO concentrations of 250 ppm and below, the 800K curve differs from the higher test temperatures and is concave in this NO concentration range. The percent reduction in ignition delay time at 800 K is also smaller than the corresponding tests at both the 850 K and 900 K for initial NO concentrations below 250 ppm. For initial NO concentrations of 250 ppm and higher, reduction levels are larger at 800 K than those at either 850 K or 900 K.

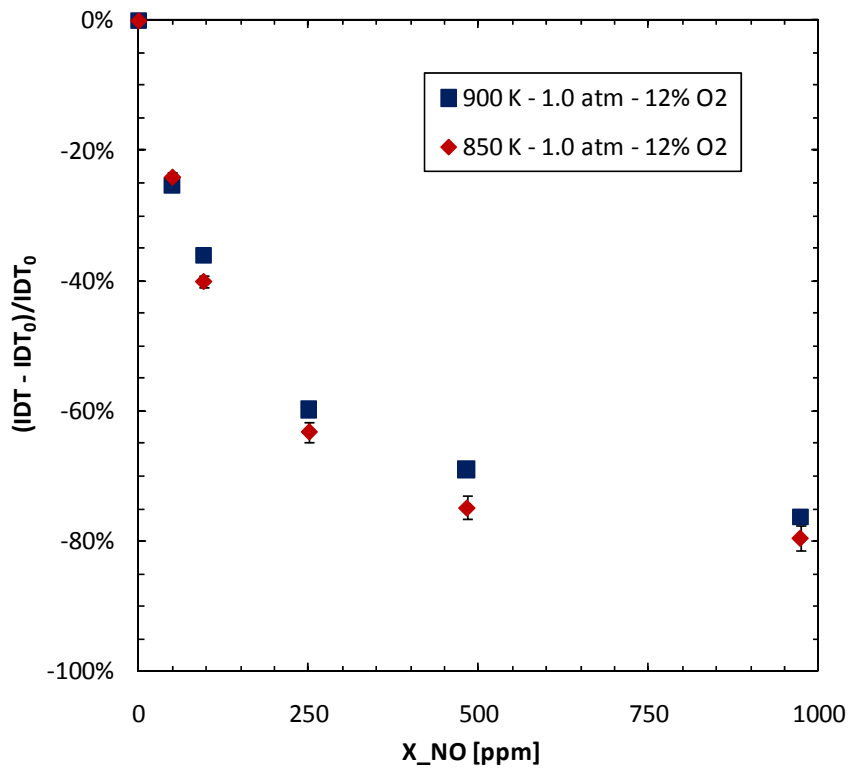


Figure 4–5: Comparison of temperature-NO interaction on reduction of atmospheric JP-8 ignition and vitiated air comprised of 12% O₂ and 88% N₂.

Two possible reasons for this variation in ignition delay time reduction trends can be considered at this point. The first is that the measurements are inaccurate and the trend is a false representation of the effect of NO in this regime. While a possibility, average 95% confidence interval for the data shown in **Figure 4–4** is $\pm 1.6\%$, due to high repeatability of the ignition delay time measurements. Another possibility is that the reaction chemistry of

JP-8 has begun to shift from the high temperature regime to the intermediate temperature regime, resulting in varied effect of NO on ignition. As shown in **Figure 4–3**, 800 K appears, based on the validated surrogate model, to be within the intermediate temperature regime for which ignition chemistry becomes influenced by the NTC effect for non-vitiated combustion of JP-8. This shift in chemistry results in different reaction pathways for the oxidation of JP-8 but also variation in the effect of NO on ignition as well. Studies by Moréac et al. [22] and Dubreuil et al. [24] found that for heavily diluted mixtures of jet fuel surrogate components and mixtures (*iso*-octane, *n*-heptane, and toluene), the presence of 50 ppm to 500 ppm of NO enhances oxidation in the high temperature regime, but significantly inhibits it at low to intermediate temperatures.

Unfortunately, ignition measurements were unable to be made at temperatures below 800 K without the presence of NO, preventing further analysis of its effect on ignition delay time reduction and a single temperature case does not allow for strong conclusions to be made regarding the effect on ignition that NO has as temperatures transition from high to intermediate and low temperature regimes. The fact that ignition did occur and decreased exponentially for the cases with NO in the oxidizer suggests that its presence in large enough concentrations does enhance ignition down to 700 K. It must be noted, however, that questions remain regarding possible experimental effects (i.e. surface effects and radical diffusion discussed in section 4.2) could alter the reaction pathways being used for oxidation and therefore further analysis is necessary to fully understand this phenomena.

4.2.3 Interaction of O₂ with NO

As shown in **Figure 3–2**, the only interaction effect examined in the screening study

that falls outside the range of normal probability is that of temperature and NO, which has a normalized effect value of 0.118 (compared to a value of 1.0 for temperature). The interaction of NO and other screening design variables are found to have comparatively low significance within the envelope of conditions tested in the screening study. For example, the interaction of O₂ and NO has a normalized effect value of only 0.034 as listed in **Table 0-4**. In the detailed investigation, however, the interaction of NO and O₂ was examined in further detail and is found to have a measureable effect on the ignition delay time of JP-8 in the expanded experimental conditions, i.e. lower temperatures and a larger range of initial NO concentration. **Figure 4-6** compares the reduction of the ignition delay time of JP-8 with 20% O₂ vs. 12% O₂ in the oxidizer at atmospheric pressure and reactor temperatures of 850 K and 900 K. The results plotted in **Figure 4-6** show that reducing the concentration of O₂ in the oxidizer stream enhances the effect of NO to reduce ignition delay time. This is determined from the observation that the average percent reduction in ignition delay time at the 12 % O₂ level is larger than that of the 20% O₂ level for both constant temperature cases at 850 K and 900 K.

At 850 K, the average difference in the percent reduction of ignition delay time between the 12% O₂ and 20% O₂ cases is approximately 8% with the largest differences of 10% and 13% corresponding to initial NO concentrations of 50 ppm and 100 ppm respectively. At 900 K, the average difference across all NO concentrations is larger, approximately 11%, with a maximum difference of 15% corresponding to initial NO concentrations of 50 ppm and 100 ppm. In both temperature cases, the smallest difference in reduction is found with approximately 1000 ppm NO in the oxidizer. At 850 K the difference is only 2%, while at 900 K it increases to 5%. Based on these differences, the

effect that NO has on ignition delay time of JP-8 is found to be measurably coupled with the level of O₂ in the oxidizer. It is also observed that the temperature and initial NO concentration of the system affects this coupling. As temperature decreases, the interaction effect of NO and O₂ decreases as well, based on the smaller differences in ignition delay time reduction. Also, when larger concentrations of NO are present in the oxidizer, e.g. 1000 ppm, the difference in ignition delay time reduction is very small between the 12% O₂ and 20% O₂ cases. This, along with the asymptotic shape of the reduction curve, suggests that NO can only enhance oxidation so far, even as ignition inhibitors such as lower temperature or O₂ concentration increase.

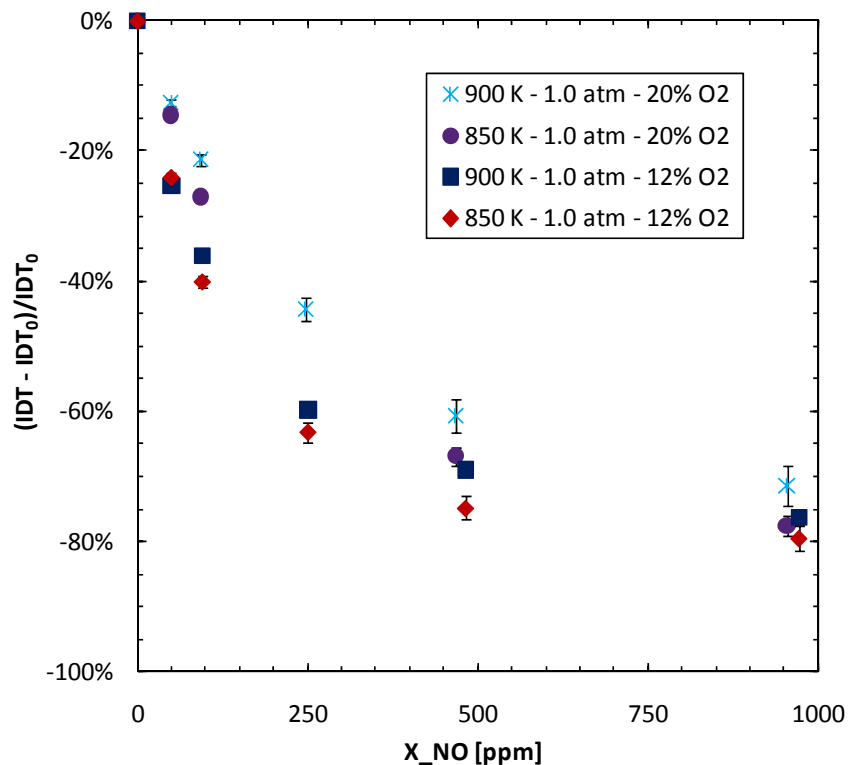


Figure 4-6: Comparison of O₂-NO interaction on reduction of atmospheric JP-8 ignition and vitiated air at 850 K and 900 K.

4.2.4 Empirical Ignition Delay Time Correlation

As found in previous works [40][39][44][59], the ignition delay time of hydrocarbon fuels in the high-temperature oxidation regime can be predicted using some form of the Arrhenius equation:

$$\tau_{ign} = A \exp\left(\frac{E}{RT}\right) \quad \text{eq. 5}$$

where A is an empirical coefficient, E is the global activation energy, R is the universal gas constant, and T is the system temperature. The effect of composition variation on ignition, namely fuel or oxidizer, is typically represented in the following modified form of the equation [39]:

$$\tau_{ign} = A \exp\left(\frac{E}{RT}\right) [\text{Fuel}]^m [\text{Oxygen}]^n \quad \text{eq. 6}$$

where [Fuel] and [Oxygen] are the respective concentrations of fuel and O_2 in the reactant stream. The empirical coefficients m and n represent the power dependency that τ_{ign} has on fuel and O_2 respectively.

As discussed previously, temperature, NO and O_2 are each found to influence ignition both individually as well as coupled with the other design variables (i.e. the NO-temperature interaction). In order to determine an empirical correlation for ignition delay time that accounts for each of these variables, the effect of NO for a constant temperature and O_2 concentration is first examined. For a given *constant* temperature and oxidizer O_2 concentration, the approximation of ignition delay time with respect to NO concentration can be predicted by an equation of the following form:

$$\tau_{ign} = C \exp(-bX_{NO}) \quad \text{eq. 7}$$

where [NO] is the initial concentration of NO in the oxidizer, C is an empirical coefficient related to temperature and O_2 content for a given curve, and b is an empirical constant related to the concentration of NO in the oxidizer stream and its effect on ignition.

This equation can be expanded upon to also account for multiple temperatures and O_2 concentrations by separating it into two parts. The coefficient C from **eq. 7** at a given temperature and O_2 concentration can be converted to an empirical function with respect to temperature and O_2 written in the following Arrhenius form similar to **eq. 6**:

$$C(T, X_{O_2}) = A' X_{O_2}^{-\gamma} \exp\left(\frac{E' X_{O_2}^{-\beta}}{RT}\right) \quad \text{eq. 8}$$

where [O_2] is the concentration of O_2 in oxidizer, T is the reactor temperature, and R is the universal gas constant. A' and E' represent the Arrhenius coefficient and global activation energy components of the equation, respectively. β and γ are exponential coefficients for O_2 . The coefficient b from **eq. 7**, used to determine the effect of NO at a specific temperature, can also be converted to an empirical function with respect to different temperatures in the following temperature dependent power function:

$$b(T) = \frac{b' T^{-\alpha}}{RT} \quad \text{eq. 9}$$

where T is the reactor temperature, R is the universal gas constant, b' represents the effect of NO on activation energy, and α is a coefficient that represents the power dependence the effect of NO has with temperature. The function $b(T)$ is in the same form as the activation energy component within the exponential of the Arrhenius equation shown in **eq. 5**.

Implementation of the sub-functions $C(T, [O_2])$ and $b(T)$ from **eq. 8** and **eq. 9** respectively into **eq. 7** results in the following modified form of an Arrhenius expression to predict the ignition delay time of JP-8 in and $O_2/N_2/NO$ oxidizer stream:

$$\tau_{ign} = A' X_{O_2}^{-\gamma} \exp\left(\frac{E' X_{O_2}^{-\beta} - b' X_{NO} T^{-\alpha}}{RT}\right) \quad \text{eq. 10}$$

Values for the empirical constants in **eq. 10** were determined using the atmospheric pressure experimental JP-8 ignition delay time data from **Table 0-6**. The following empirical correlation can be used to predict the ignition delay time of stoichiometric JP-8/ $O_2/N_2/NO$ mixtures at the atmospheric pressure test conditions used in the detailed portion of this study (i.e., temperature: 700 K – 900 K; NO: 0 ppm – 1000 ppm; O_2 : 12% - 20%):

$$\tau_{ign} = 5.31e-07 * X_{O_2}^{-0.425} * \exp\left(\frac{20700 * X_{O_2}^{-0.0487} - 1.23e12 * X_{NO} * T^{-1.934}}{RT}\right) \quad \text{eq. 11}$$

where τ_{ign} is in seconds, X_{O_2} and X_{NO} are mole fractions, T is in Kelvin, and R is in cal/mol-K. The model predictions based on the empirical correlation in **eq. 11** are compared with the experimental data in **Figure 4-7** and **Figure 4-8**. The average goodness of the fit as well as the goodness for each isotherm is provided in **Table 4-1**.

Table 4-1: Goodness of Emperical Model Fits at 1 atm

1 atm - 20 vol% O_2		1 atm - 12 vol% O_2	
Temperature [K]	R^2	Temperature [K]	R^2
900	92.6%	900	78.3%
850	90.2%	850	77.4%
800	96.8%	800	85.8%
750	95.1%		
700	95.0%		
20% vol O_2 Avg.	94.0%	12% vol O_2 Avg.	80.5%
1 atm Average		$R^2 = 88.9\%$	

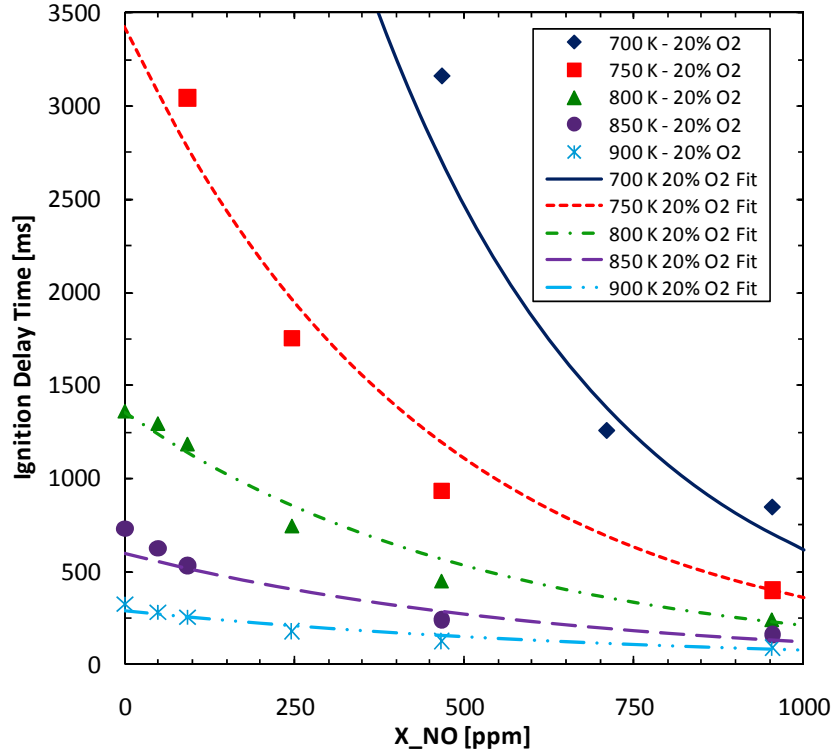


Figure 4-7: Atmospheric ignition delay time results of JP-8 and vitiated air comprised of 20% O₂ and 80% N₂ with emirical predictions using eq. 11.

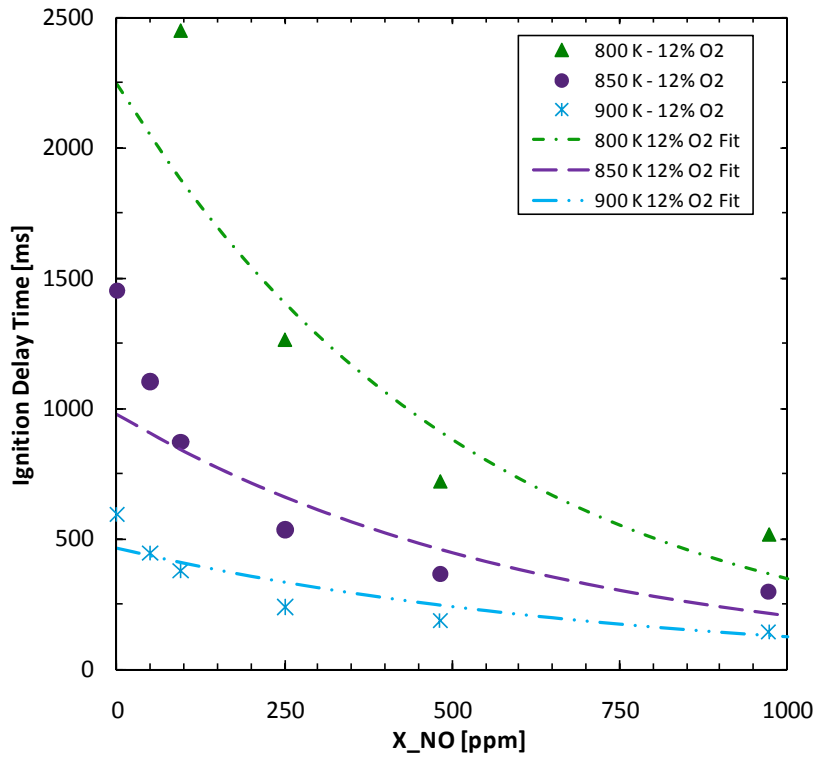


Figure 4-8: Atmospheric ignition delay time results of JP-8 and vitiated air comprised of 12% O₂ and 88% N₂ with emirical predictions using eq. 11.

The parameters from **eq. 10** and their values given in **eq. 11** can be used to better understand how NO, temperature, and O₂ affect the ignition delay time as well as through interaction with other the other design variables. Typically the concentrations of fuel or oxygen are represented as power functions outside of the exponential term of an Arrhenius equation used for ignition delay time, as seen in **eq. 6**. The presence of NO is found to directly affect the activation energy of the system. As the initial oxidizer concentration of NO increases, the value of the NO term, $b'X_{\text{NO}}T^{-\alpha}$, increases as well, resulting in an overall reduction in the activation energy of the system. The effect of NO_x on activation energy of the system has been observed before in the ignition study performed by Dabora [15]. In this study, concentrations of NO₂ ranging from 0 to 2 mol% were added to stoichiometric mixtures of methane and air. It was observed that as the concentration of NO₂ increased, both the ignition delay time of the mixture and the activation energy of the system decreased. Activation energy decreased by 24% with an initial NO₂ concentration of 0.12% and by 51% with an initial NO₂ concentration of 1% to 2%. The results support the findings in this study in which an initial NO concentration of 954 ppm (20% O₂ and 1 atm case) reduces the activation energy of the system by 38% compared to the similar case without an initial presence of NO in the oxidizer stream. Using the model prediction, this reduction in activation energy is calculated to be 36%. The reductions in activation energy for the experimental data and the model predictions are calculated from the Arrhenius plot shown in **Figure 4–9**. The calculated values for E in **Figure 4–9** are temperature averaged.

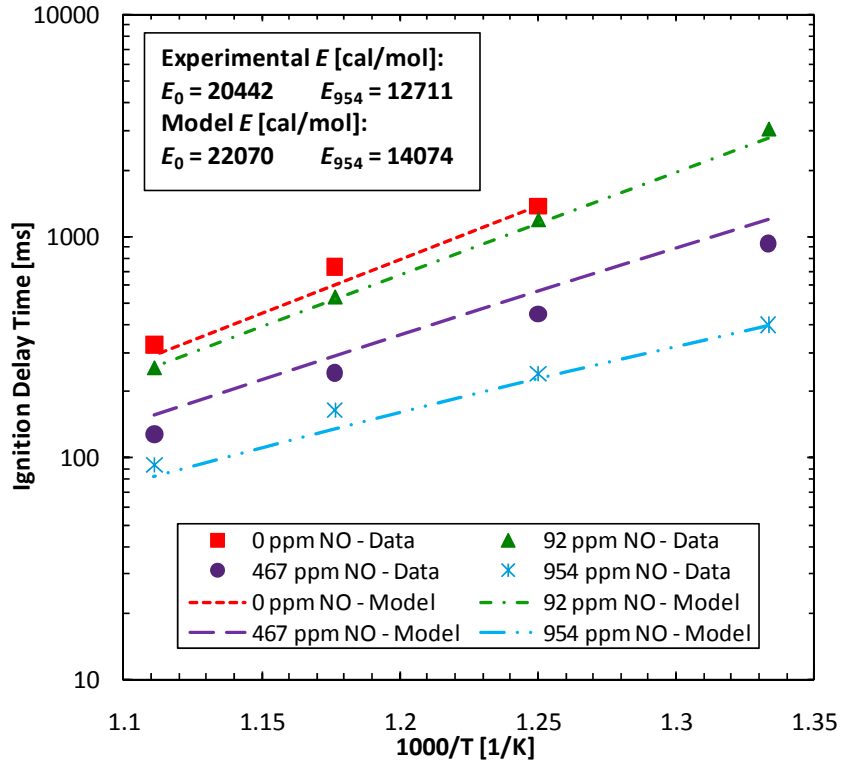


Figure 4-9: Arrhenius plot for atmospheric ignition delay time results of JP-8 and vitiated air comprised of 20% O₂ and 80% N₂ with empirical predictions.

Temperature is represented in two parts of **eq. 11**. The first, T , is in the denominator of the exponential function and is the same temperature component found in a traditional Arrhenius rate equation (**eq. 5**). Combined with A' and E' , this temperature component determines the effect of temperature on ignition delay time without regard to the O₂ and NO concentrations in oxidizer stream. Through its presence in the denominator, it's shown that increasing the temperature of the system reduces the magnitude of the exponential function, thereby lowering the overall ignition delay time of a given set of conditions. The second temperature component, $T^{-\alpha}$, is a power function found in the numerator of the exponential function and is connected to the concentration of NO in the oxidizer stream. For cases with 0 ppm NO in the oxidizer, this temperature component is nullified since the NO component of the activation energy goes to zero. For cases with NO in the oxidizer, however, the

temperature-NO interaction is determined by this component. The negative coefficient, -1.934, from the fit in **eq. 11**, signifies that increased temperatures lower the effect that NO has on the activation energy of the system and therefore also lower the effect of NO on enhancing oxidation and reducing ignition delay time.

The concentration of O₂ in the oxidizer is also found in two components of the ignition delay time prediction equation. The first component is found outside of the exponential, $X_{O_2}^{-\gamma}$ and is analogous to the [Oxygen] term in **eq. 6**. As O₂ concentration decreases, the value of this O₂ component increases, corresponding to an increase in the ignition delay time of the system. The second O₂ concentration component, $X_{O_2}^{-\beta}$ is found in the numerator of the exponential function linked to the activation energy of the system. As O₂ concentration decreases, there is a small increase of the activation energy (approximately 2% as the concentration of O₂ decreases from 21% to 12%) due to this term. The exponential O₂ component is linked to the effect of NO as its effect on the activation energy becomes more significant as increasing concentrations of NO lower the overall activation energy of the system.

Due to having a larger data set, the empirical model, **eq. 11**, was tuned to better fit the 20% O₂ data than the 12% O₂ data. The larger deviation of the empirical model in **Figure 4–8** compared to **Figure 4–7** is partially due to this fact. The deviation in the shape of the empirical curves to the measured data in **Figure 4–8** also suggests that a stronger relationship between O₂ and NO exists than that presented in **eq. 10**, especially for lower concentrations of NO. However, due to the investigation of only two concentrations of O₂, this relationship has not been developed further as part of the empirical IDT correlation. Even with the need to better understand the relationship between O₂ and NO, the empirical correlation **eq. 11**,

does provide a solid method to predict ignition delay time and how it is influenced by NO within these temperature and O₂ regimes.

4.3 Sub-Atmospheric Results

Measurements of the ignition delay time of JP-8 at sub-atmospheric pressure and the investigation of the corresponding effects of temperature, O₂ and NO were also performed at 0.5 atm using 12% and 20% O₂ in the oxidizer in the detailed study. The sub-atmospheric ignition delay time results provided in **Table 0-7** are plotted in **Figure 4-10**. It can be seen that the overall effects of temperature, O₂ and NO on ignition delay time at 0.5 atm are very similar to those found at the atmospheric pressure tests. Experimental results also show that reducing the pressure from 1.0 atm to 0.5 atm corresponds to an increase in ignition delay time for JP-8 as expected. Ignition across the full range of initial NO concentration was measured at 900 K for both mixtures with 12% O₂ and 20% O₂. For tests performed at 800 K and 850 K, limitations in the residence time of the flow reactor resulted in measurable ignition only occurring with the presence of NO in the oxidizer.

Comparison of the reduction of ignition delay time of JP-8 at both pressures at 900 K is provided in **Figure 4-11**. Decreasing the system pressure from 1.0 atm to 0.5 atm at 900 K and with both 20% and 12% O₂ in the oxidizer results in greater reduction of ignition delay time as the NO concentration is increased to 1000 ppm. For the 20% O₂ cases, the average difference in ignition delay time reduction between 0.5 and 1.0 atm is approximately 11%, ranging from 17% with approximately 100 ppm NO in the oxidizer down to 5% when approximately 1000 ppm NO is present. With 12% O₂ in the oxidizer, two aspects of the reduction are of note. The first is that an inflection in reduction curve occurs from 0 ppm to

100 ppm NO at 0.5 atm. With 50 ppm NO in the oxidizer, the reduction in ignition delay time is approximately 9% compared 25% under the similar conditions at atmospheric pressure. The inflection seen in the 0.5 atm / 900 K / 12% O₂ ignition delay time reduction curve is similar to the inflection found in the 1.0 atm / 800 K / 20% O₂ curve in **Figure 4–1**.

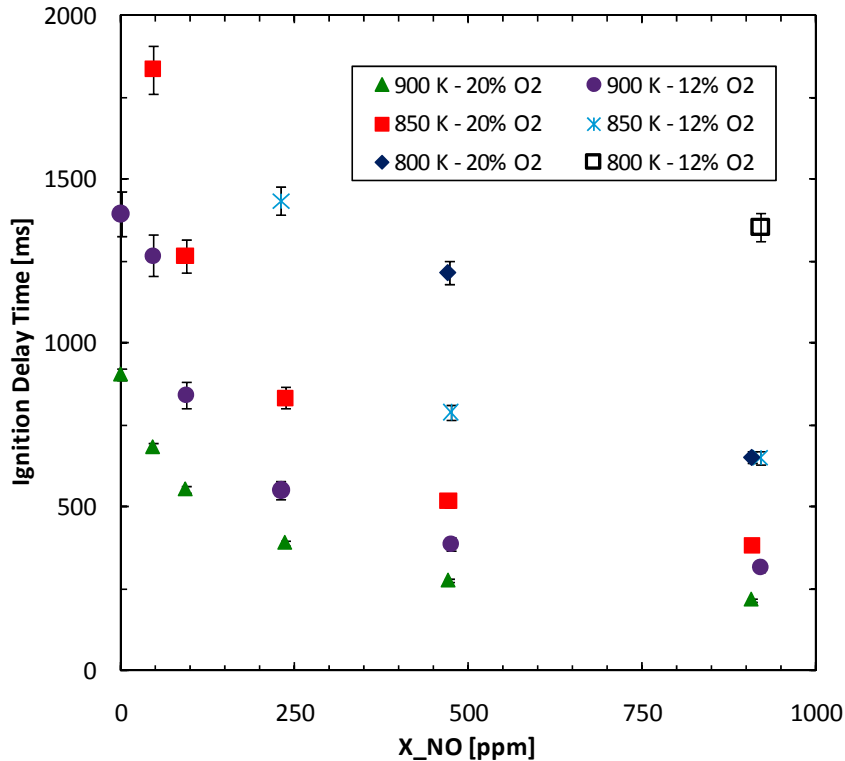


Figure 4–10: Sub-atmospheric ignition delay time results of JP-8 and vitiated air comprised of 20% O₂/80% N₂ and 12%O₂ /88% N₂.

The second notable aspect occurs after the inflection point from 100 ppm to 1000 ppm NO addition to the oxidizer. **Figure 4–11** shows that although the reduction of ignition delay time at 12% O₂ is larger than that at 20% O₂, the difference is very small. As NO is added in concentrations from 100 ppm to 1000 ppm, the average difference in reduction is only approximately 1%. The small difference in reduction seen between the 1.0 atm and 0.5 atm cases with 12 vol% O₂ in the oxidizer suggests that, similar to the interaction of NO and

O₂ at lower temperatures, the effect of NO enhancement on the reduction of ignition delay time approaches a limit even as variables that inhibit ignition are increased and that the majority of the effect of NO occurs in lower concentrations.

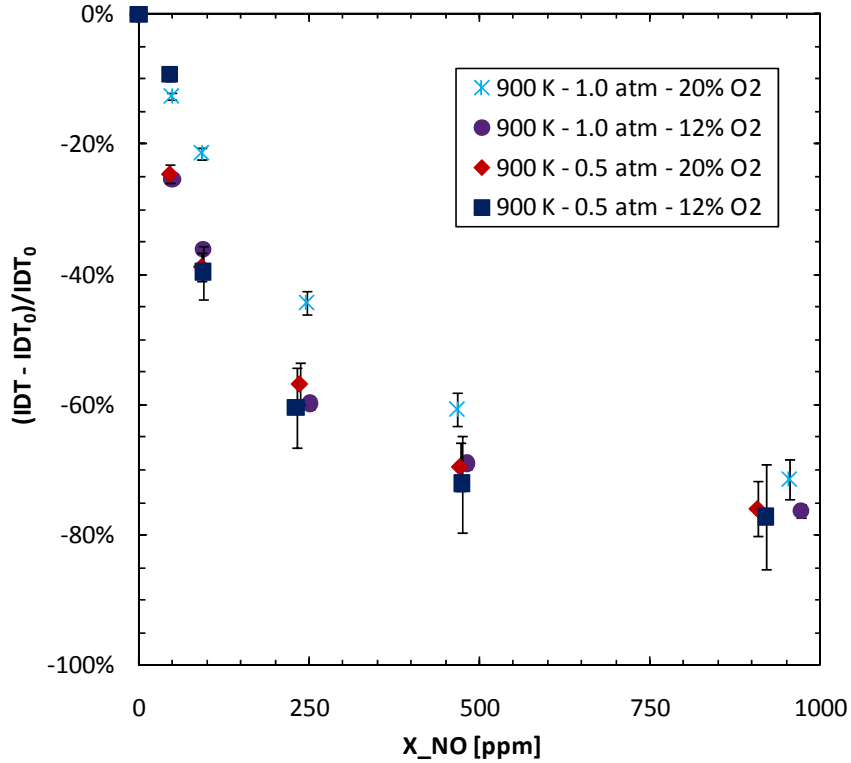


Figure 4-11: Comparison of the relative reduction of JP-8 ignition delay time from the 0 ppm NO condition along 900 K temperature test cases at 0.5 and 1.0 atm with vitiated air comprised of 20% O₂/80% N₂ and 12%O₂ /88% N₂

The limited number of sub-atmospheric data points obtained in this investigation currently prevent implementation of the contribution of pressure into the empirical model for ignition delay time shown in **eq. 11**. It can be hypothesized, however, that the effect of pressure will contribute similarly to the effect of O₂. As pressure is reduced, the available data shows that the ignition delay time of JP-8 shifts to a higher range and that the shape of the curve with respect NO concentration sharpens at lower concentrations, much like the effect of O₂ reduction. Further study across an expanded range of pressure, O₂ concentration

and temperature will increase the ability to model these effects in relation to their interaction with NO on jet fuel ignition.

Chapter 5: Summary, Conclusions, and Future Work

The overall goal of this research is to better understand the ignition behavior of multi-component jet fuels at low pressure, vitiated conditions across the range of intermediate to high temperature regimes in order to improve combustor design and predictive kinetic model capabilities. Examination of the autoignition of JP-8 under conditions relevant to those found in low pressure, vitiated combustors provides insight into the chemical kinetics of these systems as well as a key tool in the development of chemical kinetic models. In order to obtain this information, this study was broken down into two phases: a screening study used to determine which components of vitiated air are most significant to the autoignition of jet fuel and a detailed investigation of these components, with special attention paid to the effect of nitric oxide. A concise summary of the results discussed in the previous chapters are provided in the following sections followed by conclusions and a look into future work.

5.1 Summary of Results

5.1.1 Summary of Screening Study Results (Phase I)

The first testing phase examined the effect of vitiated conditions on the autoignition of jet fuels at low pressure through a broad experimental program looking at the ignition delay time of JP-8 in an atmospheric flow reactor. A rotatable design of experiment approach, the Box-Behnken Design (BBD), that allowed for the examination of both the main and two-factor interaction effects of 7 experimental variables in an efficient manner was used for the screening study. The BBD established a test matrix with 56 unique experimental combinations of 7 design variables: temperature, equivalence ratio and the concentration of CO₂, CO, H₂O and NO. The ranges of these variables can be found in

Table 0-1. Of the 7 main effects and 21 two factor interaction effects, four were found to be statistically significant to vitiated combustion: temperature, O₂ reduction, the presence of initial concentrations of NO and the interaction of NO and temperature. The results of the screening study can be found in **Table 0-2**, **Table 0-3**, and **Table 0-4**.

The results of most interest are the direct effect of NO as well as how its effect changes with temperature. Within the design of this study, the addition of 100 ppm of NO to the vitiated air stream results in an average reduction in the ignition delay time of JP-8 by approximately 40%. Regardless of the other vitiated composition components or test temperatures, the addition of NO consistently results in a reduction in ignition delay time. The effect of NO is also temperature dependent in that it appears to be more effective at reducing ignition delay time as temperature is lowered. It is postulated that a catalytic effect of NO promotes the oxidation of JP-8 at lower temperatures. Based on the results of this screening study, further experimentation to investigate the effect of NO at lower temperatures, as well as lower O₂ concentrations and pressures was undertaken in detailed portion of this study.

5.1.2 Summary of Detailed Investigation Results (Phase II)

The second phase of testing investigated the effects of temperature, O₂ oxidizer concentration and the initial concentration of NO in the oxidizer stream in more detail than the screening study as well as at lower temperatures and pressures that are relevant to combustors using gas turbine exhaust as all or part of their oxidizer stream [3]. Examining the results of the detailed investigation, provided in **Table 0-7** and **Table 0-8**, the following effects were observed by varying the four main design variables of temperature, NO

concentration in the oxidizer, O₂ concentration in the oxidizer, and system pressure:

- increasing the steady temperature of the reactor within the range of 700 K to 900 K reduces ignition delay time,
- increasing the initial concentration of NO in the oxidizer within the range of 0 ppm to 1000 ppm reduces ignition delay time,
- decreasing the concentration of O₂ in the oxidizer from 20 % to 12% increases ignition delay time,
- and decreasing the pressure of the reactor from 1.0 atm to 0.5 atm increases ignition delay time.

The effect of NO was found to be coupled with temperature, O₂ concentration and pressure. The reduction in ignition delay time by NO was generally found to be larger as temperature, O₂ concentration or pressure were reduced. This was not always the case however, as the effect of small traces of NO (50 - 100 ppm) was lessened at 800 K for 20% O₂ atmospheric cases compared to 850 K and 900 K. This difference in reduction is possibly related to the proximity of 800 K to the transition to the NTC reaction region, denoting different chemical pathways for oxidation and ignition. The interaction found between temperature and NO was expected based on the significance of the interaction in the screening study. The interaction between NO and O₂ was not found to be significant in the screening study, however in the detailed investigation its effect was found to be quite measureable.

Ignition results obtained in this study were used to develop an empirical correlation to predict ignition delay time of JP-8 at atmospheric pressure in relation to temperature, O₂, and NO concentration. The following empirical correlation can be used to predict the ignition

delay time of stoichiometric JP-8/O₂/N₂/NO mixtures at the atmospheric pressure test conditions used in the detailed portion of this study (i.e., temperature: 700 K – 900 K; NO: 0 ppm – 1000 ppm; O₂: 12% - 20%):

$$\tau_{ign} = 5.31e-07 * X_{O_2}^{-0.425} * \exp\left(\frac{20700 * X_{O_2}^{-0.0487} - 1.23e12 * X_{NO} * T^{-1.934}}{RT}\right)$$

where τ_{ign} is in seconds, X_{O_2} and X_{NO} are mole fractions, T is in Kelvin, and R is in cal/mol-K.

5.2 Conclusions

The objective stated at the beginning of this study is the following: to investigate the role and determine the significance that vitiated conditions have on jet fuel oxidation by acquiring atmospheric and sub-atmospheric pressure ignition delay time data at intermediate to high temperatures using vitiated air comprised of varying compositions of O₂, CO₂, H₂O, CO, and NO in N₂.

Within the envelope of temperature, equivalence ratio, and composition relevant to vitiated combustion at low pressures, the influence of air vitiation significantly effects the ignition of jet fuel. The aspect of vitiation of the greatest interest is the presence of nitric oxides in the oxidizer stream. The presence of NO in trace quantities as low as 50 ppm reduces ignition by 5% - 25% while initial concentrations of NO up to 1000 ppm result in ignition delay reductions of nearly 80%. This phenomenon is important for two reasons. The first is from the aspect of kinetic model development. Current kinetic models account for the fuel-independent pathways of NO_x oxidation of fuels but do not fully describe the fuel dependent pathways related to higher order hydrocarbons and multi-fuel surrogates. The

addition of jet fuel ignition data with NO present in the oxidizer will allow for further development of kinetic models and improved predictive abilities. The second reason for the importance of understanding this phenomenon is from the combustor design point of view. For systems in which ignition is difficult within the prescribed operating envelope, the ability to use NO_x species from a separate exhaust stream can provide the ability to run at a wider range of conditions. Application of the knowledge gained from this and future studies will allow for more efficient vitiated combustors.

5.3 Future Work

The findings of this study have answered certain questions regarding the significance that vitiated combustion plays on jet fuel ignition but they have also raised new topics and issues to be addressed in the future. Important questions remain about the effect of NO and other nitric oxides, especially at temperatures below the intermediate regime.

The aspect of two phases of experimentation in this study provided the opportunity to thoroughly examine the flow reactor apparatus and methodology used in Phase I and then make modifications for improvement in Phase II. Based on the experimental process in Phase II, further improvements could be made for future flow reactor ignition measurements. A constant goal with flow reactor experimentation is the minimization of the uncertainty regarding the transit, mixing, and, in the case of higher temperature tests, heat up time of the fuel and oxidizer prior to entering the constant temperature test section. One improvement could be the implementation of a laser system to make adsorption measurements across the transition from the mixing section to the diffuser and/or from the diffuser to the test section. This technique was used by Beerer [60] in a high pressure and temperature flow reactor to

measure the ignition of natural gas constituents. Not only can this technique assist in determining the time in which the fuel/oxidizer mixture enters the test section, it can also be used to examine the extent of pre-ignition fuel decomposition.

A second possible improvement to the flow reactor apparatus is the examination and reduction of possible wall effects in the flow test section. Alumina tubes are currently used to form the test section of the flow reactor is due to their ability to withstand high temperatures and provide a surface with low chemical reactivity. For tests performed at temperatures above the expected NTC region of JP-8 and *n*-decane, the ignition measurements both with and without initial concentrations of NO behaved differently than would be expected based on previous high pressure ignition [38] and oxidation experiments [23][24][26] in which jet fuel has lower ignition delay times in the NTC region and is inhibited by NO rather than enhanced. A hypothesis for this discrepancy is that the combination of long residence times (greater than 1 second) and a relative small surface area to volume ratio of the flow reactor tube allow for low temperature oxidation radicals to diffuse to the reactor walls. This would result in ignition being driven only by the thermal process and with a diminishing NTC effect. Future testing that examines and possibly limits radical diffusion could be done through variation in bulk dilution (He or Ar vs. N₂), of the surface area to volume ratio of the test section, and of the test section material.

Outside of changes made to the apparatus, examination of expanded ranges of temperature and pressure can also provide further insight. In this study, at temperatures as low as 700 K, small amounts of NO significantly reduce ignition delay time. Ignition data is still lacking however in the low (NTC to sub-NTC) temperature regime where previous fuel oxidation studies[22][24] have found that NO has little or no enhancement effect and in some

cases inhibits oxidation. Further ignition experimentation, possibly at higher pressures to reduce residence times, is necessary to examine the effect of NO at these low temperatures. Further investigation may also include examination of the effects that other NO_x species, NO₂ and N₂O, have on jet fuel ignition.

Another question that arises is in regard to the time scale of ignition and the effectiveness of enhancement by NO at shorter residence times. In the temperature regimes examined in this study there are many cases of ignition times surpassing hundreds of milliseconds, even with the enhancement of nearly 1000 ppm in the oxidizer. While the strong effect that NO has on ignition is quite apparent, for combustion processes within this temperature regime that require residence times much smaller than those required for full autoignition, the effect of NO to enhance oxidation is still not fully known. Examining the intermediate specie generation of jet fuel oxidation due to NO enhancement would provide insight into this issue.

Appendix

A.1 Measurement Variability

As discussed in Chapter 2Chapter 2:, the flow reactor system made use of both gaseous and liquid fluids to measure the ignition delay time of JP-8, *n*-heptane, and *n*-decane in vitiated air. In both phases of testing, gaseous N₂, O₂, CO₂, CO, and NO were supplied via high pressure cylinders. N₂, O₂, and CO₂ were supplied as pure components while CO and NO were supplied as part of certified mixtures balanced with N₂. In Phase II, air was supplied via a compressor. The liquids fuels used in this study, JP-8, *n*-heptane, and were supplied via cylinders pressurized by N₂. Water was supplied via the lab tap.

Each of these fluids was metered using a variable area flowmeter (rotameter) that was calibrated for a specific fluid in the specific rotameter for which it was used. Gaseous calibration was performed using an Elster American Dry Test Meter (DTM-200A) for flow rates of 12 slpm and higher. Gaseous flowrates below 12 slpm were calibrated using a bubble meter. Calibrations with both systems accounted for temperature and pressure corrections. Liquid calibration was performed using graduated cylinders.

Each flowmeter, gaseous and liquid, was calibrated at a minimum of several points spanning the entire range of flowrates examined in this study for a given fluid. Measurements were repeated no less than three times for each rotameter point that was calibrated. For both gaseous and liquid fuels, the reproducibility at a given rotameter point was very good with average standard deviations of approximately 2% of the mean.

Gas analysis measurements were also made in the exhaust stream of the flow reactor to check the composition. In the Phase I screening study, the O₂ concentration of the

oxidizer was verified at 21% for non-vitiated cases. At the end of Phase II, the flowrates of the system were re-verified using the overall exit flow of the reactor and the actual concentrations of O₂ and NO were determined. For the high O₂ cases, the average O₂ concentration was 19.8% with a standard deviation of 0.2%. It's therefore represented as 20% in the results section above. For the low O₂ cases, the average concentration was 11.5% with a standard deviation of 0.1%. It's therefore represented as 20% O₂ in the results section above. The nominal NO concentrations examined in this study were 0, 50, 100, 250, 500, 750 and 1000 ppm, however analysis of the flows determined values that differed from the nominal targets. These actual values are shown in the tables and plots of the Phase II data and were used in the development of the empirical model.

A.2 Test Reproducibility

A.2.1 Phase I Screening Study

Four separate center point tests of the BBD were run for a total of 15 individual test iterations. The standard error (S_E) is defined as follows:

$$S_E = \frac{s}{\sqrt{n}}$$

eq. 12

where s is the standard deviation of a sample and n = the number of samples. For a given test, the sample is represented by the test iterations for that given test point. The overall standard error of the 15 center point ignition delay time measurements is 1.6% of the mean experimental ignition delay time value of 269 ms. This center point error value is used to represent the standard error of the BBD as a whole.

For the individual test cases, the maximum and average standard errors for all tests

are respectively 4.8% and 2.4% of the average mean ignition delay time for a given test. Summing the average standard error with the standard error for the center point, the overall average standard error for the system is approximately 4.0%. For a normal distribution, the upper and lower 95% confidence limits are calculated as follows:

$$\bar{x} \pm (S_E \cdot 1.96) \quad \text{eq. 13}$$

where \bar{x} is the mean of a given sample. Using the overall average standard error, the 95% confidence limits for the experimental ignition delay time measurements are $\pm 7.8\%$ of the mean measured ignition delay time for a given test.

A.2.1 Phase II Detailed Investigation

DOE techniques were not applied in the detailed investigation which aimed to examine the sensitivity of fewer design variables rather than determine the significance of many. Due to significant variations in certain test conditions, namely fuel and pressure, the standard error of these groupings is useful in order to understand variability for different test conditions. The variability of different combinations of tests broken down by pressure and fuel source is provided in **Table 0-1**.

The maximum and mean standard errors for all tests recorded in the detailed study are respectively 12.4% and 2.4% of the mean ignition delay time for a given test. Using this average standard error, the 95% confidence limits for the experimental ignition delay time measurements in the detailed study are $\pm 4.7\%$ of the mean of the measured ignition delay times for all experimental runs of a given test case. The variability for each single test case examined in the detailed investigation is provided in Table 0-7, and Table 0-8. The error and confidence level for all tests examined in the detailed investigation as well as the errors for

significant subsets are provided in **Table 0-1**.

Table 0-1: Measurement Variability - Detailed Investigation

Test Group	Mean τ_{exp}[ms]	Mean SE%	Max SE%	Avg 95% Confidence
All Tests	824	2.4%	12.4%	$\tau_{exp} \pm 4.7\%$
All Tests @ 1.0 atm	843	1.9%	12.4%	$\tau_{exp} \pm 3.8\%$
All Tests @ 0.5 atm	781	3.4%	9.8%	$\tau_{exp} \pm 6.7\%$
All JP-8 Tests	803	2.4%	12.4%	$\tau_{exp} \pm 4.7\%$
All JP-8 Tests @ 1.0 atm	796	2.1%	12.4%	$\tau_{exp} \pm 4.2\%$
All JP-8 Tests @ 0.5 atm	815	2.9%	9.3%	$\tau_{exp} \pm 5.6\%$
All n -C ₁₀ Tests	867	2.4%	9.8%	$\tau_{exp} \pm 4.6\%$
All n -C ₁₀ Tests @ 1.0 atm	918	1.6%	3.9%	$\tau_{exp} \pm 3.2\%$
All n -C ₁₀ Tests @ 0.5 atm	650	5.5%	9.8%	$\tau_{exp} \pm 10.8\%$

A.3 Phase I Screening Study Test and Effects Matrices

Table 0-2: Screening Study Test Matrix and Results

Test #	x_1	x_2	x_3	x_4	x_5	x_6	x_7	Experimental		Corrected
	Temp. [K]	Φ	X_{O_2}	X_{CO_2}	X_{CO}	X_{H_2O}	X_{NO}	τ_{exp} [ms]	Std. Err.%	τ_{ig} [ms]
0	1038	1	18%	3%	0.10%	3%	50	269	1.6%	35.8
1	1038	1	18%	6%	0.20%	6%	50	285	0.7%	41.4
2	1038	1	18%	6%	0.20%	0%	50	277	1.3%	38.7
3	1038	1	18%	6%	0.00%	6%	50	285	1.0%	41.4
4	1038	1	18%	6%	0.00%	0%	50	268	2.4%	35.5
5	1038	1	18%	0%	0.20%	6%	50	256	2.6%	31.2
6	1038	1	18%	0%	0.20%	0%	50	254	1.8%	30.5
7	1038	1	18%	0%	0.00%	6%	50	268	1.4%	35.4
8	1038	1	18%	0%	0.00%	0%	50	261	2.2%	33.0
9	1125	1	18%	3%	0.10%	6%	100	214	3.3%	16.2
10	1125	1	18%	3%	0.10%	6%	0	227	1.2%	20.8
11	1125	1	18%	3%	0.10%	0%	100	194	0.6%	8.9
12	1125	1	18%	3%	0.10%	0%	0	218	4.7%	17.8
13	950	1	18%	3%	0.10%	6%	100	305	1.7%	48.5
14	950	1	18%	3%	0.10%	6%	0	440	4.6%	97.0
15	950	1	18%	3%	0.10%	0%	100	339	3.6%	60.6
16	950	1	18%	3%	0.10%	0%	0	499	2.1%	118
17	1038	1.5	18%	3%	0.20%	3%	100	226	2.2%	23.4
18	1038	1.5	18%	3%	0.20%	3%	0	268	3.5%	39.9
19	1038	1.5	18%	3%	0.00%	3%	100	232	3.1%	26.0
20	1038	1.5	18%	3%	0.00%	3%	0	266	0.9%	38.9
21	1038	0.5	18%	3%	0.20%	3%	100	275	4.0%	24.2
22	1038	0.5	18%	3%	0.20%	3%	0	318	2.6%	42.0
23	1038	0.5	18%	3%	0.00%	3%	100	290	0.9%	30.4
24	1038	0.5	18%	3%	0.00%	3%	0	357	3.0%	58.4
25	1125	1.5	18%	6%	0.10%	3%	50	201	3.7%	13.9
26	1125	1.5	18%	0%	0.10%	3%	50	189	3.5%	9.1
27	1125	0.5	18%	6%	0.10%	3%	50	224	2.7%	3.2
28	1125	0.5	18%	0%	0.10%	3%	50	242	2.4%	10.8

Table 0-2b: Screening Study Test Matrix and Results

Test #	x_1	x_2	x_3	x_4	x_5	x_6	x_7	Experimental		Corrected
	Temp. [K]	Φ	X_{O_2}	X_{CO_2}	X_{CO}	X_{H_2O}	X_{NO}	τ_{exp} [ms]	Std. Err.%	τ_{ig} [ms]
29	950	1.5	18%	6%	0.10%	3%	50	349	4.1%	71.4
30	950	1.5	18%	0%	0.10%	3%	50	353	2.2%	72.8
31	950	0.5	18%	6%	0.10%	3%	50	444	1.4%	94.4
32	950	0.5	18%	0%	0.10%	3%	50	423	1.6%	85.7
33	1038	1	15%	6%	0.10%	3%	100	283	1.1%	40.7
34	1038	1	15%	6%	0.10%	3%	0	354	1.5%	66.3
35	1038	1	15%	0%	0.10%	3%	100	286	0.1%	41.7
36	1038	1	15%	0%	0.10%	3%	0	361	1.6%	68.8
37	1038	1	21%	6%	0.10%	3%	100	243	4.3%	26.4
38	1038	1	21%	6%	0.10%	3%	0	295	2.2%	45.2
39	1038	1	21%	0%	0.10%	3%	100	227	2.8%	20.7
40	1038	1	21%	0%	0.10%	3%	0	265	3.6%	34.2
41	1125	1	15%	3%	0.20%	3%	50	206	0.7%	13.2
42	1125	1	15%	3%	0.00%	3%	50	227	2.1%	20.9
43	1125	1	21%	3%	0.20%	3%	50	207	4.8%	11.8
44	1125	1	21%	3%	0.00%	3%	50	212	4.4%	15.3
45	950	1	15%	3%	0.20%	3%	50	408	2.2%	85.2
46	950	1	15%	3%	0.00%	3%	50	410	1.9%	86.2
47	950	1	21%	3%	0.20%	3%	50	338	2.5%	60.4
48	950	1	21%	3%	0.00%	3%	50	343	2.1%	62.3
49	1038	1.5	15%	3%	0.10%	6%	50	267	3.6%	39.5
50	1038	1.5	15%	3%	0.10%	0%	50	266	1.8%	39.2
51	1038	1.5	21%	3%	0.10%	6%	50	245	2.6%	30.7
52	1038	1.5	21%	3%	0.10%	0%	50	234	1.5%	26.5
53	1038	0.5	15%	3%	0.10%	6%	50	318	2.9%	42.2
54	1038	0.5	15%	3%	0.10%	0%	50	318	3.3%	42.0
55	1038	0.5	21%	3%	0.10%	6%	50	291	2.3%	31.1
56	1038	0.5	21%	3%	0.10%	0%	50	282	1.9%	27.2
NV 950	950	1	21%	0%	0%	0%	0	482	1.1%	111.8
NV 1038	1038	1	21%	0%	0%	0%	0	246	1.8%	27.6
NV 1125	1125	1	21%	0%	0%	0%	0	195	2.8%	9.2

Table 0-3: Matrix of Main Effects

	x_1	x_2	x_3	x_4	x_5	x_6	x_7
Test #	Temp.	Φ	X_{O_2}	X_{CO_2}	X_{CO}	X_{H_2O}	X_{NO}
1	0.0	0.0	0.0	41.4	41.4	41.4	0.0
2	0.0	0.0	0.0	38.7	38.7	-38.7	0.0
3	0.0	0.0	0.0	41.4	-41.4	41.4	0.0
4	0.0	0.0	0.0	35.5	-35.5	-35.5	0.0
5	0.0	0.0	0.0	-31.2	31.2	31.2	0.0
6	0.0	0.0	0.0	-30.5	30.5	-30.5	0.0
7	0.0	0.0	0.0	-35.4	-35.4	35.4	0.0
8	0.0	0.0	0.0	-33.0	-33.0	-33.0	0.0
9	16.2	0.0	0.0	0.0	0.0	16.2	16.2
10	20.8	0.0	0.0	0.0	0.0	20.8	-20.8
11	8.9	0.0	0.0	0.0	0.0	-8.9	8.9
12	17.8	0.0	0.0	0.0	0.0	-17.8	-17.8
13	-48.5	0.0	0.0	0.0	0.0	48.5	48.5
14	-97.0	0.0	0.0	0.0	0.0	97.0	-97.0
15	-60.6	0.0	0.0	0.0	0.0	-60.6	60.6
16	-118.0	0.0	0.0	0.0	0.0	-118.	-118.
17	0.0	23.4	0.0	0.0	23.4	0.0	23.4
18	0.0	39.9	0.0	0.0	39.9	0.0	-39.9
19	0.0	26.0	0.0	0.0	0.0	0.0	26.0
20	0.0	38.9	0.0	0.0	-38.9	0.0	-38.9
21	0.0	-24.2	0.0	0.0	24.2	0.0	24.2
22	0.0	-42.0	0.0	0.0	42.0	0.0	-42.0
23	0.0	-30.4	0.0	0.0	-30.4	0.0	30.4
24	0.0	-58.4	0.0	0.0	-58.4	0.0	-58.4
25	13.9	13.9	0.0	13.9	0.0	0.0	0.0
26	9.1	9.1	0.0	-9.1	0.0	0.0	0.0
27	3.2	-3.2	0.0	3.2	0.0	0.0	0.0
28	10.8	-10.8	0.0	-10.8	0.0	0.0	0.0
29	-71.4	71.4	0.0	71.4	0.0	0.0	0.0
30	-72.8	72.8	0.0	-72.8	0.0	0.0	0.0
31	-94.4	-94.4	0.0	94.4	0.0	0.0	0.0
32	-85.7	-85.7	0.0	-85.7	0.0	0.0	0.0
33	0.0	0.0	40.7	40.7	0.0	0.0	40.7
34	0.0	0.0	66.3	66.3	0.0	0.0	-66.3
35	0.0	0.0	41.7	-41.7	0.0	0.0	41.7
36	0.0	0.0	68.8	-68.8	0.0	0.0	-68.8
37	0.0	0.0	-26.4	26.4	0.0	0.0	26.4
38	0.0	0.0	-45.2	45.2	0.0	0.0	-45.2
39	0.0	0.0	-20.7	-20.7	0.0	0.0	20.7
40	0.0	0.0	-34.2	-34.2	0.0	0.0	-34.2
41	13.2	0.0	13.2	0.0	13.2	0.0	0.0
42	20.9	0.0	20.9	0.0	-20.9	0.0	0.0
43	11.8	0.0	-11.8	0.0	11.8	0.0	0.0
44	15.3	0.0	-15.3	0.0	-15.3	0.0	0.0
45	-85.2	0.0	85.2	0.0	85.2	0.0	0.0
46	-86.2	0.0	86.2	0.0	-86.2	0.0	0.0
47	-60.4	0.0	-60.4	0.0	60.4	0.0	0.0
48	-62.3	0.0	-62.3	0.0	-62.3	0.0	0.0
49	0.0	39.5	39.5	0.0	0.0	39.5	0.0
50	0.0	39.2	39.2	0.0	0.0	-39.2	0.0
51	0.0	30.7	-30.7	0.0	0.0	30.7	0.0
52	0.0	26.5	-26.5	0.0	0.0	-26.5	0.0
53	0.0	-42.2	42.2	0.0	0.0	42.2	0.0
54	0.0	-42.0	42.0	0.0	0.0	-42.0	0.0
55	0.0	-31.1	-31.1	0.0	0.0	31.1	0.0
56	0.0	-27.2	-27.2	0.0	0.0	-27.2	0.0
Main Effect	-780.6	-60.0	194.2	44.8	-41.8	-2.4	-279.5
Normalized Effect	-1.00	-0.08	0.25	0.06	-0.05	0.00	-0.36

Table 0-4: Matrix of Two-Factor Interaction Effects

	T Φ	T O ₂	T CO ₂	T CO	T H ₂ O	T NO	Φ O ₂	Φ CO ₂	Φ CO	Φ H ₂ O	Φ NO
Test #	x1x2	x1x3	x1x4	x1x5	x1x6	x1x7	x2x3	x2x4	x2x5	x2x6	x2x7
1	0.0	0.0	0.0	0.0	0.0	0.0	0.0	0.0	0.0	0.0	0.0
2	0.0	0.0	0.0	0.0	0.0	0.0	0.0	0.0	0.0	0.0	0.0
3	0.0	0.0	0.0	0.0	0.0	0.0	0.0	0.0	0.0	0.0	0.0
4	0.0	0.0	0.0	0.0	0.0	0.0	0.0	0.0	0.0	0.0	0.0
5	0.0	0.0	0.0	0.0	0.0	0.0	0.0	0.0	0.0	0.0	0.0
6	0.0	0.0	0.0	0.0	0.0	0.0	0.0	0.0	0.0	0.0	0.0
7	0.0	0.0	0.0	0.0	0.0	0.0	0.0	0.0	0.0	0.0	0.0
8	0.0	0.0	0.0	0.0	0.0	0.0	0.0	0.0	0.0	0.0	0.0
9	0.0	0.0	0.0	0.0	16.2	16.2	0.0	0.0	0.0	0.0	0.0
10	0.0	0.0	0.0	0.0	20.8	-20.8	0.0	0.0	0.0	0.0	0.0
11	0.0	0.0	0.0	0.0	-8.9	8.9	0.0	0.0	0.0	0.0	0.0
12	0.0	0.0	0.0	0.0	-17.8	-17.8	0.0	0.0	0.0	0.0	0.0
13	0.0	0.0	0.0	0.0	-48.5	-48.5	0.0	0.0	0.0	0.0	0.0
14	0.0	0.0	0.0	0.0	-97.0	97.0	0.0	0.0	0.0	0.0	0.0
15	0.0	0.0	0.0	0.0	60.6	-60.6	0.0	0.0	0.0	0.0	0.0
16	0.0	0.0	0.0	0.0	118.0	118.0	0.0	0.0	0.0	0.0	0.0
17	0.0	0.0	0.0	0.0	0.0	0.0	0.0	0.0	23.4	0.0	23.4
18	0.0	0.0	0.0	0.0	0.0	0.0	0.0	0.0	39.9	0.0	-39.9
19	0.0	0.0	0.0	0.0	0.0	0.0	0.0	0.0	-26.0	0.0	26.0
20	0.0	0.0	0.0	0.0	0.0	0.0	0.0	0.0	-38.9	0.0	-38.9
21	0.0	0.0	0.0	0.0	0.0	0.0	0.0	0.0	-24.2	0.0	-24.2
22	0.0	0.0	0.0	0.0	0.0	0.0	0.0	0.0	-42.0	0.0	42.0
23	0.0	0.0	0.0	0.0	0.0	0.0	0.0	0.0	30.4	0.0	-30.4
24	0.0	0.0	0.0	0.0	0.0	0.0	0.0	0.0	58.4	0.0	58.4
25	13.9	0.0	13.9	0.0	0.0	0.0	0.0	13.9	0.0	0.0	0.0
26	9.1	0.0	-9.1	0.0	0.0	0.0	0.0	-9.1	0.0	0.0	0.0
27	-3.2	0.0	3.2	0.0	0.0	0.0	0.0	-3.2	0.0	0.0	0.0
28	-10.8	0.0	-10.8	0.0	0.0	0.0	0.0	10.8	0.0	0.0	0.0
29	-71.4	0.0	-71.4	0.0	0.0	0.0	0.0	71.4	0.0	0.0	0.0
30	-72.8	0.0	72.8	0.0	0.0	0.0	0.0	-72.8	0.0	0.0	0.0
31	94.4	0.0	-94.4	0.0	0.0	0.0	0.0	-94.4	0.0	0.0	0.0
32	85.7	0.0	85.7	0.0	0.0	0.0	0.0	85.7	0.0	0.0	0.0
33	0.0	0.0	0.0	0.0	0.0	0.0	0.0	0.0	0.0	0.0	0.0
34	0.0	0.0	0.0	0.0	0.0	0.0	0.0	0.0	0.0	0.0	0.0
35	0.0	0.0	0.0	0.0	0.0	0.0	0.0	0.0	0.0	0.0	0.0
36	0.0	0.0	0.0	0.0	0.0	0.0	0.0	0.0	0.0	0.0	0.0
37	0.0	0.0	0.0	0.0	0.0	0.0	0.0	0.0	0.0	0.0	0.0
38	0.0	0.0	0.0	0.0	0.0	0.0	0.0	0.0	0.0	0.0	0.0
39	0.0	0.0	0.0	0.0	0.0	0.0	0.0	0.0	0.0	0.0	0.0
40	0.0	0.0	0.0	0.0	0.0	0.0	0.0	0.0	0.0	0.0	0.0
41	0.0	13.2	0.0	13.2	0.0	0.0	0.0	0.0	0.0	0.0	0.0
42	0.0	20.9	0.0	-20.9	0.0	0.0	0.0	0.0	0.0	0.0	0.0
43	0.0	-11.8	0.0	11.8	0.0	0.0	0.0	0.0	0.0	0.0	0.0
44	0.0	-15.3	0.0	-15.3	0.0	0.0	0.0	0.0	0.0	0.0	0.0
45	0.0	-85.2	0.0	-85.2	0.0	0.0	0.0	0.0	0.0	0.0	0.0
46	0.0	-86.2	0.0	86.2	0.0	0.0	0.0	0.0	0.0	0.0	0.0
47	0.0	60.4	0.0	-60.4	0.0	0.0	0.0	0.0	0.0	0.0	0.0
48	0.0	62.3	0.0	62.3	0.0	0.0	0.0	0.0	0.0	0.0	0.0
49	0.0	0.0	0.0	0.0	0.0	0.0	39.5	0.0	0.0	39.5	0.0
50	0.0	0.0	0.0	0.0	0.0	0.0	39.2	0.0	0.0	-39.2	0.0
51	0.0	0.0	0.0	0.0	0.0	0.0	-30.7	0.0	0.0	30.7	0.0
52	0.0	0.0	0.0	0.0	0.0	0.0	-26.5	0.0	0.0	-26.5	0.0
53	0.0	0.0	0.0	0.0	0.0	0.0	-42.2	0.0	0.0	-42.2	0.0
54	0.0	0.0	0.0	0.0	0.0	0.0	-42.0	0.0	0.0	42.0	0.0
55	0.0	0.0	0.0	0.0	0.0	0.0	31.1	0.0	0.0	-31.1	0.0
56	0.0	0.0	0.0	0.0	0.0	0.0	27.2	0.0	0.0	27.2	0.0
Main Effect	44.8	-41.7	-10.1	-8.4	43.5	92.4	-4.4	2.4	20.9	0.4	16.3
Norm. Effect	0.057	-0.053	-0.013	-0.011	0.056	0.118	-0.006	0.003	0.027	0.001	0.021

Table 0-4b: Matrix of Two-Factor Interaction Effects

	O ₂ CO ₂	O ₂ CO	O ₂ H ₂ O	O ₂ NO	CO ₂ CO	CO ₂ H ₂ O	CO ₂ NO	CO H ₂ O	CO NO	H ₂ O NO
Test #	x3x4	x3x5	x3x6	x3x7	x4x5	x4x6	x4x7	x5x6	x5x7	x6x7
1	0.0	0.0	0.0	0.0	41.4	41.4	0.0	41.4	0.0	0.0
2	0.0	0.0	0.0	0.0	38.7	-38.7	0.0	-38.7	0.0	0.0
3	0.0	0.0	0.0	0.0	-41.4	41.4	0.0	-41.4	0.0	0.0
4	0.0	0.0	0.0	0.0	-35.5	-35.5	0.0	35.5	0.0	0.0
5	0.0	0.0	0.0	0.0	-31.2	-31.2	0.0	31.2	0.0	0.0
6	0.0	0.0	0.0	0.0	-30.5	30.5	0.0	-30.5	0.0	0.0
7	0.0	0.0	0.0	0.0	35.4	-35.4	0.0	-35.4	0.0	0.0
8	0.0	0.0	0.0	0.0	33.0	33.0	0.0	33.0	0.0	0.0
9	0.0	0.0	0.0	0.0	0.0	0.0	0.0	0.0	0.0	16.2
10	0.0	0.0	0.0	0.0	0.0	0.0	0.0	0.0	0.0	-20.8
11	0.0	0.0	0.0	0.0	0.0	0.0	0.0	0.0	0.0	-8.9
12	0.0	0.0	0.0	0.0	0.0	0.0	0.0	0.0	0.0	17.8
13	0.0	0.0	0.0	0.0	0.0	0.0	0.0	0.0	0.0	48.5
14	0.0	0.0	0.0	0.0	0.0	0.0	0.0	0.0	0.0	-97.0
15	0.0	0.0	0.0	0.0	0.0	0.0	0.0	0.0	0.0	-60.6
16	0.0	0.0	0.0	0.0	0.0	0.0	0.0	0.0	0.0	118.0
17	0.0	0.0	0.0	0.0	0.0	0.0	0.0	0.0	23.4	0.0
18	0.0	0.0	0.0	0.0	0.0	0.0	0.0	0.0	-39.9	0.0
19	0.0	0.0	0.0	0.0	0.0	0.0	0.0	0.0	-26.0	0.0
20	0.0	0.0	0.0	0.0	0.0	0.0	0.0	0.0	38.9	0.0
21	0.0	0.0	0.0	0.0	0.0	0.0	0.0	0.0	24.2	0.0
22	0.0	0.0	0.0	0.0	0.0	0.0	0.0	0.0	-42.0	0.0
23	0.0	0.0	0.0	0.0	0.0	0.0	0.0	0.0	-30.4	0.0
24	0.0	0.0	0.0	0.0	0.0	0.0	0.0	0.0	58.4	0.0
25	0.0	0.0	0.0	0.0	0.0	0.0	0.0	0.0	0.0	0.0
26	0.0	0.0	0.0	0.0	0.0	0.0	0.0	0.0	0.0	0.0
27	0.0	0.0	0.0	0.0	0.0	0.0	0.0	0.0	0.0	0.0
28	0.0	0.0	0.0	0.0	0.0	0.0	0.0	0.0	0.0	0.0
29	0.0	0.0	0.0	0.0	0.0	0.0	0.0	0.0	0.0	0.0
30	0.0	0.0	0.0	0.0	0.0	0.0	0.0	0.0	0.0	0.0
31	0.0	0.0	0.0	0.0	0.0	0.0	0.0	0.0	0.0	0.0
32	0.0	0.0	0.0	0.0	0.0	0.0	0.0	0.0	0.0	0.0
33	40.7	0.0	0.0	40.7	0.0	0.0	40.7	0.0	0.0	0.0
34	66.3	0.0	0.0	-66.3	0.0	0.0	-66.3	0.0	0.0	0.0
35	-41.7	0.0	0.0	41.7	0.0	0.0	-41.7	0.0	0.0	0.0
36	-68.8	0.0	0.0	-68.8	0.0	0.0	68.8	0.0	0.0	0.0
37	-26.4	0.0	0.0	-26.4	0.0	0.0	26.4	0.0	0.0	0.0
38	-45.2	0.0	0.0	45.2	0.0	0.0	-45.2	0.0	0.0	0.0
39	20.7	0.0	0.0	-20.7	0.0	0.0	-20.7	0.0	0.0	0.0
40	34.2	0.0	0.0	34.2	0.0	0.0	34.2	0.0	0.0	0.0
41	0.0	13.2	0.0	0.0	0.0	0.0	0.0	0.0	0.0	0.0
42	0.0	-20.9	0.0	0.0	0.0	0.0	0.0	0.0	0.0	0.0
43	0.0	-11.8	0.0	0.0	0.0	0.0	0.0	0.0	0.0	0.0
44	0.0	15.3	0.0	0.0	0.0	0.0	0.0	0.0	0.0	0.0
45	0.0	85.2	0.0	0.0	0.0	0.0	0.0	0.0	0.0	0.0
46	0.0	-86.2	0.0	0.0	0.0	0.0	0.0	0.0	0.0	0.0
47	0.0	-60.4	0.0	0.0	0.0	0.0	0.0	0.0	0.0	0.0
48	0.0	62.3	0.0	0.0	0.0	0.0	0.0	0.0	0.0	0.0
49	0.0	0.0	39.5	0.0	0.0	0.0	0.0	0.0	0.0	0.0
50	0.0	0.0	-39.2	0.0	0.0	0.0	0.0	0.0	0.0	0.0
51	0.0	0.0	-30.7	0.0	0.0	0.0	0.0	0.0	0.0	0.0
52	0.0	0.0	26.5	0.0	0.0	0.0	0.0	0.0	0.0	0.0
53	0.0	0.0	42.2	0.0	0.0	0.0	0.0	0.0	0.0	0.0
54	0.0	0.0	-42.0	0.0	0.0	0.0	0.0	0.0	0.0	0.0
55	0.0	0.0	-31.1	0.0	0.0	0.0	0.0	0.0	0.0	0.0
56	0.0	0.0	27.2	0.0	0.0	0.0	0.0	0.0	0.0	0.0
Main Eff.	-20.2	-3.2	-7.8	-20.3	9.9	5.5	-3.8	-4.8	6.4	13.2
Norm.Eff	-0.026	-0.004	-0.010	-0.026	0.013	0.007	-0.005	-0.006	0.008	0.017

A.4 Phase II Detailed Investigation Test Matrices

Table 0-5: Detailed Investigation Atmospheric Test Matrix - Nominal Values

Temp [K]	X _{O2}	X _{NO}	Temp [K]	X _{O2}	X _{NO}
900	20%	0	900	12%	0
900	20%	50	900	12%	50
900	20%	100	900	12%	100
900	20%	250	900	12%	250
900	20%	500	900	12%	500
900	20%	1000	900	12%	1000
850	20%	0	850	12%	0
850	20%	50	850	12%	50
850	20%	100	850	12%	100
850	20%	250	850	12%	250
850	20%	500	850	12%	500
850	20%	1000	850	12%	1000
800	20%	0	800	12%	0
800	20%	50	800	12%	50
800	20%	100	800	12%	100
800	20%	250	800	12%	250
800	20%	500	800	12%	500
800	20%	1000	800	12%	1000
750	20%	0	750	12%	0
750	20%	50	750	12%	50
750	20%	100	750	12%	100
750	20%	250	750	12%	250
750	20%	500	750	12%	500
750	20%	1000	750	12%	1000
700	20%	0	700	12%	0
700	20%	50	700	12%	50
700	20%	100	700	12%	100
700	20%	250	700	12%	250
700	20%	500	700	12%	500
700	20%	1000	700	12%	1000

Table 0-6: Results for Atmospheric Tests of JP-8 and O₂/N₂/NO Mixtures

1.0 atm 20% O ₂ - JP-8 Tests w/ NO						1.0 atm 12% O ₂ - JP-8 Tests w/ NO											
Fuel	X _{O2}	Temp. [K]	X _{NO}	τ _{ig} [ms]	SE%	Fuel	X _{O2}	Temp. [K]	X _{NO}	τ _{ig} [ms]	SE%						
JP-8	20%	900	0	325	2.0%	JP-8	12%	900	0	593	0.9%						
JP-8	20%	900	49	284	1.8%	JP-8	12%	900	49	443	0.8%						
JP-8	20%	900	92	256	0.5%	JP-8	12%	900	95	379	2.1%						
JP-8	20%	900	246	181	1.4%	JP-8	12%	900	251	239	1.0%						
JP-8	20%	900	467	128	5.3%	JP-8	12%	900	482	184	2.3%						
JP-8	20%	900	954	93	1.5%	JP-8	12%	900	972	141	1.4%						
Fuel	X _{O2}	Temp. [K]	X _{NO}	τ _{ig} [ms]	SE%	Fuel	X _{O2}	Temp. [K]	X _{NO}	τ _{ig} [ms]	SE%						
JP-8	20%	850	0	731	1.8%	JP-8	12%	850	0	1452	1.5%						
JP-8	20%	850	49	626	0.2%	JP-8	12%	850	49	1103	0.9%						
JP-8	20%	850	92	533	0.3%	JP-8	12%	850	95	870	2.4%						
JP-8	20%	850	246	Did Not Run		JP-8	12%	850	250	251	1.4%						
JP-8	20%	850	467	242	1.2%	JP-8	12%	850	482	365	1.3%						
JP-8	20%	850	954	164	2.1%	JP-8	12%	850	972	298	1.7%						
Fuel	X _{O2}	Temp. [K]	X _{NO}	τ _{ig} [ms]	SE%	Fuel	X _{O2}	Temp. [K]	X _{NO}	τ _{ig} [ms]	SE%						
JP-8	20%	800	0	1365	2.1%	JP-8	12%	800	0	No Ign.							
JP-8	20%	800	49	1298	3.1%	JP-8	12%	800	49	No Ign.							
JP-8	20%	800	92	1188	2.5%	JP-8	12%	800	95	2446	4.1%						
JP-8	20%	800	246	745	1.0%	JP-8	12%	800	251	1261	1.6%						
JP-8	20%	800	467	448	0.3%	JP-8	12%	800	482	717	1.7%						
JP-8	20%	800	954	239	0.5%	JP-8	12%	800	972	514	2.5%						
Fuel	X _{O2}	Temp. [K]	X _{NO}	τ _{ig} [ms]	SE%	705 ppm NO case added for this temperature only at 1 atm and 20% O ₂											
JP-8	20%	750	0	No Ign.													
JP-8	20%	750	49	No Ign.													
JP-8	20%	750	92	3044	1.7%												
JP-8	20%	750	246	1752	2.5%												
JP-8	20%	750	467	932	2.9%												
JP-8	20%	750	954	401	1.9%												
Fuel	X _{O2}	Temp. [K]	X _{NO}	τ _{ig} [ms]	SE%												
JP-8	20%	700	0	No Ign.													
JP-8	20%	700	49	No Ign.													
JP-8	20%	700	92	No Ign.													
JP-8	20%	700	246	No Ign.													
JP-8	20%	700	467	3166	12.4%												
JP-8	20%	700	705	1314	4.4%												
JP-8	20%	700	954	845	4.0%												

Table 0-7: Results for Sub-atmospheric Tests of JP-8 and O₂/N₂/NO Mixtures

0.5 atm 20% O ₂ - JP-8 Tests w/ NO						0.5 atm 12% O ₂ - JP-8 Tests w/ NO					
Fuel	X _{O2}	Temp. [K]	X _{NO}	τ _{ig} [ms]	SE%	Fuel	X _{O2}	Temp. [K]	X _{NO}	τ _{ig} [ms]	SE%
JP-8	20%	900	46	905	2.9%	JP-8	12%	900	46	1396	7.2%
JP-8	20%	900	46	683	3.1%	JP-8	12%	900	46	1268	4.6%
JP-8	20%	900	93	555	2.2%	JP-8	12%	900	94	844	4.9%
JP-8	20%	900	236	392	0.9%	JP-8	12%	900	231	552	4.4%
JP-8	20%	900	472	276	1.5%	JP-8	12%	900	475	390	3.9%
JP-8	20%	900	908	218	0.8%	JP-8	12%	900	921	319	5.4%
Fuel	X _{O2}	Temp. [K]	X _{NO}	τ _{ig} [ms]	SE%	Fuel	X _{O2}	Temp. [K]	X _{NO}	τ _{ig} [ms]	SE%
JP-8	2%	850	49	No Ign.		JP-8	12%	850	49	No Ign.	
JP-8	20%	850	46	1837	9.3%	JP-8	12%	850	49	No Ign.	
JP-8	20%	850	93	1268	3.0%	JP-8	12%	850	49	No Ign.	
JP-8	20%	850	236	834	3.3%	JP-8	12%	850	231	1435	3.9%
JP-8	20%	850	472	521	2.4%	JP-8	12%	850	475	789	1.4%
JP-8	20%	850	908	384	1.9%	JP-8	12%	850	921	650	3.5%
Fuel	X _{O2}	Temp. [K]	X _{NO}	τ _{ig} [ms]	SE%	Fuel	X _{O2}	Temp. [K]	X _{NO}	τ _{ig} [ms]	SE%
JP-8	20%	800	0	No Ign.		JP-8	12%	800	49	No Ign.	
JP-8	20%	800	49	No Ign.		JP-8	12%	800	49	No Ign.	
JP-8	20%	800	92	No Ign.		JP-8	12%	800	49	No Ign.	
JP-8	20%	800	246	No Ign.		JP-8	12%	800	49	No Ign.	
JP-8	20%	800	472	1217	3.3%	JP-8	12%	800	49	No Ign.	
JP-8	20%	800	908	654	2.5%	JP-8	12%	800	921	1355	3.1%

Table 0-8: Results for all Tests of *n*-Decane (*n*-C₁₀) and O₂/N₂/NO Mixtures

1 atm - 20% O₂ - <i>n</i>-Decane Tests w/ NO						1 - atm 20% O₂ - <i>n</i>-Decane Tests w/o NO					
Fuel	X _{O2}	Temp. [K]	X _{NO}	τ _{ig} [ms]	SE%	Fuel	X _{O2}	Temp. [K]	X _{NO}	τ _{ig} [ms]	SE%
<i>n</i> -C ₁₀	20%	900	0	470	2.1%	<i>n</i> -C ₁₀	21%	900	0	470	2.1%
<i>n</i> -C ₁₀	20%	900	49	395	0.9%	<i>n</i> -C ₁₀	21%	850	0	848	1.6%
<i>n</i> -C ₁₀	20%	900	92	343	0.4%	<i>n</i> -C ₁₀	21%	800	0	1382	1.7%
<i>n</i> -C ₁₀	20%	900	246	284	0.7%	<i>n</i> -C ₁₀	21%	750	0	1539	0.8%
<i>n</i> -C ₁₀	20%	900	467	200	0.0%	<i>n</i> -C ₁₀	21%	700	0	2391	3.1%
<i>n</i> -C ₁₀	20%	900	954	126	0.4%	1 - atm 12% O₂ - <i>n</i>-Decane Tests w/o NO					
Fuel	X _{O2}	Temp. [K]	X _{NO}	τ _{ig} [ms]	SE%	Fuel	X _{O2}	Temp. [K]	X _{NO}	τ _{ig} [ms]	SE%
<i>n</i> -C ₁₀	20%	700	0	1798	1.3%	<i>n</i> -C ₁₀	12%	900	0	803	3.9%
<i>n</i> -C ₁₀	20%	700	49	1344	3.0%	<i>n</i> -C ₁₀	12%	850	0	1833	1.5%
<i>n</i> -C ₁₀	20%	700	92	1157	2.4%	<i>n</i> -C ₁₀	12%	800	0	No Ign.	
<i>n</i> -C ₁₀	20%	700	246	769	1.4%	<i>n</i> -C ₁₀	12%	750	0	No Ign.	
<i>n</i> -C ₁₀	20%	700	467	501	1.4%	<i>n</i> -C ₁₀	12%	700	0	No Ign.	
<i>n</i> -C ₁₀	20%	700	954	350	1.3%	1 atm - 12% O₂ - <i>n</i>-Decane Tests w/ NO					
Fuel	X _{O2}	Temp. [K]	X _{NO}	τ _{ig} [ms]	SE%	Fuel	X _{O2}	Temp. [K]	X _{NO}	τ _{ig} [ms]	SE%
<i>n</i> -C ₁₀	12%	850	0	1798	1.3%	<i>n</i> -C ₁₀	20%	900	0	1116	8.8%
<i>n</i> -C ₁₀	12%	850	49	1386	2.7%	<i>n</i> -C ₁₀	20%	900	50	936	6.0%
<i>n</i> -C ₁₀	12%	850	95	1157	2.4%	<i>n</i> -C ₁₀	20%	900	100	800	9.8%
<i>n</i> -C ₁₀	12%	850	251	769	1.4%	<i>n</i> -C ₁₀	20%	900	250	490	2.6%
<i>n</i> -C ₁₀	12%	850	482	499	0.8%	<i>n</i> -C ₁₀	20%	900	500	334	1.4%
<i>n</i> -C ₁₀	12%	850	972	350	1.5%	<i>n</i> -C ₁₀	20%	900	1000	225	4.4%

References

- [1] *Vitiate* | *Define Vitiate at Dictionary.com*. (n.d.). Retrieved April 17th, 2010, from Dictionary.com: <http://dictionary.reference.com/browse/vitiate>
- [2] Cavaliere, A., & de Joannon, M. (2004). Mild Combustion. *Progress in Energy and Combustion Science* , 30, 329-366.
- [3] Lovett, J. A., Brogan, T. P., Derk, S. P., Kiel, B. V., & Thompson, T. V. (2004). Development Needs for Advanced Afterburner Designs. *40th AIAA/ASME/SAE/ASEE Joint Propulsion Conference and Exhibit, AIAA 2004-4192*. Fort Lauderdale, Florida.
- [4] Gokulakrishnan, P. G. (2007). Experimental and Kinetic Modeling of Kerosene-Type Fuels at Gas Turbine Operating Conditions. *Journal of Engineering for Gas Turbines and Power* , 129, 655-663.
- [5] Curran, H. J., Gaffuri, P., Pitz, W. J., & Westbrook, C. K. (1998). A Comprehensive Modeling Study of n-Heptane Oxidation. *Combustion and Flame* , 114, 149-177.
- [6] Dooley, S., Won, S. H., Chaos, M., Heyne, J., Ju, Y., Dryer, F. L., et al. (2010). A jet fuel surrogate formulated by real fuel properties. *Combustion and Flame* , 157 (12), 2333-2339.
- [7] Dagaut, P., Reuillon, M., Boettner, J. -C., & Cathonnet, M. (1994). "Kerosene Combustion at Pressures upto 40 atm: Experimental Study and Detailed Chemical Kinetic Modeling. *Proceeding of the Combustion Institute* , 25, 919-926.
- [8] Ranzi, E., Dente, M., Goldaniga, A., Bozzano, G., & Faravelli, T. (2001). Lumping procedures in detailed kinetic modeling of gasification, pyrolysis, partial oxidation and combustion of hydrocarbon mixtures. *Progress in Energy and Combustion Science* , 27 (1), 99-139 .
- [9] Faravelli, T., Frassoldati, A., & Ranzi, E. (2003). Kinetic modeling of the interactions between NO and hydrocarbons in the oxidation of hydrocarbons at low temperatures. *Combustion and Flame* , 132, 188-207.
- [10] Frassoldati, A., Faravelli, T., & Ranzi, E. (2003). Kinetic modeling of the interactions between NO and hydrocarbons at high temperature. *Combustion and Flame* , 135, 97-122.
- [11] Seiser, R., & Seshadri, K. (2005). The influence of water on extinction and ignition of hydrogen and methane flames. *Proceedings of the Combustion Institute* , 30, 407-414.
- [12] Le Cong, T., Dagaut, P., & Dayma, G. (2008). Oxidation of Natural Gas, Natural Gas/Syngas Mixtures, and Effect of Burnt Gas Recirculation: Experimental and Detailed Modeling Study. *Journal of Engineering for Gas Turbines and Power* , 130 (4).
- [13] Thompson, H. W., & Hinshelwood, C. N. (1929). The Influence of Nitrogen Peroxide on the Combination of Hydrogen and Oxygen. *Proceedings of the Royal Society of London* , A124, 219-227.

- [14] Norrish, R. G., & Wallace, J. (1934). The Reaction of Methane and Oxygen Sensitized by Nitrogen Peroxide. Part I – Thermal Ignition. *Proceedings of the Royal Society of London*, 134, 307-321.
- [15] Dabora, E. K. (1975). Effect of NO₂ on the Ignition Delay of CH₄-Air Mixtures. *Combustion and Flame*, 24, 181-184.
- [16] Slack, M. W., & Grillo, A. R. (1981). Shock Tube Investigation of Methane-Oxygen Ignition Sensitized by NO₂. *Combustion and Flame*, 40, 155-172.
- [17] Bromly, J. H., Barnes, F. J., Muris, S., You, X., & Haynes, B. S. (1996). Kinetic and Thermodynamic Sensitivity Analysis of the NO-Sensitized Oxidation of Methane. *Combustion Science and Technology*, 115, 259-296.
- [18] Bromly, J. H., Barnes, F. J., Mandyczewsky, R., Edwards, T. J., & Haynes, B. S. (1992). An experimental investigation of the mutually sensitised oxidation of nitric oxide and n-butane. *24th Symposium (International) on Combustion* (24), 899-907.
- [19] Dagaut, P., & Nicolle, A. (2005). Experimental study and detailed kinetic modeling of the effect of exhaust gas on fuel combustion: mutual sensitization of the oxidation of nitric oxide and methane over extended temperature and pressure ranges. *Combustion and Flame*, 140, 161-171.
- [20] Bendtsen, A. B., Glarborg, P., & Dam-Johansen, K. (2000). Low Temperature Oxidation of Methane: The Influence of Nitrogen Oxides. *Combustion Science and Technology*, 151, 31-71.
- [21] Konnov, A. A., Zhu, J. N., Bromly, J. H., & Zhang, D. (2005). The effect of NO and NO₂ on the partial oxidation of methane: experiments and modeling. *Proceedings of the Combustion Institute*, 30, 1093-1100.
- [22] Moréac, G., Dagaut, P., Roesler, J. F., & Cathonnet, M. (2006). Nitric oxide interactions with hydrocarbon oxidation in jet-stirred reactor at 10 atm. *Combustion and Flame*, 145, 512-520.
- [23] Moréac, G., Dagaut, P., Roesler, J. F., & Cathonnet, M. (2002). Impact of Trace NO and other residual burnt gas components from piston engines on the oxidation of various hydrocarbons in a jet stirred reactor at atmospheric pressure. *Proceedings of the Second Mediterranean Combustion Symposium 6-11 January 2002*, (pp. 240-251). Sharm El-Sheikh, Egypt.
- [24] Dubreuil, A., Foucher, F., Mounáim-Rousselle, C., Dayma, G., & Dagaut, P. (2007). HCCI combustion: Effect of NO in EGR. *Proceedings of the Combustion Institute*. 31, pp. 2879-2886. The Combustion Institute.
- [25] Anderlohr, J. M., Piprel, A., Pires da Cruz, A., Bounaceur, R., Battin-Leclerc, F., Dagaut, P., et al. (2009). Influence of EGR compounds on the oxidation of an HCCI-diesel surrogate. *Proceedings of the Combustion Institute*, 32, pp. 2852-2859.
- [26] Kowalski, S. (1993). *A Study of the Low and Intermediate Temperature Oxidation Chemistry of a Primary Reference Fuel Blend and Two Gasolines at High Pressure*. Masters Thesis, Princeton University, Department of Mechanical and Aerospace Engineering.

- [27] Dagaut, P. (2002). On the Kinetics of Hydrocarbons Oxidation from Natural Gas to Kerosene and Diesel Fuel". *Physical Chemistry and Chemical Physics* , 4, 2079 –2094.
- [28] Violi, A., Yan, S., Eddings, E. G., Sarofim, A. F., Granata, S., Faravelli, T., et al. (2002). Experimental Formulation and Kinetic Model for JP-8 Surrogate Mixtures. *Combustion Science and Technology* , 174, 399-417.
- [29] Lindstedt, R. P., & Maurice, L. Q. (2000). Detailed Chemical-Kinetic Model for Aviation Fuels. *Journal of Propulsion and Power* , 16, 187-195.
- [30] Starkman, E. (1946). Ignition delay in diesel engines. *American Institute of Chemical Engineers -- Transactions* , 42 (1), 107-207.
- [31] Geir, F. (1985). Investigations of Combustion Properties of Liquid Fuels in a Constant Volume Bomb. *ASTM Special Technical Publication* , 190-203.
- [32] Granata, S., Faravelli, T., & Ranzi, E. (2003). A Wide Range Kinetic Modeling Study of the Pyrolysis and Combustion of Naphthenes. *Combustion and Flame* , 132, 533–544.
- [33] Wurmel, J., Silke, E. J., O Conaire, M. S., & Simmie, J. M. (2007). The effect of diluent gases on ignition delay times in the shock tube and in the rapid compression machine. *Combustion and Flame* , 151 (1-2), 289-302 .
- [34] Mullaney, G. J. (1958). Shock tube technique for study of autoignition of liquid fuel sprays. *Industrial and Engineering Chemistry* , 50, 53-58.
- [35] Miyasaka, K., & Mizutani, Y. (1975). Ignition of Sprays by an Incident Shock. *Combustion and Flame* , 25, 177-186.
- [36] Ciezki, H. K., & Adomeit, G. (1993). Shock-Tube Investigation of Self-Ignition of n-Heptane Mixtures Under Engine Relevant Conditions. *Combustion and Flame* , 93, 421-433.
- [37] Dean, A. J., Penyazkov, O. G., Sevruck, K. L., & Varatharajan, B. (2005). Ignition of Aviation Kerosene at High Temperatures. *20th International Colloquium on Dynamics of Explosions and Reactive Systems*. Montreal, Canada.
- [38] Vasu, S. S., Davidson, D. F., & Hanson, R. K. (2006). Shock Tube Ignition Delay Times and Modeling of Jet Fuel Mixtures. *42nd AIAA/ASME/SAE/ASEE Joint Propulsion Conference and Exhibit, AIAA-2006-4402*. Sacramento, CA.
- [39] Freeman, G., & Lefebvre, A. H. (1984). Spontaneous Ignition Characteristics of Gaseous Hydrocarbon-Air Mixtures. *Combustion and Flame* , 58, 153-162.
- [40] Spadaccini, L. J., & TeVelde, J. A. (1980). Autoignition Characteristics of Aircraft-Type Fuels. *Report No. NASA CR-159886*. United Technologies Research Center, East Hartford, CT.
- [41] Gokulakrishnan, P., Gaines, G. G., Klassen, M. S., & Roby, R. J. (2007). Autoignition of Aviation Fuels: Experimental and Modeling Study. *AIAA/ASME/SAE/ASEE 43rd Joint Propulsion Conference, AIAA 2007-5701*. Cincinnati, OH.

- [42] Fuller, C. C., Gokulakrishnan, P., Klassen, M. S., Roby, R. J., & Kiel, B. V. (2009). Investigation of the Effects of Vitiated Conditions on the Autoignition of JP-8. *45th AIAA/ASME/SAE/ASEE Joint Propulsion Conference & Exhibit*. Denver, CO: American Institute of Aeronautics and Astronautics, Inc.
- [43] Fuller, C. C., Gokulakrishnan, P., Klassen, M. S., Roby, R. J., & Kiel, B. V. (2011). Investigation of the Effect of Nitric Oxide on the Autoignition of JP-8 at Low Pressure Vitiated Conditions. *49th AIAA Aerospace Sciences Meeting including the New Horizons Forum and Aerospace Exposition*. Orlando, FL: American Institute of Aeronautics and Astronautics, Inc.
- [44] Holton, M. M., Gokulakrishnan, P., Klassen, M. S., Roby, R. J., & Jackson, G. S. (2010). Autoignition Delay Time Measurements of Methane, Ethane, Propane Pure Fuels and Methane-Based Fuel Blends. *Journal of Engineering for Gas Turbines and Power*, 132 (9).
- [45] ASTM Standard D2425. (2004). *Standard Test Method for Hydrocarbon Types in Middle Distillates by Mass Spectrometry*. ASTM International, West Conshohocken, PA, 2004: DOI: 10.1520/D2425-04, www.astm.org.
- [46] ASTM Standard D6379. (2004). *Standard Test Method for Determination of Aromatic Hydrocarbon Types in Aviation Fuels and Petroleum Distillates—High Performance Liquid Chromatography Method with Refractive Index Detection*. ASTM International, West Conshohocken, PA: DOI: 10.1520/D6379-04, www.astm.org.
- [47] Yetter, R. A., Dryer, F. L., & Rabitz, H. (1991). Flow Reactor Studies of Carbon Monoxide/Hydrogen/ Oxygen Kinetics. *Combustion Science and Technology*, 27 (1-3), 129-140.
- [48] Li, J., Kazakov, A., & Dryer, F. L. (2001). Ethanol pyrolysis experiments in a variable pressure flow reactor. *International Journal of Chemical Kinetics*, 33 (12), 859–867.
- [49] Schmidt, C. (2001). *Flow Reactor Study on the Effect of Pressure on the Thermal De-NOx Reaction*. Phd. Thesis, Stanford University, Stanford, CA.
- [50] Gokulakrishnan, P., Kazakov, A., & Dryer, F. L. (2003). Comparison of Numerical and Experimental Kinetic Data for Flow Reactor Systems: Mixing Effects. *Proceedings of the Third US Combustion Meeting*. Chicago, IL: The Combustion Institute.
- [51] Myers, R. H., & Montgomery, D. C. (1995). *Response Surface Methodology: Process and Product Optimization Using Designed Experiments*. Wiley and Sons.
- [52] Box, G. E., Hunter, W. G., & Hunter, J. S. (1978). *Statistics for Experimenters: An Introduction to Design, Data Analysis and Model Building*. Wiley-Interscience.
- [53] *NIST/SEMATECH e-Handbook of Statistical Methods*. (n.d.). Retrieved November 20, 2008, from <http://www.itl.nist.gov/div898/handbook>
- [54] Holton, M. M. (2008). *Autoignition Delay Time Measurements for Natural Gas Fuel Components and their Mixtures*. M.S. Thesis, University of Maryland, College Park, Mechanical Engineering.

- [55] Joklik, R., Fuller, C., Turner, B., & Gokulakrishnan, P. (2010). The Effect of Multi-Component Fuel Evaporation on the Ignition of JP-8. *ASME Turbo Expo 2010: Power for Land, Sea, and Air (GT2010)* (pp. 813-822). Glasgow, UK: ASME.
- [56] Burcat, A. (2006, March 13th). *Burcat's Thermodynamic Data*. Retrieved from Burcat's Thermodynamic Data: <http://garfield.chem.elte.hu/Burcat/burcat.html>
- [57] Gracia-Salcedo, C. M., Brabbs, T. A., & McBride, B. J. (1988). Experimental verification of the thermodynamic properties of a Jet-A fuel. *Coal combustion and soot formation* (pp. 875-882). Los Angeles, CA: NASA.
- [58] Gokulakrishnan, P., McLellan, P. J., Lawrence, A. D., & Grandmaison, E. W. (2005). Kinetic analysis of NO-sensitized methane oxidation. *Chemical Engineering Science*, 60, 3683 - 3692.
- [59] Beerer, D., McDonell, V., & Samuelsen, S. (2009). Interpretation of Flow Reactor Based Ignition Delay Measurements. *Proceedings of the ASME Turbo Expo*, v2, pp. 1011-1026. Orlando, FL.
- [60] Beerer, D. J. (2009). *Autoignition of Methane, Ethane, Propane and Hydrogen in Turbulent High Pressure and Temperature Flows*. Master's Thesis, University of California, Irvine, Mechanical and Aerospace Engineering.